

Impacts of climate change on the fire weather in Indian forests

by

Anasuya Barik

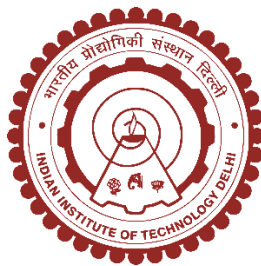
(Entry No. 2018ASZ8004)

in fulfilment of the requirements of the degree of

DOCTOR OF PHILOSOPHY

Under the Supervision of

Professor Somnath Baidya Roy



Centre for Atmospheric Sciences

INDIAN INSTITUTE OF TECHNOLOGY DELHI

April 2025

© 2025. Anasuya Barik. All rights reserved.

Certificate

This is to certify that the thesis entitled " **Impacts of climate change on the fire weather in Indian forests**" being submitted by **Anasuya Barik** to the Indian Institute of Technology Delhi for the award of the degree of **DOCTOR OF PHILOSOPHY** is a record of original bonafide research carried out by her. Anasuya has worked under my guidance and supervision and has fulfilled the requirements for the submission of this thesis. The results contained in this thesis have not been submitted part or full to any other University or Institute for the award of any degree or diploma.

(Prof. Somnath Baidya Roy)
Professor,
Centre for Atmospheric Sciences
Indian Institute of Technology
New Delhi-110016, India

Acknowledgements

First and foremost, I would like to express my gratitude to my research supervisor, Prof. Somnath Baidya Roy, for his constant guidance, encouragement, and insightful discussions throughout the course of this research. His scientific rigor and clarity of perspective have shaped my approach to research and problem-solving, both within and beyond academic settings. I am also thankful to the members of my Student Research Committee — Prof. Krishna AchutaRao, Prof. Dhanya C T, and Prof. Ravi Kumar Kunchala — for their valuable suggestions and feedback that have substantially improved the quality of this work.

I extend my appreciation to all the faculty members of the Centre for Atmospheric Sciences (CAS), IIT Delhi, whose teachings and advice have, directly or indirectly, contributed to this research journey. The academic atmosphere within the department has been instrumental in my PhD journey.

I gratefully acknowledge IIT Delhi for providing a conducive research environment, excellent infrastructure, and opportunities for academic exposure, including travel support. I sincerely thank the Industrial Research and Development (IRD) Unit for their financial support and for granting me the research excellence travel award, which enabled me to share my work on wider global platforms. I also thank the administrative staff of the CAS for their support in facilitating various official matters. Additionally, I am grateful to the Board for Hostel Management for ensuring a comfortable and well-managed residential experience during my stay at IIT Delhi.

Among those who shared this academic journey closely, I would like to thank my labmates and batchmates, especially Saran and Jaswant, for the camaraderie, discussions, and everyday conversations that have been an indispensable part of this experience. I also extend my heartfelt thanks to my juniors — Narender, Chaithra, Pawan, Shankar, Chiranjit, Shubhojit, and Pragya - who both personally and professionally created an environment where my efforts were constantly appreciated and cheered. The welcoming space they created made this journey lighter, brighter, and deeply meaningful.

I also acknowledge my colleagues at BISA, where I have had the opportunity to work alongside some remarkable individuals — Riya, Saumya, Aniket, Kaushik, and Uttam. I am especially grateful to my mentors at BISA, Dr. Pramod Aggarwal, Dr. Paresh Shirsath, and Dr. Prasun Gangopadhyay, whose mentorship and encouragement continue to guide my professional growth.

I am fortunate to have friends who feel like family. I would like to express my heartfelt thanks to Yash and Abhishek for their unwavering support and for standing by me through the most demanding phases of this work. Lastly, a special mention to Kunal and Akash, whose enduring support, intellectual engagement, and honest conversations have significantly contributed to my personal and professional growth. Above all, I owe everything to my parents, Anupam and Swati, for their boundless support, patience, and belief in me. Their quiet strength and best wishes have been the foundation on which this entire journey rests.

Abstract

Forest fires are influenced by changing climatic conditions. The changing climate and its impact on fire frequencies have led to increased interest within the research community in investigating climate-fire interactions at both global and regional scales. India experiences a large number of forest fires. This thesis presents a detailed analysis of the forest fire patterns across India, the influence of meteorological conditions, and the projected impact of climate change on fire weather regimes by the end-century over forests in India. For this study, Indian forests were classified into five zones: Himalayan, Northeast, Central India, Deccan, and Western Ghat. This classification was based on the climate and forest types of these zones. A comprehensive analysis of MODIS active fire data from 2003 to 2021 shows spatial heterogeneity in fire activity across India's forest zones. The highest fire occurrence is observed in the Northeast (NE) zone, with concentrations up to 250 fires per year in some of the 25km grids. Temporal analysis reveals a clear seasonality, with fires occurring mainly in the pre-monsoon months with high temperatures and low humidity.

Next, the Canadian Forest Fire Danger Rating System Fire Weather Index (CFFDRS-FWI) system was evaluated under Indian climatic conditions. It was found that with a spin-up period of about 365 days, the algorithm produced stable values of FWI over the Indian forest zones. Further analysis shows that high FWI is an essential requirement for fire occurrence. This makes FWI a good metric for estimating fire danger. After this, a Fire Danger Rating System (FDRS) was developed and tailored to each forest zone. This FDRS was based on the simulated FWI from the CFFDRS, ERA5 reanalysis data as meteorological input to CFFDRS and MODIS active fire

observations from 2003 to 2021 for validation. An ensemble of methods using logistic regression, FWI percentiles, fire occurrence percentages, and k-means clustering was employed to classify FWI values into five fire danger categories. Machine learning techniques were introduced to reduce the subjective decisions in these methods. This increased the efficiency of the FDRS to detect fire probability by 30-50%.

To drive this CFFDRS and compute baseline and future FWI, a high-resolution dynamically downscaled climate projection DSCESM was used for a baseline (2006-2015) and an end-century (2091-2100) period. DSCESM dataset is a 10-km gridded hydrometeorological dataset over India developed by dynamic downscaling of the bias-corrected Community Earth System Model (CESMv1) climate projections under RCP8.5 scenario using the state-of-the-art Weather Research and Forecasting (WRF) model. It is archived in the World Data Center for Climate (WDCC) portal at three temporal resolutions (daily, monthly, and monthly climatology) for current (2006–2015), mid-century (2041–2050) and end-century (2091–2100) periods. All the DSCESM variables were extensively evaluated against reanalysis data and station observations for the period 2006–2015. Variables such as 2-m air temperature, total accumulated precipitation, wind speed, and relative humidity were used as input for the CFFDRS algorithm.

To assess the impact of climate change on the Fire Weather Index (FWI) across Indian forest zones, this study compared various aspects of baseline and future FWI, fire weather danger, Seasonal Severity Ratings (SSR), and seasonal characteristics of fire danger. Results indicated substantial variability in both baseline and projected fire weather danger across different zones and within forest zones. Climate change is

anticipated to significantly impact fire weather, with days exceeding the Very High FWI threshold projected to increase by 30–40 days by the end of the century, despite only a 5% rise in annual FWI values. In dry forests, severe fire weather days could increase by up to 60% by the century's end due to rising temperatures. In contrast, humid forests may experience a reduction of up to 40% in severe fire weather days, attributed to an expected increase in precipitation by the century's end. The fire season is also expected to extend by 3–61 days throughout India. SSR analysis suggests a peak in fire disturbances during the pre-monsoon months (March–April–May), affecting about 55% of India's forest area, while the post-monsoon season (September–October–November) is likely to show minimal impact. Forests at highest risk of fire disturbances by century's end include moist deciduous and evergreen forests in the northern Western Ghats (WG), mixed dry deciduous forests in central and southern Central India (CEN), Pine and Sal forests in the Himalayas (HIM), and scrub forests in the Deccan (DEC) zone.

This research represents one of the first efforts to quantify climate change effects on forest fire hazards in India. The high-resolution analysis shows intricate patterns of the relationship between weather variables and fire occurrences, which are different from those suggested by coarser-resolution global studies. This study counters the conventional view that fire regimes will intensify homogeneously with rising temperatures. Precipitation and humidity are likely to moderate the impact of temperature increases under changing climate, particularly in humid zones. Such findings highlight the importance of considering changes in monsoon dynamics alongside temperature changes for fire-climate interaction studies. This study also has significant policy implications and can be valuable in targeted efforts towards regional fire hazards under evolving climate conditions.

सारांश

वनाग्रियाँ परिवर्तित होते जलवायु परिस्थितियों से प्रभावित होती हैं। जलवायु परिवर्तन तथा इसके कारण आग की आवृत्तियों में हो रहे बदलावों ने वैश्विक एवं क्षेत्रीय स्तर पर आग-जलवायु अंतःक्रियाओं के अध्ययन में शोध समुदाय की रुचि बढ़ाई है। भारत में प्रतिवर्ष बड़ी संख्या में वनाग्रियाँ घटित होती हैं। यह शोध प्रबंध भारत में वनाग्नि प्रवृत्तियों, मौसमीय परिस्थितियों के प्रभाव, तथा भविष्य में जलवायु परिवर्तन के कारण आग के मौसम पर संभावित प्रभावों का विश्लेषण प्रस्तुत करता है। इस अध्ययन में भारतीय वनों को उनके जलवायु एवं वन प्रकारों के आधार पर पाँच क्षेत्रों — हिमालय, उत्तर-पूर्व, मध्य भारत, दक्कन तथा पश्चिमी घाट — में वर्गीकृत किया गया है।

2003 से 2021 तक के MODIS सक्रिय अग्नि डेटा का विश्लेषण भारत के वन क्षेत्रों में आग की स्थानिक विषमता को दर्शाता है। सर्वाधिक अग्नि घटनाएँ उत्तर-पूर्व (NE) क्षेत्र में पाई गईं, जहाँ कुछ 25-किमी ग्रिड में प्रतिवर्ष 250 तक आग की घटनाएँ दर्ज हुईं। कालानुक्रमिक विश्लेषण में पूर्व मानसून महीनों में उच्च तापमान एवं कम आर्द्रता के साथ आग की मौसमी प्रवृत्ति स्पष्ट रूप से परिलक्षित होती है।

अगले चरण में, Canadian Forest Fire Danger Rating System Fire Weather Index (CFFDRS-FWI) प्रणाली का भारतीय परिस्थितियों में परीक्षण किया गया। पाया गया कि लगभग 365 दिन के स्पिन-अप काल के साथ, यह एल्गोरिद्म भारतीय वन क्षेत्रों में स्थिर FWI मान प्रदान करता है। उच्च FWI मान को आग की घटनाओं के लिए अनिवार्य पाया गया, जिससे यह FWI को आग के खतरे के आकलन का उपयुक्त संकेतक बनाता है। इसके पश्चात, CFFDRS सिम्पुलेटेड FWI, ERA5 पुनःविश्लेषण डेटा तथा MODIS आग प्रेक्षणों (2003–2021) पर आधारित, प्रत्येक वन क्षेत्र के अनुरूप एक Fire Danger Rating System (FDRS) विकसित किया गया। लॉजिस्टिक रिग्रेशन, FWI परसेंटाइल, आग की घटना प्रतिशत एवं k-means क्लस्टरिंग जैसी तकनीकों के संयोजन से FWI को पाँच श्रेणियों में वर्गीकृत किया गया। मशीन लर्निंग तकनीकों को शामिल कर इन विधियों में व्यक्तिपरक निर्णयों को कम किया गया, जिससे FDRS की भविष्यवाणी क्षमता में 30–50% तक सुधार हुआ। इस प्रणाली को चलाने तथा वर्तमान एवं भविष्य की FWI की गणना के लिए उच्च-रिज़ॉल्यूशन, डायनामिकली डाउनस्केल्ड जलवायु प्रक्षेपण DSCESM का उपयोग किया गया। यह डेटा सेट 10-किमी ग्रिड आकार में CESMv1 जलवायु प्रक्षेपणों को RCP8.5 परिदृश्य के अंतर्गत WRF मॉडल द्वारा डाउनस्केल कर विकसित किया गया है। यह World Data Center for Climate (WDCC) पोर्टल

पर दैनिक, मासिक तथा मासिक औसत स्तर पर वर्तमान (2006–2015), मध्य-शती (2041–2050) एवं शताब्दी-अंत (2091–2100) कालखंडों के लिए उपलब्ध है। 2006–2015 की अवधि में DSCESM चरमानों का पुनःविश्लेषण तथा प्रेक्षण डेटा के साथ गहन परीक्षण किया गया।

वन क्षेत्रों में जलवायु परिवर्तन के FWI पर प्रभाव का आकलन करने हेतु आधारभूत एवं भविष्य FWI, आग मौसम खतरा, Seasonal Severity Ratings (SSR), तथा आग मौसम की मौसमी प्रवृत्तियों की तुलना की गई। परिणामों से स्पष्ट होता है कि अलग-अलग क्षेत्रों एवं वन क्षेत्रों के भीतर आग मौसम खतरे में पर्याप्त अंतर है। शताब्दी-अंत तक, अत्यंत उच्च FWI वाले दिनों की संख्या में 30–40 दिन की वृद्धि संभावित है, जबकि वार्षिक FWI में मात्र 5% की वृद्धि अनुमानित है। शुष्क वनों में, तीव्र आग मौसम वाले दिनों में तापमान वृद्धि के कारण 60% तक वृद्धि हो सकती है। दूसरी ओर, आर्द्र वनों में वर्षा वृद्धि के कारण 40% तक की कमी संभव है। पूरे भारत में आग का मौसम 3–61 दिन तक बढ़ सकता है। SSR विश्लेषण से पूर्व-मानसून महीनों (मार्च-अप्रैल-मई) में सर्वाधिक (~55%) वन क्षेत्र प्रभावित होने की संभावना है, जबकि उत्तर-मानसून (सितंबर-अक्टूबर-नवंबर) में प्रभाव न्यूनतम होगा। सर्वाधिक जोखिम वाले वन क्षेत्र शताब्दी-अंत तक उत्तरी पश्चिमी घाट के नम पतझड़ी एवं सदाबहार वन, मध्य एवं दक्षिणी मध्य भारत के मिश्रित शुष्क पतझड़ी वन, हिमालय के चीड़ एवं साल वन तथा दक्कन के स्क्रब वन हो सकते हैं।

यह अध्ययन भारत में वनाग्नि जोखिमों पर जलवायु परिवर्तन के प्रभाव का मात्रात्मक आकलन करने का प्रथम प्रयास है। उच्च-रिज़ॉल्यूशन विश्लेषण से यह स्पष्ट हुआ कि मौसमीय कारकों एवं आग की घटनाओं के बीच संबंध वैश्विक स्तर पर प्राप्त निष्कर्षों से भिन्न हैं। यह अध्ययन पारंपरिक धारणा का खंडन करता है कि तापमान वृद्धि के साथ आग की घटनाएँ समान रूप से बढ़ेंगी। आर्द्रता एवं वर्षा तापमान वृद्धि के प्रभाव को विशेषकर आर्द्र क्षेत्रों में संतुलित कर सकती हैं। यह परिणाम मानसूनी प्रवृत्तियों के परिवर्तनों को तापमान के साथ मिलाकर विचार करने की आवश्यकता को रेखांकित करता है। यह शोध नीति निर्माण में भी उपयोगी हो सकता है एवं क्षेत्रीय स्तर पर आग के खतरों के प्रबंधन हेतु महत्वपूर्ण दिशा-निर्देश प्रदान कर सकता है।

Contents

Chapter 1: Introduction and Literature Review

Chapter 2: Materials and Methods

2.1 Study area

2.1.1 Extent of Indian mainland

2.1.2 Topographical features

2.1.3 Forest cover of India

2.1.4 Climate of India

2.2 Descriptions of models used

2.2.1 High-resolution land use/ land cover (LULC) dataset

2.2.2 Koppen climate data

2.2.3 MODIS active fire data

2.2.4 ERA5 reanalysis

2.2.5 CESMv1

2.2.6 DSCESM

2.2.7 GSOD

2.3 Models

2.3.1 CFFDRS-FWI

2.3.2 WRF-ARW

2.4 Methods

Chapter 3: Spatial and temporal patterns of forest fires in India

3.1 Introduction

3.2 Forest zones of India

3.3 Removal of non-forest fires

3.4 Fire occurrence patterns in forest zones of India

3.4.1 Spatial signature of fire events in forest zones

3.4.2 Temporal signatures of fire events in forest zones

Chapter 4: Fire Danger Rating System (FDRS) for Indian forest zones

4.1 Evaluation of CFFDRS-FWI in Indian climate

4.2 Association between FWI and fire frequency

4.3 Fire danger rating system

4.4 Evaluation of FDRS

4.5 Summary

Chapter 5: High-resolution climate scenarios

5.1 WRF model configuration

5.2 Sensitivity analysis of parametrization schemes

5.3 Validation of the downscaled data

5.4 DSCESM data archival with DKRZ

5.5 Bias correction of DSCESM wind speed

Chapter 6: Effects of climate change on Fire Weather Index

6.1 Introduction

6.2 FWI computation for baseline and end-century

6.3 Change in mean annual FWI by end-century

6.4 Change in spatial pattern of severe FWI days

6.5 Change in seasonal pattern of fire weather severity

6.6 Change in fire weather danger season

Chapter 7: Conclusions and future work

List of Publications Based on This Thesis

Journal articles

Barik, A., & Baidya Roy, S. (2023). Climate change strongly affects future fire weather danger in Indian forests. *Communications Earth & Environment*, 4(1), 452.

Barik, A., Sahoo, S. K., Kumari, S., & Baidya Roy, S. (2024). High-resolution climate projection dataset over India using dynamical downscaling. *Geoscience Data Journal*, 11(4), 921-935.

Barik, A., & Baidya Roy, S. Modelling Fire Weather Hazard and Risk in Fragmented Tropical Forests: A Machine Learning Approach. *npj Natural Hazards* (under review)

Datasets

Barik, A., Sahoo, S. K., Kumari, S., & Baidya Roy, S. (2021). 10 km gridded hydrometeorological dataset developed by dynamical downscaling of the bias-corrected CMIP5 CESM RCP8.5 projections over India for current (2006-2015) and future (2091-2100) periods using WRF, World Data Center for Climate (WDCC) at DKRZ.

Conferences

Barik, A., & Roy, S. B. (2023). Impact of climate change on the fire weather in Indian forests. In *EGU General Assembly Conference Abstracts* (No. EGU23-10618). Copernicus Meetings.

Barik, A., & Baidya Roy, S. (2022, December). Impact of climate change on the fire weather in Indian forests. In *AGU Fall Meeting Abstracts*

Barik, A., & Baidya Roy, S. (2021, April). Sensitivity of the CFFDRS Fire Weather Index parameters for Indian weather conditions. In *EGU General Assembly Conference Abstracts* (pp. EGU21-14231).

Barik, A., & Baidya Roy, S. (2020, May). Effects of meteorology on forest fires in India: A modeling study. In *EGU General Assembly Conference Abstracts* (p. 18317).

List of figures and tables

List of figures

Figure 2.1: Map of the Indian mainland featuring (a) topographical classification, (b) forest cover and (c) climate zones.

Figure 2.2: Comparison of CESM precipitation and temperatures under RCP 2.6, RCP 4.5, and RCP 8.5 with observational (GPCP) and reanalysis (ERA5) datasets for the years 2005 and 2015

Figure 2.3: Structure of CFFDRS-FWI

Figure 2.4: Structure of the WRF model

Figure 2.5: Graphical illustration of the overall methodology used in this study

Figure 3.1: (a) Forest cover percentages and (b) Shapefiles of the classified forest zones of India

Figure 3.2: Exclusion of non-forest fires

Figure 3.3: Annual fire count data in a 25km grid over forest zones of India

Figure 3.4: Seasonal forest fire occurrences over Indian forest zones

Figure 3.5: Time series of aggregated fire over a year in a zone

Figure 4.1: Spin-up simulation for (a) FPMC, (b) DMC, and (c) DC)

Figure 4.2: Idealistic (i and iii) and realistic (ii and iv) model performance with Indian Climate for varying (a) temperature, (b) relative humidity, and (c) wind speed for (i and ii) no precipitation grids and (iii and iv) precipitation occurring grids respectively.

Figure 4.3: Relationship between fire counts and percentiles of FWI. (i) Spatial map of percentiles of annual mean FWI and b MODIS observed annual fire count and (ii) scatterplot of fire count for each FWI percentile bin for a HIM, b NE, c CEN, d DEC, and e WG FWI zones for the baseline period (2006–2015). R^2 represents the coefficient of determination.

Figure 4.4: Kernel Density Estimation of FWI corresponding to that of fire-occurring grids and non-fire grids for different zones.

Figure 4.5: Graphical illustration of ROC curves of the percentile-based method for every zone

Figure 4.6: Graphical illustration of classes developed using percentage of fires beyond PI and hierarchical clustering for every zone

Figure 4.7: Graphical illustration of classes developed using logistic regression probabilities and hierarchical clustering for every zone

Figure 4.8: Graphical illustration of classes developed using K-means clustering for every zone

Figure 4.9: Violin plots for danger class thresholds developed using different methods along with the mean and median for different zones

Figure 4.10: Fire occurrence probability at fire danger classes for different zones

Figure 4.11: Critical Success Rate (CSR) of thresholds for each danger class developed without machine learning (dashed lines) and with machine learning (solid lines) for different zones.

Figure 5.1: WRF simulation domains showing the elevation and three nested grids d01, d02 and d03 at resolutions 90 km, 30 km, and 10 km, respectively

Figure 5. 2: Taylor Diagram of sensitivity experiments vs IMDAA reanalysis dataset of monthly mean 2m-temperature for (a) January and (b) July, and (c) total monthly precipitation for July.

Figure 5.3: (a) Taylor Diagram and (b) the RMSE vs BIAS diagram of DSCESM daily variables against IMDAA and ERA5 reanalysis variables.

Figure 5.4: RMSE of (a) monthly accumulated precipitation and monthly means of (b) 2m temperature (K), (c) wind speed (m/s), (d) relative humidity (%), (e) sensible heat flux (W/m²), (f) latent heat flux (W/m²), (g) downward surface shortwave radiation (W/m²) and (h) outgoing longwave radiation (W/m²) with respect to IMDAA (column i and iii) and ERA5 (column ii and iv) reanalyses.

Figure 5.5: Seasonal cycle of DSCESM variables (black) in comparison with the IMDAA (orange) and ERA5 (blue). The grey shaded area represents the DSCESM uncertainty (one standard deviation).

Figure 5.6: Probability distribution functions (PDFs) of the 10-year average values of DSCESM variables (blue), IMDAA (Green) and ERA5 (red).

Figure 5.7: Location-wise Pearson's correlation coefficients for daily climatology of CESMv1 and DSCESM against GSOD station observations from 2006-2015

Figure 5.8: Comparison of correlation coefficients of GSOD observations with DSCESM and CORDEX-SA for monthly mean 2m temperature and monthly accumulated precipitation.

Figure 5.9: Bias of DSCESM climatology with GSOD station data observations

Figure 5.10: Quantile-quantile plot of daily ERA5 wind speed with (a) linear scaling bias corrected wind speed and (b) variance scaling bias corrected wind speed. The dotted red line denotes the normal reference line, and the blue markers denote the quantile of x quantity plotted against the quantiles of y quantity.

Figure 5.11: Comparison of correlation coefficients of GSOD observations with DSCESM and CORDEX-SA for monthly mean 2m temperature and monthly accumulated precipitation.

Figure 6.1: (i)(a) Spatial map of the change in mean annual FWI between baseline and end-century, (b) variable contribution resulting in this change, pie charts of dominant contributor in (c) arid, (d) intermediate, and (e) humid regions and (ii) Kernel density estimation (KDE) for baseline and future daily FWI for different FWI zones

Figure 6.2: Number of days per year exceeding (a) Medium, (b) High, and (c) Very High thresholds of FWI for (i) the baseline period and (ii) change in these numbers of days expected by end-century.

Figure 6. 3: Spatial Seasonal Severity Rating (SSR) of the (i) baseline and (ii) the difference between the end-century and baseline SSR for different seasons

Figure 6.4: Daily FWI climatology for baseline (blue) and end-century (red) for (a) HIM, (b) NE, (c) CEN, (d) DEC, and (e)WG. The shaded region denotes the bootstrap uncertainty computed at 95% significance.

List of tables

Table 3.1 Forest zones of India

Table 4.1 Sensitivity experiment sets to determine FFMC, DMC, and DC initialization

Table 4.2: Sensitivity experiments for assessing ideal CFFDRS behaviour

Table 4.3: Upper thresholds of fire danger classes in percentiles of FWI for the different zones

Table 4.4: Evaluative parameters to test the skill of the developed system in fire prediction

Table 5.1: Nested Grid Configuration in WRF Simulations

Table 5.2: Physics parameterization combinations for the sensitivity experiments

Table 5.3: List of variables in the DSCESM dataset

Table 6.1: Zone-wise severe fire weather danger season for baseline and end-century

List of abbreviations

BMJ	Betts Miller Janjic
BUI	Buildup Index
C3S	Copernicus Climate Change Service
CDS	Climate Data Store
CEN	Central India
CESM	Community Earth System Model
CFFDRS	Canadian Forest Fire Weather Rating System
CISL	Computational and Information Systems Laboratory
CMIP	Coupled Model Intercomparison Project
CORDEX-SA	Coordinated Regional Climate Downscaling Experiment-South Asia
CRU TS	Climate Research Unit Time Series
CSI	Critical Success Index
CSR	Critical Success Rate
DC	Drought Code
DEC	Deccan
DMC	Duff Moisture Code
DSCESM	Downscaled CESM
DSR	Daily Severity Rating
ERA5	Fifth generation ECMWF reanalysis
ETM+	Enhanced Thematic Mapper Plus
FAST 3.0	Forest Fire Alert System v3.0
FAR	False Alarm Ratio
FDRS	Fire Danger Rating System
FFMC	Fine Fuel Moisture Code
FIRMS	Fire Information for Resource Management System
FPR	False Positive Rate
FRP	Fire Radiative Power
FSI	Forest Survey of India
FWI	Fire Weather Index
GCM	General Circulation Model

GPCC	Global Precipitation Climatology Centre
GPCP	Global Precipitation Climatology Project
GSOD	Global Summary of the Day
HIM	Himalayas
IGBP	International Geosphere-Biosphere Programme
IMDAA	Indian Monsoon Data Assimilation and Analysis
IPCC AR6	Intergovernmental Panel on Climate Change Sixth Assessment Report
IRS	India Remote Sensing
ISI	Initial Spread Index
KBDI	Keetch-Byram Drought Index
KDE	Kernel Density Estimation
KF	Kain–Fritsch
LISS	Linear Imaging Self-Scanning Sensor
LULC	Land Use and Land Cover
MM5	Fifth-Generation Penn State/NCAR Mesoscale Model
MODIS	Moderate Resolution Imaging Spectroradiometer
MPAS	Model for Prediction Across Scales
MSS	Multispectral Scanner
MYJ	Mellor-Yamada-Janjic
NCAR	National Center for Atmospheric Research
NE	North East
NOAH-MP	Noah Multi-parameterization
OLR	Outgoing Longwave Radiation
ORNL-DAAC	Oak Ridge National Laboratory Distributed Active Archive Center
PBL	Planetary Boundary Layer
PDF	Probability Density Function
PET	Potential Evapotranspiration
PI	Percentile Index
RCM	Regional Climate Models
RCP	Representative Concentration Pathways
RMSE	Root Mean Square Error

ROC	Receiver Operating Characteristic curve
RRTM	Rapid Radiative Transfer Model
SSR	Seasonal Severity Rating
T2m	2m Temperature
TH	Tropical thorn
TM	Thematic Mapper
TOA	Top Of Atmosphere
TPR	True Positive Rate
TS	Time Series
WDCC	World Data Center for Climate
WG	Western Ghats
WRF	Weather Research and Forecasting
YSU	Yonsei University Scheme

Chapter 1

Introduction and Literature Review

Forest fires are an ecologically important phenomenon (Hutto et al., 2016; Pausas & Keeley, 2019). These fires play an important role in ecological processes such as nutrient cycling, seed germination, and habitat regeneration (Abedi et al., 2018; Carbutt & Kirkman, 2022; Naveh, 1994; Zackrisson et al., 1996). However, in humid tropical forests where natural regeneration is difficult, insufficient regeneration rates can pose a threat to forest cover (Scheper et al., 2021). The intensification of climate-related factors is leading to uncontrolled fires in these regions, resulting in not only forest cover reductions but also economic losses (Jones et al., 2022; Kalogiannidis et al., 2023; Mohanty & Mithal, 2022; Tyukavina et al., 2022; van Wees et al., 2021; Vancutsem et al., 2021). Indian forests also have a large number of uncontrolled fires. Forest Survey of India recorded 2,23,333 forest fires between November 2021 and June 2022 and 2,12,249 between November 2022 and June 2023 (Damage Due to Forest Fire, 2023). However, these fires remain lesser known globally owing to their smaller size and intensity than their counterparts in Australia, California, or the Amazon. As of 2021, 54.40% of India's forests experience occasional fires, 7.49% contend with moderately frequent fires, and 2.40% experience high incidence levels, accounting for a significant land area of 20,074 sq km (*India State Forest Report 2021, 2022*).

Many factors like weather, vegetation, fuel loading, and local socioeconomic conditions drive forest fires. Among the important factors, meteorological factors like temperature, humidity, wind speed, and rainfall are crucial in determining fire risk. Studies across many countries and specific forest systems have deduced evidence of changes in spatial distribution, intensity and frequency of forest fires with the changing climate (Barbero et al., 2015; Liu et al., 2013; Piñol et al., 1998). The major meteorological parameters that

forest fires depend upon are temperature, relative humidity, precipitation and wind (Barbero et al., 2015; Kirchmeier-Young et al., 2019; Liu et al., 2013). A warmer atmosphere facilitates a drier surface and increases fuel availability and distribution to a larger area (Flannigan et al., 2000). Under such conditions, any ignition will lead to an intensified fire. However, only an increase in temperature cannot ensure an increase in fire disturbance. Relative humidity also plays an important role in increasing fuel loading by lowering fuel moisture (Barbero et al., 2015; Flannigan et al., 2000). Precipitation subdues fuel availability, thus diminishing fire probability (Dimitrakopoulos & Papaioannou, 2001). The probability of fire occurrence becomes zero beyond a certain threshold value of rainfall (Vadrevu et al., 2019). Changes in regional and temporal patterns and the intensity of precipitation will, in turn, affect the intensity and frequency of fire occurrences. Changes in the fire season can also be expected with the changes in the monsoon season. However, according to (Stocks et al., 1989), the changes in fire patterns due to temperature and relative humidity subdues the effect on them due to precipitation. Once the fuel availability is ensured by the parameters mentioned above, the forest fire ignition depends largely upon wind (Flannigan et al., 2000). Wind affects moisture availability and can also influence the intensity and spread of fire individually (Liu et al., 2013).

The climate datasets generated by the General Circulation Models (GCMs) have enabled the quantitative analysis of the meteorological parameters under various emission and climate change scenarios (Barbero et al., 2015; Flannigan et al., 2000; Kirchmeier-Young et al., 2019). According to climate projections, India will experience a warming of 4.4-4.8 °C by the end-century compared to the 1976-2005 period (Chaturvedi et al., 2012;

Krishnan et al., 2020). Such warming is expected to affect forest fire occurrences and severity in India. However, other factors like future changes in humidity and precipitation are also likely to play pivotal roles in the future fire regime (Fanin et al., n.d.; Littell et al., 2016). Higher summer temperatures and delayed monsoon cause soils to be drier for longer, increasing the likelihood of drought and a more extended fire season (Flannigan et al., 2006a). The hot, dry conditions also escalate fuel availability and increase the possibility of more intense fires (Liu et al., 2013). Furthermore, climate change may affect the timing and intensity of the monsoons. As climate change alters these weather variables, we can expect shifts in the fire regime (Abatzoglou et al., 2019).

Globally, the rise in forest fires is often attributed to climate change, which alters weather patterns and exacerbates fire-prone conditions (Barbero et al., 2015; Flannigan et al., 2000; Wotton et al., 2010). Studies also show that with changes in weather patterns induced by climate change, Indian forests are becoming more susceptible to fires (Mohanty & Mithal, 2022). Despite the prevalence of forest fires and evidence of rapidly changing climate patterns, no comprehensive country-scale studies have attempted to understand and quantify the fire-climate interplay in India. Understanding how meteorological changes impact fire patterns will be vital to predicting future fire risks and developing effective mitigation strategies.

Addressing this gap, the broad goal of this thesis is to quantitatively assess how climate change can influence fire weather in Indian forests. The focus is on how shifts in key weather parameters—such as temperature, humidity, precipitation, and wind speed—may impact fire risk across different forest types under future climate scenarios. By examining these variables, the thesis seeks to not only highlight areas most vulnerable

to future fire events but also provide insight into the seasonal and spatial changes in fire risk. This understanding is critical for a more informed and targeted fire management strategies that account for the changing climate.

With this broad goal of the thesis outlined, the following section focuses on a comprehensive literature review of the state of the knowledge in the field of fire-climate relationship and probable changes expected in fire regimes in future. In this section, global efforts to understand fire-climate interactions are first discussed. Regional studies over India are examined to identify their limitations in capturing country-scale dynamics. The absence of high-resolution assessments addressing fire-climate interactions over Indian forests is highlighted. The limitations of coarse-resolution global studies in predicting future changes specific to Indian fire regimes are also discussed. Overall, the specific research gaps are highlighted, and the key objectives of this thesis are outlined.

Literature review

Climate change is leading to severe fire regimes in the global forests (Abatzoglou & Williams, 2016; Abram et al., n.d.; Canadell et al., n.d.; E. Lopez Gunn Caretta M.A. & and S. Supratid R. Morgan, 2016; Flannigan et al., 2006b; Gonzalez et al., 2010). The intensities and frequencies of fire events are likely to change in the future with the changing climate (E. Lopez Gunn Caretta M.A. & and S. Supratid R. Morgan, 2016; Krikken et al., n.d.; Liu et al., 2010, 2013; Moritz et al., 2012; Wotton et al., 2010). There is also evidence of the lengthening of fire seasons in the future (Flannigan et al., 2000; Wotton & Flannigan, 1993). Intergovernmental Panel on Climate Change Sixth Assessment Report (IPCC AR6) predicts an increase in the forest fire risk due to

increasing global temperature with high confidence and quantifies this increase to be ~30% under a 4-degree warmer climate compared to the pre-industrial level with medium confidence (John R Porter, 2022; Seneviratne et al., 2021). Despite the prevalence of forest fires, their implications on biodiversity, and evidence of rapidly changing climate patterns, very few studies explore a better understanding of the fire-climate dynamics in India.

In India, several studies have examined forest fire dynamics over a particular forest or state. Their regional focus and methodological gaps limit their use for a detailed and high-resolution analysis of fire-climate interactions on a national scale. For instance, (Jain et al., 2021) assessed changes in forest fire activity over central India from 2001 to 2020, associating increased fire incidents with warmer temperatures and multiple climate extremes. While insightful, this study is limited to central India. Similarly, (Ahmad & Goparaju, 2018) examined forest fire data using remote sensing, finding that the months of April and May and deciduous broadleaf forests have the highest fire incidences. However, this study is limited to Himachal Pradesh and Uttarakhand. Another study (Renard et al., 2012) developed a fire susceptibility model for the Western Ghats by using a framework with Moderate Resolution Imaging Spectroradiometer (MODIS) hotspots and a Maxent algorithm and using environmental factors like climate, topography, and vegetation to predict fire-prone areas. (Dhar et al., 2023) focused on fire occurrence, distribution, and risk mapping in Meghalaya using MODIS data, alongside factors like human settlement and forest health. Such regional studies ignore broader regional variability, which can address India's diverse forest types and does not provide insight into fire-climate dynamics at the national level.

Moreover, the existing studies do not assess fire behaviour in future climate change scenarios. Kale et al. (2017) analyzed fire regimes across India from 2003 to 2013, investigating links between fire occurrences and climatic factors like dry days, El Niño events, and maximum temperatures. Although this study addresses fire frequency across India's bio-geographic zones, its temporal focus on a limited decade restricts its applicability under future climate change scenario assessments. Ahmad and Goparaju (2019) conducted a national-scale assessment of long-term forest fire patterns in India, identifying hotspot districts and analyzing spatial and seasonal trends using fire event data over a nine-year period. They also examined fire-climate relationships in few hotspot regions of India using National Centers for Environmental Prediction's gridded reanalysis data and statistical measures like the Cramer V coefficient. Although the study provides a detailed understanding of local fire-climate associations, it is limited in scope both spatially and temporally. The analysis to assess fire-climate relationship was done on limited region rather than the entire country. Temporally, this study focusses on a defined fire season (February to June) thereby excluding significant fire activity occurring in other months, as indicated by MODIS active fire data. Moreover, the study does not assess potential changes in fire behaviour under future climate scenarios. Another recent study by Sagar et al. (2024) presents a comprehensive analysis of forest fire dynamics across India between 2005 and 2022. By integrating meteorological, ecological, and socio-environmental datasets, the study provides important insights into the spatial patterns of fire activity and its associations with factors such as NDVI, elevation, and disease outbreaks like anthrax. This approach highlights the complex ecology-biotic interface influencing fire behaviour. While the inclusion of multiple variables broadens the scope of

analysis, many of these parameters—such as vegetation indices, disease incidence, and population density—are inherently uncertain in future climate projections. The study's primary focus is on current fire distributions and it does not directly inform how these patterns may shift under changing climatic conditions. In addition to these studies, operational systems like the Forest Fire Alert System (FAST 3.0) developed by the Forest Survey of India have enhanced real-time monitoring of forest fire activity across the country. FAST 3.0 utilizes MODIS and VIIRS satellite data to identify active fire locations and disseminates alerts to forest departments and stakeholders, thereby contributing to fire response and preparedness. However, the system is primarily designed for real-time detection and short-term alerts. It does not incorporate climate information that can help anticipate fire hazard under changing climate conditions.

In addition to these studies that focus on current fire patterns and associated drivers, a few have attempted to explore the implications of climate change on Indian forests. Ravindranath et al. (2006) is a classic country-wide study that examined potential climate impacts on Indian forests. Regional model projections were used to project forest type shifts by 2085 under A2 and B2 climate change scenarios. Though this study addresses various aspects of climate-forest interactions in the country, outdated and low-resolution projections and lack of analysis on the forest fire aspect make this study inadequate to provide information on the fire-climate dynamics over India. A recent study (Bar et al., 2024) investigated fire regime dynamics in India, modelling burnt areas up to 2050 climate projections. Although this study applies CMIP6 data, the low resolution of their analysis cannot capture fire behaviour in India's diverse and fragmented forest landscapes. These studies provide insights into specific regions or aspects of fire-weather interactions but

are limited by geographic scope or resolution. This leaves an information gap for national-scale, high-resolution analysis essential for understanding forest fires across India's varied ecosystems.

Existing global-scale studies simulate fire weather over the entire world, including India, but they do not generally analyse the results over India. Potentially, we could gain some information on the fire danger over India by visually inspecting the global maps, but they would be inadequate for three reasons.

1. Coarse resolution: The typical 0.5-2° spatial resolution of the global studies is too coarse to resolve the fragmented forests of India.
2. Inconsistent results: The results of most of the global studies are widely divergent. For instance, (Gonzalez et al., 2010) aimed to identify areas vulnerable to climate-driven fire regime changes under IPCC scenarios globally. Pechony & Shindell (2010) also aimed to understand the relative impact of climate and human activity on global fire trends. Sun et al. (2019) examine the impacts of global warming on fire weather, aiming to identify regions most vulnerable to increased fire frequency and season length. These studies used climate model simulations for variables like temperature, precipitation, and wind under various warming scenarios. The results of all three studies indicate an overall homogenous increase in fire frequency in India in the future. Another study (Scholze et al., 2006) uses a dynamic global vegetation model and climate data from multiple models under various warming scenarios to quantify risks of climate-induced changes in forests, wildfire frequency, and freshwater availability during the 21st century. (Moritz et al., 2012) aim to project global fire activity changes over the 21st century and assess fire-

related risks to ecosystems and human well-being. Using a spatial statistical model integrating global fire datasets with environmental variables, it evaluates fire probability at a 0.5° resolution based on climate norms from 16 global climate models under the A2 emissions scenario, covering the periods 2010–2039 and 2070–2099. The common feature in the plots of these two studies is that they show fire probability to increase in the northwestern part and a decrease in the rest of India in future. Another recent study (Quilcaille et al., 2023) has projected FWI using CMIP6 climate simulations, providing a consistent global dataset for assessing fire danger under climate change. Though key indicators such as maximum FWI, extreme fire weather days, and fire season length were developed in the study, it predicts an overall decrease in the future fire weather danger over India. Such inconsistencies across the findings are likely because the fire models are not calibrated and evaluated with local observations. Moreover, recent global studies have advanced the understanding of fire-climate interactions at large scales. For example, Gincheva et al., (2024) demonstrated that interannual variability of global burned areas is predominantly driven by climatic factors, highlighting the strong influence of climate drivers in shaping fire regimes. However, the study remains at a global scale, and its findings, while valuable, lack region-specific evaluations for complex landscapes like India. Similarly, Turco et al., (2018) showed that anthropogenic warming would increase fire risk in Mediterranean Europe using non-stationary climate-fire models. Likewise, (Turco et al., 2023) reported that anthropogenic climate change has significantly exacerbated summer forest fires in California, using high-resolution regional

projections to isolate the effect of climate change. These studies emphasize the value of regionally tailored, high-resolution fire danger assessments, but similar efforts for India are still absent in the literature.

3. Lack of forest mask: Due to the lack of any forest masks in global studies, certain unrealistic results, such as high fire danger in the deserts of northwestern India, are observed. An example of this limitation can be observed in (Liu et al., 2010). This study investigates the impact of climate change on global wildfire potential using the Keetch-Byram Drought Index (KBDI) based on observed temperature and precipitation data alongside projections from general circulation models (GCMs) for the late 21st century. This study specifically points out that the high FWI calculated in northwest India is attributed to desert conditions with less rainfall and high temperatures. However, as no forests exist in this region, such results can be misleading when analysing forest fires.

These limitations highlight that to improve the state-of-science, it is necessary to simulate the fire weather at high granularity along with a forest mask using a well-calibrated and validated model to advance our understanding of fire-climate interactions in this understudied region.

Many factors like weather, vegetation, fuel loading, and local socioeconomic conditions drive forest fires. Among the important factors, climate change has a direct and the most significant impact on fire weather. “Fire weather” is the state of meteorological variables like temperature, relative humidity, precipitation, and wind over a forest ecosystem that affects the fuel loading and controls the start and spread of fires (Flannigan et al., 2005;

Kirchmeier-Young et al., 2019; Liu et al., 2013; Schroeder & Buck, 1970). FWI is a metric that systematically integrates the individual and combined effects of the meteorological variables to represent fire danger. Although various factors contribute to fire events, global agencies predominantly rely on fire weather conditions for predicting fire occurrence patterns (Amiro et al., 2004; Bedia et al., 2018; Carvalho et al., 2008; Dowdy et al., 2009). The Canadian Forest Fire Danger Rating System – Fire Weather Index (CFFDRS-FWI; (Stocks et al., 1989; Wagner, 1987; Wotton, 2009) is a widely used system for computing FWI. Originally developed in Canada, this system has evolved into a widely adopted tool for operational fire monitoring across the globe. (W. J. de Groot et al., n.d.; De Jong et al., 2016; Dimitrakopoulos et al., 2011; W. J. D. Groot et al., 2007; Karali et al., 2014; Matt Jolly et al., 2019; X. Tian et al., 2011; Wang et al., 2017). CFFDRS incorporates various meteorological parameters such as temperature, humidity, wind speed, and precipitation to calculate several fire danger indices (Stocks et al., 1989; Wagner, 1987). These indices provide a comprehensive understanding of the prevailing fuel and fire conditions, enabling fire management agencies to make informed decisions about fire prevention, preparedness, and suppression efforts (Stocks et al., 1989). Many countries have integrated CFFDRS into their operational fire monitoring systems, attesting to its effectiveness in diverse geographic and climatic contexts. The FWI is a component of CFFDRS, which is a meteorologically based index used to quantify the effects of weather variables on forest fuels and fire occurrence patterns (Stocks et al., 1989; Wagner, 1987).

Another application of CFFDRS-FWI is to be the basis of a Fire Danger Rating System (FDRS). In response to forest fires in India, the Forest Survey of India monitors and

reports on forest fires. However, unlike countries such as Australia, the UK, Indonesia etc. India lacks a country-wide FDRS for monitoring weather conditions that are conducive to forest fires. An FDRS is a tool in wildfire management which categorises fire danger on a scale ranging from "Low" to "Extreme," providing a quantitative measure of the risk and potential impact of fires (*Stocks et al., 1989; Vasilakos et al., 2007*). This systematic approach enables firefighting agencies to proactively allocate resources, plan responses, and implement preventive measures based on the anticipated fire danger level. Hence, developing a robust FDRS system is essential for informed decision-making and timely interventions associated with forest fires in the country. This thesis aims to take the first step toward developing a unified FDRS based on fire weather tailored to the diverse forest zones across India using the CFFDRS-FWI system. However, since the CFFDRS was initially developed for the Canadian climate, it is important to assess its performance and applicability in the diverse climatic conditions of India. The Indian subcontinent, with its unique monsoon-driven climate, presents a significantly different environment for fire dynamics. This evaluation can ensure that the system accurately reflects the fire-conducive weather patterns specific to India. Furthermore, integrating machine learning techniques could enhance the robustness of the FDRS system by optimising predictions through advanced algorithms (*Fathima Nuzla Ismail et al., 2024; Shah et al., 2022*). This combined approach of refining the CFFDRS for Indian conditions and leveraging machine learning holds promise for building a more effective FDRS for the country.

The effectiveness of the CFFDRS system relies heavily on accurate and timely meteorological inputs. To generate reliable fire weather indices, the system requires data

on key meteorological variables such as temperature, relative humidity, wind speed, and precipitation (Stocks et al., 1989; Wagner, 1987). These factors directly influence the fire weather conditions by determining fuel moisture and ignition potential. Hence, precise measurement and forecasting of the weather variables are important for accurate fire danger assessments. This becomes even more important in a country like India, where geographical climate and weather vary significantly across regions. Seasonal changes in weather further add to this variability. Considering these factors, high-resolution meteorological data integrated into frameworks like CFFDRS is vital for producing regionally and seasonally tailored fire danger predictions.

Global Circulation Models (GCMs) are extensively used to study the impacts of climate change on forest ecosystems and processes on a global scale (Edwards, 2000; Flato et al., 2013; Randall, 2007). These models simulate large-scale climatic shifts under various future emission scenarios, represented by Representative Concentration Pathways (RCPs) to reflect different radiative forcing levels (van Vuuren et al., 2011). While GCMs have contributed significantly to our understanding of global climate changes, their coarse spatial resolution, ranging from 100-600 km, is insufficient for conducting detailed regional impact assessments, especially for specific challenges like fire weather in India's diverse forest ecosystems (Mishra et al., 2020; Navarro-Racines et al., 2020; Trzaska & Schnarr, 2014). Accurate assessment of fire weather risks and developing appropriate strategies for forest regions in India require more granular climate data that can capture localised meteorological variations (Castro et al., 2005; Challinor et al., 2009; Flato et al., 2013). This necessity of high-resolution climate data makes it essential to downscale GCM outputs to higher spatial resolutions, enabling more precise fire weather modelling and

risk evaluations in these regions (Castro et al., 2005; Kidson & Thompson, 1998; Navarro-Racines et al., 2020; Trzaska & Schnarr, 2014).

The Community Earth System Model (CESMv1; (Hurrell et al., 2013), a part of the CMIP5 (Coupled Model Intercomparison Project 5) suite, has been widely employed for global and regional climate assessments. CESM's proven ability to simulate the distinct climatic patterns of the Indian subcontinent made it a suitable choice for this study (Choudhury et al., 2024; Thomas et al., 2023). Moreover, bias-corrected data from CESM, which improves the reliability of climate projections by correcting systematic model biases, is publicly available (Bruyère et al., 2014). These attributes ensured CESM was an optimal choice for generating high-resolution projections necessary for accurate fire weather prediction over India.

The literature review clearly highlights a research gap in the quantitative analysis of fire weather changes under a changing climate scenario, particularly in the context of India. While several countries have developed national-scale FDRS to monitor and predict fire-conducive weather, India still lacks a comprehensive FDRS to support fire-climate studies. This absence of a unified system limits the country's ability to assess and manage fire risks effectively. Moreover, the diverse climate and topographical variation in India demand high-resolution climate data for accurate regional climate impact studies. However, such fine-scale data are currently unavailable. This gap highlights the need for high-resolution downscaling to generate climate data capable of addressing these spatial complexities.

In light of the above-mentioned challenges, this thesis aims to bridge the knowledge gap by focusing on the following specific objectives:

- To understand spatial and temporal patterns of forest fire occurrences over Indian forests using satellite data.
- To develop a robust fire danger rating system for Indian forests based on the CFFDRS-FWI algorithm.
- To develop a high-resolution climate dataset by dynamically downscaling the CESMv1 climate projections for two-time slices, 2006-2015 (baseline) and 2091-2100 (end-century), to be used as meteorological drivers for CFFDRS-FWI.
- To quantify the changes in fire weather due to climate change by the end-century using the CFFDRS-FWI driven by the downscaled CESM projections.

In the subsequent chapters, the methods used to achieve these objectives are described in detail, followed by a discussion of the major findings from each section.

Chapter 2

Materials and methods

2.1 Study area

The study domain is India, an important and interesting region for studying forest fire-climate interactions. India is a vast South Asian country with diverse landscapes and a significant forest ecosystem. Almost 27% of India is covered by forests home to a wide range of species. These forests host a wide range of forest types, ranging from the Himalayas in the north to the tropical rainforests of the Western Ghats in the south. India also hosts six of the world's biodiversity hotspots, including the Western Ghats, Terai-duars savanna, Indo-Burma region, Sundaland, Himalayan region, and the Sunderbans. In this section, a comprehensive overview of the study area, focusing on the topographical features, forest cover, and climatic zones across the Indian mainland, is provided. One of the characteristic features of Indian forests is that they are heavily fragmented due to high human population density and intense land use practices. Fires occur throughout the year in most of the forest areas of India except for the peak monsoon period.

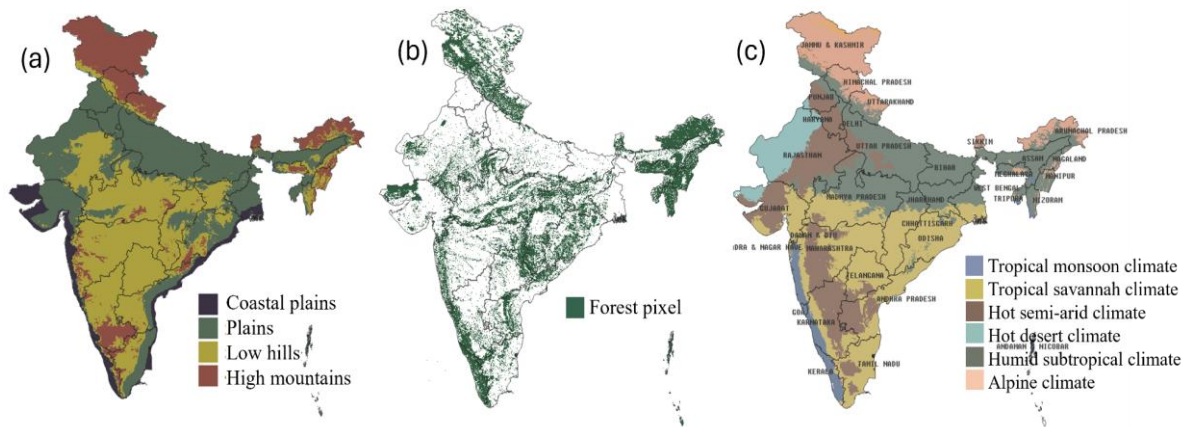


Figure 2.1: Map of the Indian mainland featuring (a) topographical classification, (b) forest cover and (c) climate zones.

2.1.1 Extents of Indian mainland:

The Indian mainland, geographically positioned between latitudes 8°4'N and 37°6'N and longitudes 68°7'E and 97°25'E, covers an area of approximately 3.287 million square kilometres. Bounded by the Arabian Sea to the west, the Bay of Bengal to the east, and the Indian Ocean to the south, India shares its borders with Pakistan, China, Nepal, Bhutan, Bangladesh, and Myanmar.

2.1.2 Topographical Features:

India's topography is characterised by diverse landforms (Figure 2.1 (a)). In the northernmost region, the Himalayan Mountain range stretches across the states of Jammu and Kashmir, Himachal Pradesh, Uttarakhand, Sikkim, and Arunachal Pradesh. South of this, India features an expansive alluvial Indo-Gangetic plain extending from Punjab in the northwest to West Bengal in the east. To the west of the plains lie the arid regions of Rajasthan and Gujarat, characterised by the vast Thar Desert. In the south, the Deccan plateau covers much of central and southern India, encompassing states such as Maharashtra, Karnataka, and Telangana. This elevated region is bordered by the Western Ghats to the west and the Eastern Ghats to the east. The Western Ghats run parallel to the western coast of India, stretching from Gujarat to Tamil Nadu. This biodiversity hotspot is renowned for its dense tropical rainforests. Additionally, an extensive coastal belt spanning over 7,500 km along the Arabian Sea and the Bay of Bengal features diverse coastal ecosystems and significant mangrove forests.

2.1.3 Forest cover of India:

According to the India State Forest Report (2021, 2022), the country's total forest cover (Figure 2.1 (b)) stands at 712,249 km², which is 21.67% of its total geographical area. Within this, very dense forests account for 3.04% of India's geographical area. These forests exhibit a tree canopy density greater than 70%, creating dense canopies that limit sunlight penetration to the forest floor. Moderately dense forests, featuring a canopy density ranging from 40% to 70%, comprise 9.33% of the total area. Open forests, accounting for 9.34% of India's geographical area, have a tree canopy density of about 10%, allowing more sunlight to reach the forest floor and supporting a greater diversity of undergrowth.

Geographically, Madhya Pradesh has the highest forest cover, followed by Arunachal Pradesh, Chhattisgarh, Odisha, and Maharashtra. However, it is noteworthy that the northeastern states of India exhibit the highest percentage of forest cover relative to their geographical area. Despite the eight northeastern states covering only 8% of the total geographical area, they collectively host 24% of the country's total forests. Overall, 64.67% of northeastern India is covered with forests. This region is crucial not only for its high forest cover but also for its unique socio-cultural practices and land-use patterns. One such practice prevalent in this region is shifting cultivation, also known as "jhum cultivation." This traditional agricultural practice involves clearing patches of forest land, cultivating crops for a short period, and then leaving the land fallow for years before reuse.

While integral to the livelihoods of many indigenous communities, shifting cultivation poses challenges in terms of fluctuations in forest cover and uncontrolled fire ignitions.

Altitude-wise, the distribution of forests in India varies significantly across different elevation ranges. Approximately 81% of India's forests are in the 0-1000 meters elevation range, including plains, Tarai, and valley regions. Low hills, ranging from 1000 to 2400 meters, host 10% of the forests, while the remaining 7% are situated in high mountainous regions at altitudes higher than 2400 meters.

2.1.4 Climate of India:

India has diverse climatic zones influenced by geographical location, topography, and seasonal monsoon winds. The Köppen climate classification system is commonly used to categorise India's climate into distinct zones based on temperature and precipitation patterns (Figure 2.1 (c)). The Western Ghats has a tropical monsoon climate (Am), characterised by hot and humid conditions with heavy rainfall during the southwest monsoon season (June-September). The Central and Southern Peninsular regions exhibit a tropical savanna climate (Aw), which is drier than the tropical monsoon climate. This class is characterised by dry winters. The Deccan Plateau and certain areas in the northwestern part of India experience a hot semi-arid climate (BSh). This climate type is characterised by hot to extremely hot summers and warm to cool winters, with limited precipitation. On the fringes of the hot semi-arid climate region in the northwest, the hot desert climate region stretches along the country's boundary that falls in the states of Rajasthan, Gujarat, and Punjab. The Indo-Gangetic plain and most of Northeast India are

characterised by a monsoon-influenced humid subtropical climate (Cwa), with hot and humid summers and cool to mild winters. The Himalayan region in the northern high-altitude zone experiences an alpine climate (ET) characterised by low temperatures. Here, temperatures remain below 10 degrees Celsius for most of the year, with at least one month warm enough to melt a substantial amount of annual snow cover.

To account for these variabilities in forest types and climate over India, the forest regions were divided into five classes in this study. The classification is described in Section 3.2.

2.2 Data

This section provides an overview of the datasets utilised in the study. A high-resolution Roy et al., (2015) land use land cover data, supplemented with Köppen climate information, was used to create a forest layer and delineate five forest zones of India. The Moderate Resolution Imaging Spectroradiometer (MODIS) active fire data (Giglio et al., 2003) was used to generate a daily gridded fire dataset, which was then utilised to study the patterns of fire occurrences across these forest zones. The ECMWF's ERA5-Land and ERA5 single-level (Muñoz-Sabater et al., 2021) meteorological reanalysis data was used as a forcing dataset for the CFFDRS system to develop the FDRS. To evaluate this FDRS, the gridded fire count data derived from the MODIS active fire data was again used. To force the CFFDRS-FWI for two-time slices, baseline (2006-2015) and end-century (2091-2100), high-resolution (10 km) gridded Downscaled CESM (DSCESM) data was developed. This was done by dynamically downscaling CESMv1 climate

projections under the RCP8.5 scenario using the Weather Research and Forecasting (WRF) model. A consistent bias in the DSCESM wind speed was observed when compared with reanalyses and ground observations. Consequently, a linear scaling approach was adopted to correct this bias with respect to Global Summary of the Day (GSOD) station observations.

Overall, various high-resolution datasets, including meteorological reanalysis, land use/land cover data, active fire data, station data, and climate projections, were used in this study. Below, the details of the sources, resolutions, and availability of each dataset used in our analysis are elaborately discussed.

2.2.1 High-resolution land use/ land cover (LULC) dataset

The LULC information from ‘Decadal Land Use and Land Cover Classifications across India, 1985, 1995, 2005’ (Roy et al., 2015) was used. This dataset provides LULC classification products for India at 100-meter resolution. Derived from Landsat 4 and 5 Thematic Mapper (TM), Enhanced Thematic Mapper Plus (ETM+), and Multispectral Scanner (MSS) data, as well as India Remote Sensing satellites (IRS) Resourcesat Linear Imaging Self-Scanning Sensor-1 or III (LISS-I, LISS-III) data, ground truth surveys, and visual interpretation, the dataset follows the International Geosphere-Biosphere Programme (IGBP) classification scheme. It comprises 19 classes. Seven forest classes from the 2005 map were aggregated to determine the forest cover layer. The Forest Survey of India (FSI) defines forest cover as any land with a tree canopy density greater

than 10% per hectare. Based on this definition, the following classes were aggregated to represent forest cover: Deciduous Broadleaf Forest, Mixed Forest, Shrublands, Mangrove Forest, Evergreen Broadleaf Forest, Deciduous Needleleaf Forest, and Evergreen Needleleaf Forest. In contrast, classes such as Cropland, Built-up Land, Barren Land, Fallow Land, Wasteland, Water Bodies, Aquaculture, Salt Pan, Grassland, Permanent Wetlands, Snow & Ice, and other Non-Forest Areas are excluded from the forest cover category.

This dataset is evaluated with ground truth data, resulting in an overall mapping accuracy of 94.46%. This data is freely available to download from the Oak Ridge National Laboratory Distributed Active Archive Center (ORNL-DAAC, https://daac.ornl.gov/VEGETATION/guides/Decadal_LULC_India.html)

2.2.2 Köppen climate data

The Köppen climate dataset (<https://datacatalog.worldbank.org/search/dataset/0042325>) provides a comprehensive picture of global climate patterns using the Köppen-Geiger climate classification system. It uses Climate Research Unit Time Series 2.1 (CRU TS 2.1) temperature data and Global Precipitation Climatology Centre Full Version 4 (GPCC Full v4) precipitation data. The baseline dataset is available from 1976 to 2000. The Köppen climate classification system divides climates into five main groups: A (tropical), B (dry), C (temperate), D (continental), and E (polar), each further subdivided based on specific criteria related to temperature and precipitation regimes. For instance, the tropical

climate group (Group A) includes subgroups such as Af (tropical rainforest), Am (tropical monsoon), and Aw (tropical savanna), distinguished by variations in precipitation distribution and temperature characteristics. In the context of India, specific Köppen climate classes hold particular relevance due to their influence on forests, agricultural practices, water resource management, and ecological dynamics. Notable Köppen climate classes observed in India include the tropical monsoon (Am), tropical savanna (Aw), subtropical (Cwa), and arid (BWh) climates.

2.2.3 MODIS active fire data

The simulated FWI was evaluated, and the modified fire danger rating thresholds were developed using fire frequency information. For that, the MODIS active fire data (Giglio et al., 2003) was used to create a daily fire frequency dataset at 25 km resolution.

MODIS, onboard the Aqua and Terra satellites, detects thermal anomalies and active fires at a 1 km resolution during satellite overpasses under relatively cloud-free conditions. The instrument captures data in both the daytime and nighttime, providing comprehensive coverage and high temporal resolution. MODIS active fire detection is based on thermal infrared bands, which allow for identifying fire pixels through their higher radiative energy than the surrounding area. Each detected fire pixel is assigned to a confidence level (low, nominal, or high) based on the detection algorithm, aiding in filtering false positives.

The MODIS active fire data includes detailed attributes for each fire, such as geographic coordinates, detection time, brightness temperature, and the estimated fire radiative power (FRP), which is an indicator of fire intensity. This dataset is publicly accessible via NASA's Fire Information for Resource Management System (FIRMS) website (<https://firms.modaps.eosdis.nasa.gov/>). FIRMS provides near real-time active fire data and historical fire information in CSV, KML, and SHP formats for 24-hour, 48-hour, and 7-day periods, supporting a wide range of applications, including wildfire monitoring, resource management, climate change studies, and validation of fire models. FIRMS integrates MODIS active fire detections with other satellite data and tools to enhance the usability and accuracy of fire monitoring efforts.

Giglio et al. (2003) reported improvements in the performance of the Collection 6 active fire detection algorithm compared to Collection 5. Collection 6 showed reduced omission errors over large fires and lower false alarm rates in tropical ecosystems. This is a well-evaluated dataset to detect fires, and the version used in this study has been shown to have low error margins and fewer false alarms over South Asia. Hence, this dataset was selected for this study.

2.2.4 ERA5 reanalysis

While developing the FDRS, ECMWF's ERA5-Land and ERA5 single-level reanalysis datasets (Muñoz-Sabater et al., 2021) were used as the meteorological input to the CFFDRS-FWI framework. These datasets have demonstrated reliable performance in India and are widely used in various applications (Mahto & Mishra, 2019), making them

suitable for computing fire weather indices in India. These datasets are available from 1981 to the present at various temporal resolutions and can be accessed through the Copernicus Climate Change Service portal (<https://cds.climate.copernicus.eu/cdsapp#!/search?type=dataset>).

The ERA5 dataset, produced by the European Centre for Medium-Range Weather Forecasts (ECMWF), provides a comprehensive range of meteorological variables essential for diverse applications. The ERA5 datasets are accessible through the Copernicus Climate Change Service (C3S) Climate Data Store (CDS), available in multiple formats with extensive documentation and user guides. This enables their use in both research and operational settings. Key variables important for such fire-related studies include daily maximum, minimum, and mean temperatures at 2 meters, daily average and minimum relative humidity values, average wind speeds, and 24-hour accumulated precipitation, which are included in this dataset. For the CFFDRS-FWI, ERA5 data was used to derive daily maximum 2m temperatures and average or minimum relative humidity from the ERA5 single-level reanalysis dataset at a 0.25° resolution. Additionally, average wind speeds were calculated from the same dataset, while daily 24-hour accumulated precipitation was obtained from the ERA5-Land dataset at a 0.1° resolution and regridded to 0.25° resolution for consistency.

ERA5's high resolution allows for detailed and accurate representations of meteorological variables. Its long-term data availability supports extensive climate studies and trend

analyses. Continuous assimilation of observational data ensures high accuracy and reliability, making ERA5 a versatile tool suitable for such calibration applications.

2.2.5 CESMv1 climate projections

The climate data which was downscaled in this study is the output from the Community Earth System Model version 1 (CESM1; *Hurrell et al., 2013*), a coupled global climate model (GCM) developed by the National Center for Atmospheric Research (NCAR). This model is part of the phase 5 of the Coupled Model Intercomparison Project (CMIP5), which supported the Intergovernmental Panel on Climate Change's Fifth Assessment Report (IPCC AR5). The CESM1 dataset provides a horizontal resolution of approximately 1° and is available at six-hourly intervals, interpolated to 26 pressure levels. This high-resolution data supports detailed regional downscaling efforts, such as those performed using the WRF model in this study. The dataset encompasses the variables necessary for initial and boundary conditions for simulations with regional models such as the WRF model and the Model for Prediction Across Scales (MPAS).

The output from the CESM version 1 (*Hurrell et al., 2013*) was bias-corrected using ECMWF's ERA-Interim Global reanalysis (*Berrisford et al., 2011*) by Computational and Information Systems Laboratory (CISL), National Center for Atmospheric Research (NCAR) (*Bruyère et al., 2014*). The regional scale biases in the CESM1 output were removed by mean state correction, which involves replacing the CESM annual signal with the ERA-Interim annual signal and retaining the GCM simulated perturbations. As this

dataset lacks the GCM output biases that could significantly affect the regional scale processes after downscaling, it is an appropriate choice to be dynamically downscaled. This bias correction was applied to the historic (1951-2005) and 3 RCP future scenarios, RCP4.5, RCP6.0, and RCP8.5, for 2006-2100 of the CESM outputs. In our study, the extreme case scenario RCP8.5 was downscaled and analysed. This scenario assumes an addition of 8.5 W/m^2 of Radiative forcing due to emissions by 2100. The results obtained by this assumption are consistent with the 2005-2020 CO_2 emissions (Schwalm et al., 2020) and hence provide better future climate estimates than the other RCP scenarios. Moreover, we observed that over the Indian region, RCP8.5 estimates of the current monthly mean temperature and precipitation provide a better match representation when compared with observations during the period 2005-2015. A comparison was carried out between CESM simulations under RCP2.6, RCP4.5, and RCP8.5 scenarios and observational datasets for the years 2005 and 2015 (Figure 2.2). In this figure, the top panel shows the monthly accumulated precipitation from CESM and Global Precipitation Climatology Project (GPCP), the middle panel shows maximum temperature from CESM and ERA5, and the lower panel shows minimum temperature from CESM and ERA5. All variables were averaged over the Indian region. The Pearson's correlation coefficient (r) and Root Mean Square Error (RMSE) of the RCP8.5 2m-temperature with ERA5 reanalyses are 0.98 and 3.942°C , respectively. The highest r of 0.92 and the lowest RMSE of 31.6 mm for RCP8.5 were observed when the monthly accumulated precipitation was compared with the GPCP observations.

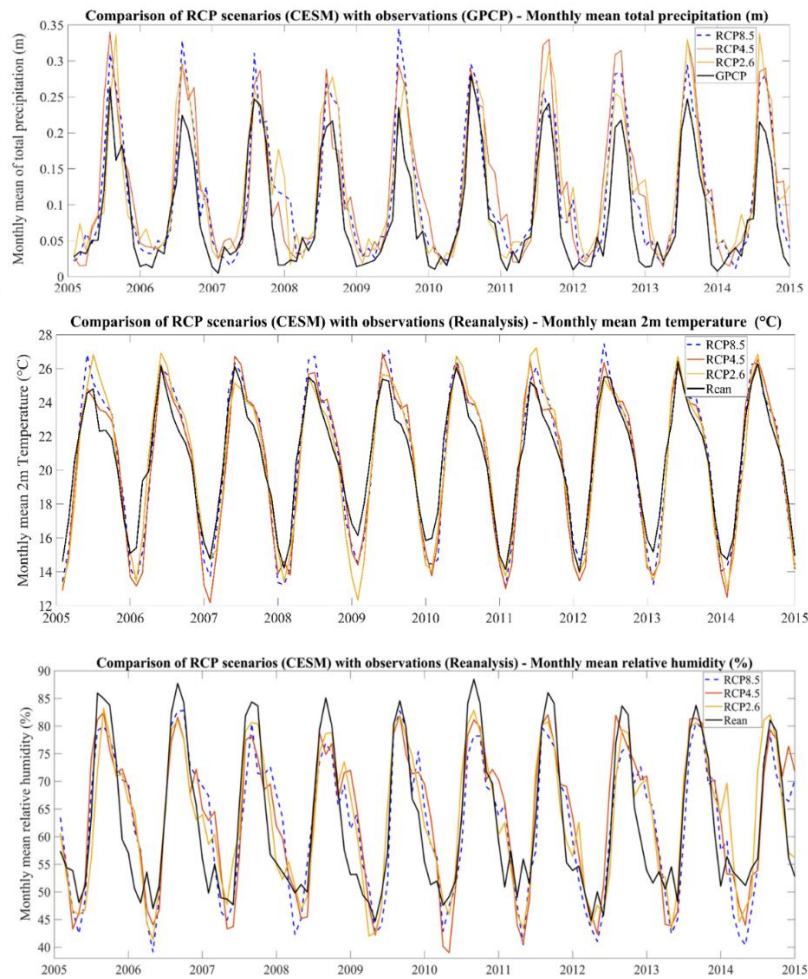


Figure 2.2: Comparison of CESM precipitation and temperatures under RCP 2.6, RCP 4.5, and RCP 8.5 with observational (GPCP) and reanalysis (ERA5) datasets for the years 2005 and 2015

The variables in the GCM output required for the initial and boundary conditions of RCMs like WRF are provided in 6-hourly intermediate files by the National Centre for Atmospheric Research (NCAR) CESM Global bias-corrected CMIP5 Output to Support WRF/MPAS Research dataset, which is available in NCAR CISL's Research Data Archive (Monaghan et al., 2014). This dataset is useful for conducting dynamic

downscaling to enable accurate assessments of regional climate dynamics and future projections, facilitating informed decision-making in various climate-related studies and applications.

The CESM1 data, with its extensive temporal coverage and rigorous bias correction, provides a robust foundation for evaluating future climate impacts on forest fire risk in India. This comprehensive dataset ensures that the fire danger assessments are based on high-quality, consistent, and comprehensive meteorological inputs, thereby increasing the reliability and accuracy of fire danger predictions.

2.2.6 DSCESM downscaled climate projections

For forcing the CFFDRS-FWI for the baseline and end-century, the high-resolution (10 km) gridded Downscaled CESM (DSCESM) data (Barik et al., 2021) was used. This dataset is archived with the World Data Centre for Climate, which can be accessed from (https://doi.org/10.26050/WDCC/WRF10km_wbc_C5_forc_oIndia and https://doi.org/10.26050/WDCC/WRF10_wbc_C5_forcIndia_MC_V2). This dataset was developed by dynamically downscaling the bias-corrected Community Earth System Model (CESMv1) climate projection under emission scenario RCP8.5 using the Weather Research and Forecasting (WRF) model over India. The performance of CESMv1 for the baseline period was extensively analysed, and it was found to work well in India. This dataset consists of baseline (2006-2015), mid-century (2041-2050) and end-century (2091-2100) climate projections for the RCP8.5 scenario over India at 10 km spatial

resolution. The dataset covers the Indian region with a 369 x 369 grid, but the area outside India is masked out. The data is available at three temporal resolutions: Daily time series (TS), Monthly TS, and Monthly Climatology. The data contains ten meteorological variables and information on latitude, longitude, and time. The dataset has been structured into a total of 90 files (10 variables x 3 temporal resolutions x 3 periods) packed in self-explanatory and universally accepted NetCDF format. The daily, monthly, and monthly climatology files contain 369 x 369 x 365, 369 x 369 x 12, and 369 x 369 x 30 data points, respectively. This entire dataset is about 120 GB in size. Details about all files are available in the dataset's metadata information. These datasets were evaluated over the baseline 10-year period against the reanalysis datasets and station observations. The evaluation of the dataset is described in detail in chapter 4 of this thesis. It can also be observed that the downscaled product performed better than the raw GCM output. The downscaled dataset includes all atmospheric variables that are relevant for real-world applications in agriculture, forestry, and water resource management, such as 2m air temperature, precipitation, relative humidity, wind, radiation, and heat fluxes. If CESM RCP8.5 is considered to be a reasonable future scenario, this high-resolution dataset is expected to be of value for a wide range of purposes including understanding regional climate change, climate change impact assessment, and developing adaptation and mitigation strategies over India.

2.2.7 GSOD station observations

To evaluate the DSCESM and for bias-correction of DSCESM wind speed, the Global Summary of the Day (GSOD) dataset was used. This dataset is provided by the National Centers for Environmental Information. This dataset comprises daily 24-hour averages computed from hourly station observations of over 9000 stations across the globe. This dataset can be accessed from <https://www.ncei.noaa.gov/access/search/data-search/global-summary-of-the-day>. There are 60 GSOD stations within India that have complete daily averages of variables relevant to our study, such as temperature, precipitation, and wind speed during the 2006-2015 period. These station data were used to evaluate DSCESM variables. The relative humidity was calculated from the dew point temperature. The DSCESM daily values of the grid corresponding to the GSOD station location were extracted and compared statistically with the observations. The coarse-resolution raw CESMv1 data was also compared to the station observations to determine whether downscaling was beneficial. For bias correction, DSCESM wind speed was corrected using a linear scaling approach with respect to GSOD station wind speed observations. The details of the bias correction are in section 5.6.

2.3 Models

In this section, two models used in this study are described. The CFFDRS-FWI was used to simulate fire weather in the study region. The WRF-ARW model was used to dynamically downscale the climate scenario data to a finer resolution suitable for this study. This section elaborates on the structure and sub-modules of these models in detail.

2.3.1 Canadian Forest Fire Danger Rating System - Fire Weather Index

The CFFDRS-FWI (Bedia et al., 2015; Wagner, 1987; Figure 2.3) is a meteorologically based numerical index used by researchers worldwide to account for the effects of weather variables on forest fuels and fires and study fire severity patterns. It consists of three moisture codes, namely the Fine Fuel Moisture Code (FFMC), the Duff Moisture Code (DMC), and the Drought Code (DC). These codes numerically quantify the moisture content at 0-1, 2-4-, and 4-8-inches depths under rainfall and drying phases. These components collectively reflect the moisture content of various fuel layers within the forest environment, including surface litter, shallow organic layers, and deeper soil depths.

The FFMC quantifies the moisture content of surface fuels, such as litter and grass, and is primarily influenced by recent weather conditions, including temperature, humidity, and precipitation. The DMC assesses moisture levels in the organic layer beneath the forest floor. At the same time, the DC represents the deeper soil moisture content and integrates longer-term weather patterns and climatic influences.

In addition to these core components, the CFFDRS FWI model incorporates secondary indices, including the Initial Spread Index (ISI) and the Buildup Index (BUI), which provide further insights into fire ignition and growth potential. The ISI combines the effect of wind speed and top layer moisture from FFMC to compute the rate of spread of fire. Meanwhile, the BUI reflects the cumulative effect of drying conditions on deeper organic layers and serves as a proxy for fire intensity and resistance to control. FWI is calculated from ISI and BUI.

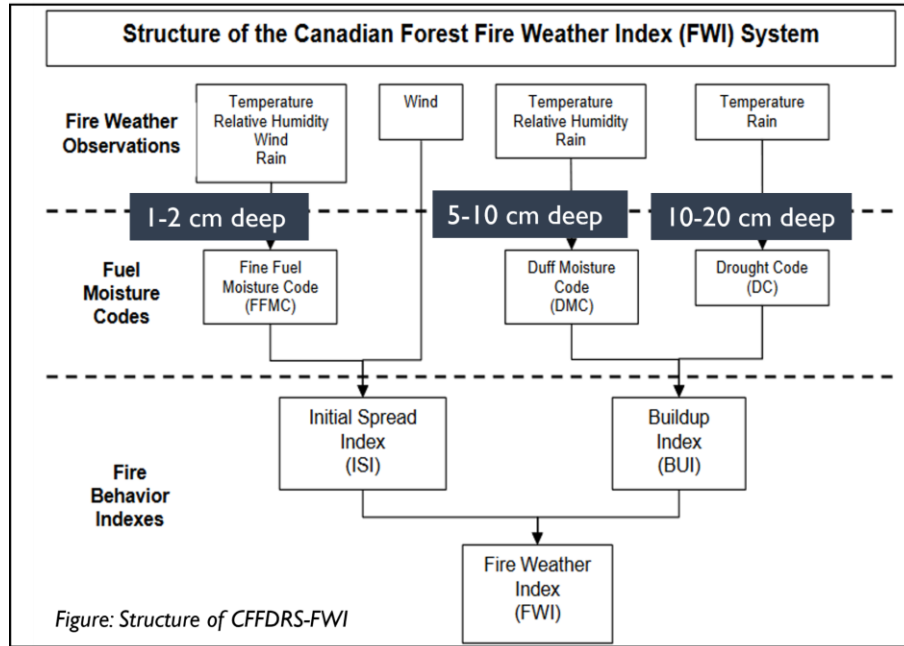


Figure 2.3: Structure of CFFDRS-FWI

2.3.2 WRF-ARW mesoscale atmospheric model

The regional climate model (RCM) used for dynamical downscaling in this study is the WRF model (Version 3.8.1) (et al. Skamarock WC, 2008). WRF is a state-of-the-art mesoscale model that has been widely used for regional climate downscaling (Prathipati et al., 2021; Wang et al., 2021). This model integrates fully compressible, Euler non-hydrostatic equations and includes full Coriolis and curvature terms. The model uses a terrain-following hydrostatic pressure vertical coordinate system with vertical grid stretching permitted. The horizontal grid is the Arakawa C-grid staggering, where velocities are computed at the centre of each grid and the thermodynamic variables at the intersections of grid cells. The numerical discretisation uses a 2nd or 3rd-order Runge-Kutta scheme for time integration and 2nd to 6th-order horizontal advection schemes on the C-grid. It also provides multiple nesting options. Key features of WRF-ARW include

its non-hydrostatic, fully compressible equations, allowing for accurate representation of convective storms, boundary layer processes, and complex terrain interactions from the perspective of dynamical downscaling. WRF is a popular tool for developing high-resolution outputs from coarser GCM outputs that capture fine-scale atmospheric processes. The model supports multiple nested domains, enabling users to focus on specific regions of interest while maintaining smooth interactions between domains.

Additionally, WRF includes physics parameterisations for processes like microphysics, radiation, and surface exchanges, and it is customisable to suit applications, research, and operational needs. From the perspective of dynamical downscaling, WRF-ARW plays a pivotal role in refining coarse-resolution GCM outputs, providing localised climate information essential for climate impact assessments, regional climate modelling, and weather forecasting. By leveraging its advanced capabilities, WRF-ARW enhances the understanding of regional climate variability and change, aiding in the development of targeted adaptation and mitigation strategies in response to evolving climate conditions.

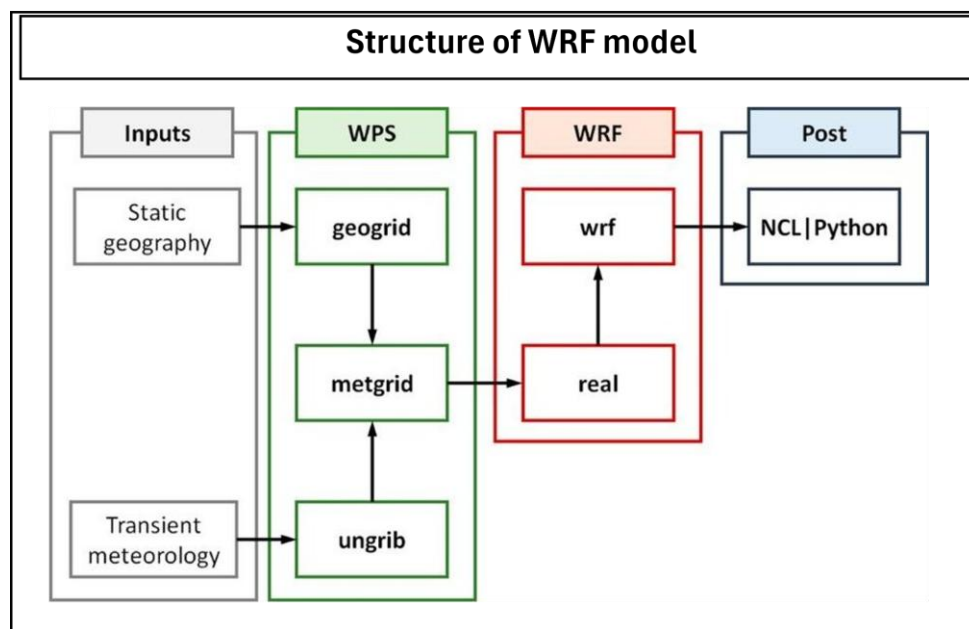


Figure 2.4: Structure of the WRF model

The WRF model comprises several components working together to simulate atmospheric processes at various scales with high accuracy (Figure 2.4). One key component is the WRF Preprocessing System (WPS), which includes programs like geogrid, ungrib, and metgrid.

The geogrid program defines the computational domain, specifying its geographic extent, horizontal grid resolution, and map projection. It prepares the static geographical and topographical datasets required for the simulation. Ungrib, or Universal Gridded Data Translator, is responsible for extracting meteorological fields from input datasets in various formats (e.g., GRIB, netCDF) and interpolating them to the model's grid. These fields typically include temperature, humidity, wind, and pressure, sourced from global reanalysis datasets or GCM outputs, as in this case. Metgrid, the final component in the preprocessing chain, interpolates the meteorological fields obtained by ungrib to the operating computational grid. It also computes necessary derivatives of the fields, such as horizontal and vertical gradients, to facilitate the numerical integration in the WRF model.

Once the preprocessing is complete, the WRF model, specifically the Advanced Research WRF (WRF-ARW) core—solves the governing equations of atmospheric motion using a finite-difference numerical scheme. The model employs a split-explicit time integration scheme to handle different physical processes separately, such as dynamics, radiation, and microphysics. This approach ensures efficient computation and includes sophisticated physics parameterisations tailored to specific atmospheric phenomena.

Overall, the WRF model, with its preprocessing system and advanced numerical core, provides a framework for simulating and studying meteorological phenomena at regional scales. Hence, it was chosen for the downscaling application in this study.

2.4 General Methodology

In this section, the methodology of this study has been outlined in brief. It is also illustrated in Figure 2.5.

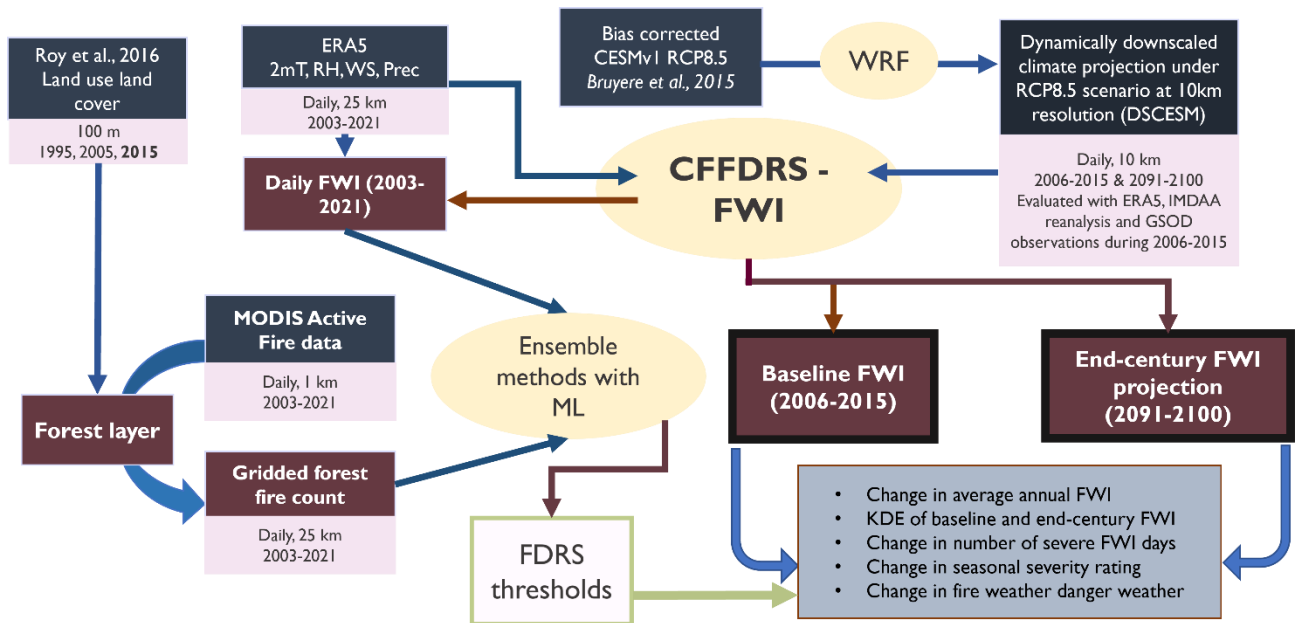


Figure 2.5: Graphical illustration of the overall methodology used in this study

First, to analyse the spatial and temporal patterns of fire events in India, a gridded fire count dataset from the MODIS active fire data (Giglio et al., 2003) was created at 25km resolution detected over the period 2003-2021. This gridded data is the total count of daily

active fires occurring within the 25km grid. Next, to eliminate the non-forest/ agricultural fires, a forest layer in the analysis was introduced. Ten different forest classes from a high-resolution land use land cover dataset (Roy et al., 2015) were clubbed to classify forest pixels at 100m. Then, the percentage of forest pixels within every 25 km grid was computed, and all the fires occurring in pixels where the forest percentage was less than 20% were filtered out. Finally, this forest area was classified into five major forest-climate zones by combining Koppen's classification of climatic zones over India and the (Roy et al., 2015) forest class information. The spatial pattern and the seasonal variations of the fire count dataset was analysed distinctly over the five forest-climate zones.

To test the capability of CFFDRS to operate in Indian weather, the ideal behaviour of the system was compared to realistic behaviour with Indian meteorological conditions using ERA5 reanalysis as the input at 25km resolution. This testing was carried out for the period of 2003-2021 on a daily temporal scale. The spin-up period required for the system to produce stable values of intermediate indices and FWI was also determined. The simulated FWI was tested against a gridded fire count dataset. The evaluation included non-parametric statistical tests and Epanechnikov kernel density estimations (KDE) between FWIs associated with fire and no-fire events. These approaches evaluated the statistical association and distinct differences in FWI spread during fire events. This rendered FWI an effective metric for identifying conditions conducive to fire occurrence.

Then, an FDRS was developed by classifying the FWI values into five classes: Low, Medium, High, Very high, and Extreme. For this, an ensemble of four methods were used,

including the fire count information and FWI data, to characterise limiting FWI thresholds for each danger class. These methods are based on percentiles of FWI, percentage of fire events, logistic regression and K-means clustering. To reduce the subjective decisions involved in these methods, machine learning techniques like receiver operating characteristic curves and hierarchical clustering techniques were integrated.

The next step was to develop downscaled climate projections. A 10 km gridded dataset was developed by dynamically downscaling the bias-corrected Community Earth System Model (CESMv1) climate projections under the RCP8.5 scenario using the WRF model. The downscaled CESM dataset (DSCESM) is archived in the World Data Center for Climate (WDCC) portal at three temporal resolutions (daily, monthly, and monthly climatology) for Baseline (2006-2015), Mid-Century (2041-2050) and End-Century (2091-2100) periods (Barik et al., 2021). The DSCESM variables were evaluated against ERA5 and IMDAA reanalysis data and Global State of the Day (GSOD) station observations for the period 2006-2015. The baseline and end-century DSCESM were used as an input to CFFDRS-FWI to compute the baseline and end-century FWI at a spatial resolution of 10km x 10km. A consistent bias was observed in the DSCESM wind speed compared to reanalyses and ground observations. Hence, a linear scaling approach (Li et al., 2019) was adopted to correct this bias with respect to Global Summary of the Day (GSOD) observations.

The changes expected in end-century FWI were estimated by comparing various aspects with the baseline FWI. First, the climatological change in FWI was computed by subtracting the baseline 10-year average from the end-century 10-year average of FWI.

Then, the major contributor variable causing the climatological change in FWI was identified by four sensitivity experiments in which we simulated end-century FWI by using end-century values of one variable and retaining the baseline values of other variables. Then, the KDE of daily FWI within a particular FWI zone were computed for both periods. From this, the shift in average daily FWI for each zone was calculated using the bootstrap confidence interval for the mean parameter at a $p < 0.05$. The number of days exceeding a certain threshold like Medium, High, and Very High fire dangers for both periods was also computed.

SSR, an additional seasonal component of the FWI system, is a numeric measure of the difficulty of controlling fires. A value of 90th percentile SSR was considered in the baseline scenario as a threshold beyond which the fire potential becomes severe. This metric was used to study the seasonal pattern of fire weather severity and how it may change due to changing climate. Lastly, a 'fire weather danger season' was defined as a period in which the daily climatology values are beyond the Medium threshold. The future fire weather danger season was then compared to the baseline.

These methods have been elaborated in detail, and the results have been reported and discussed in the upcoming chapters.

Chapter 3

Spatial and temporal patterns of forest fires in India

3.1 Introduction

India's diverse climate and ecological characteristics result in varying fire regimes across different parts of the country. To account for these differences, a zonal approach was adopted to understand the forest fire and weather dynamics better. Hence, India was divided into five distinct forest zones, each with unique ecological traits and fire patterns. This section provides a comprehensive overview of these forest zones, setting the foundation for subsequent zone-specific analyses of spatial and temporal fire occurrence and fire-weather patterns.

Next, it was important to exclude non-forest fires. This was necessary because the MODIS satellite captures agricultural fires, particularly prevalent in northwestern India, in addition to the forest fires. Filtering out non-forest fires ensures that the analysis focuses solely on forest fires. This section also explains the methodology adopted to perform this filtering.

The following subsection studies the geographic distribution of forest fires across different zones in India. By mapping the filtered fire occurrences, regions with higher fire frequencies were identified, and the spatial variability of fire events in the country and across zones were analyzed. Studying the temporal patterns of forest fires was essential to understanding the prevalent variability in fire seasons across zones.

Overall, this chapter lays the foundation for subsequent fire-weather modelling efforts by providing detailed background on forest fire patterns in India.

3.2 Forest zones of India

Indian forests have diverse species types and climates, as discussed in sections 2.1.3 and 2.1.4. So, the danger rating system must be developed, and climate impacts must be analysed considering these diversities. To cater to that, high-resolution LULC data was first used to segregate the forest pixels. First, the country was divided into 25 x 25 km pixels and the pixels with more than 20% of their area were classified as forest pixels (Figure 3.1. (a)).

Then, these forest pixels were classified into five zones. This classification was done by combining Koppen's classification of climatic zones over India and the vegetation types in the forest pixels (Table 3.1). The five zones are

- (1) HIM: the cold, dry Himalayan mountainous region covered by alpine and subtropical pine forests,
- (2) NE: the warm, humid North-east with wet evergreen and deciduous forests,
- (3) CEN: the hot, dry Central India with mixed deciduous and tropical thorn forests,
- (4) DEC: the hot, dry Deccan thorn forest and
- (5) WG: the warm, humid Western Ghats with semi-evergreen forests.

To smoothen the sharp edges of these zones, the shapefiles of these zones were created using the ArcGIS software (Figure 3.1(b)). As the range of fire occurrences and FWI computed varied across these zones, the FDRS and associated thresholds were developed separately for each zone. The CFFDRS-FWI model was also evaluated, and the future fire projections were analysed separately for each zone.

Table 3.1 Forest zones of India

FWI zones	Aggregated forest types	Climate zones
Himalayan (HIM)	Dry and moist temperate, alpine, subtropical pine forests	Montane
North East (NE)	Tropical wet evergreen and deciduous	Humid subtropical
Central deciduous (CEN)	Dry and moist deciduous forests	Tropical dry
Deccan thorn (DEC)	Tropical thorn forests	Semi-arid
Western Ghats (WG)	Wet and semi evergreen forests	Tropical wet

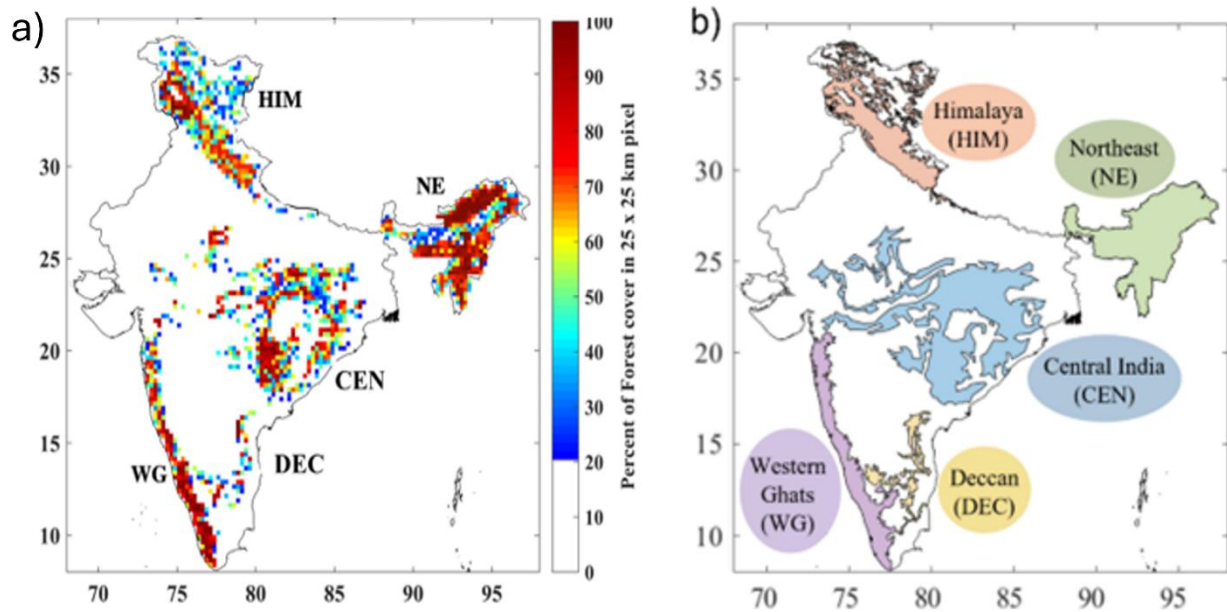


Figure 3.1: (a) Forest cover percentages and (b) Shapefiles of the classified forest zones of India

After identifying the zones, the next step was to understand the variability in fire occurrence patterns within these zones. Before proceeding, non-forest fires detected by MODIS were removed to retain only the forest fires.

3.3 Removal of non-forest fires

The active forest fire data includes forest and non-forest/ agricultural fires. This data was used for three purposes in this study. Firstly, it was used to understand the spatial and temporal pattern of forest fire occurrences in Indian forest zones. Secondly, it was used to evaluate the simulated FWI from CFFDRS using statistical methods. Third, it was used to calibrate the fire danger rating thresholds for each zone. For all these purposes, the spatial and temporal information in the active fire data was converted into a gridded daily fire count dataset at 25 km resolution. For this, the MODIS fire data from January 1, 2003, to December 31, 2021, was utilised, and only those fires occurring in the forest zones of India were retrieved. This step is important as it removes all the intentional agricultural fires prevalent in the northwestern part of India. Subsequently, these filtered forest fire data were counted into a daily count of fires in a grid with a 25 km resolution matching the resolution of ERA5 weather data and the simulated FWI information. Additionally, zone-wise daily and monthly aggregated climatological fire datasets were computed from this daily fire frequency information.

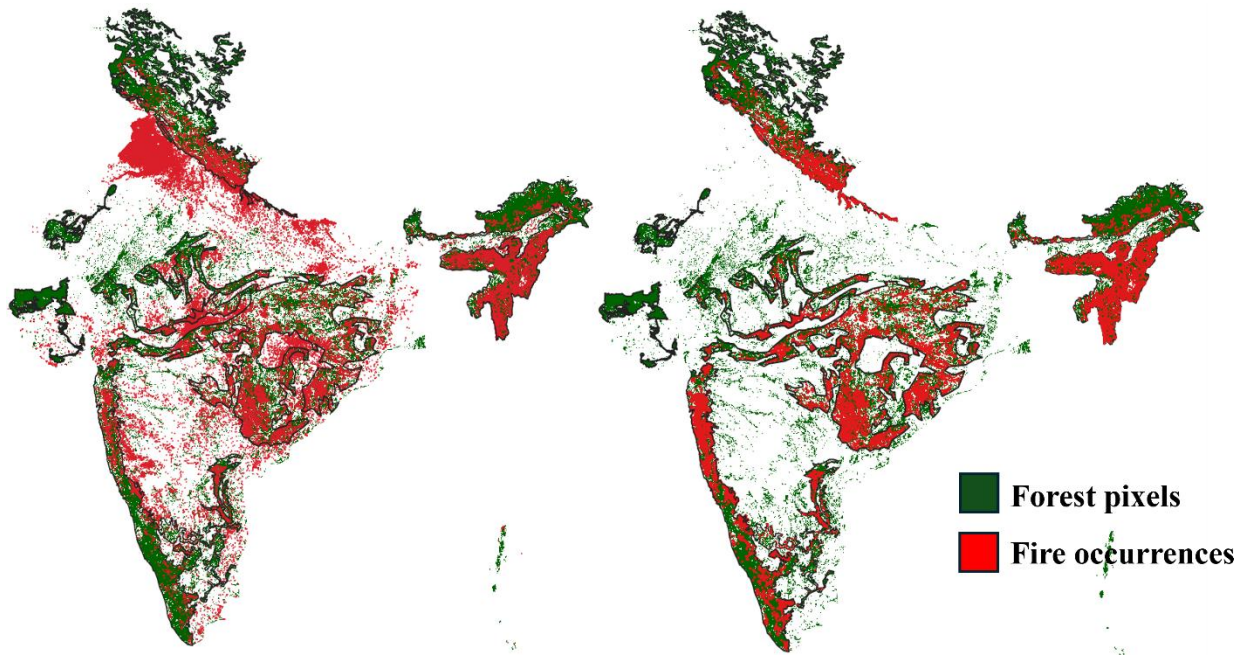


Figure 3.2: Exclusion of non-forest fires

This fire count data was used to analyse the spatial and temporal patterns of forest fires occurring in different forest zones of India.

3.4 Fire occurrence patterns in forest zones of India

In this section, the spatial and temporal variations of forest fire occurrences in each zone are discussed. Spatial analysis helps identify the geographic distribution and regional hotspots of fire occurrences within and across zones. For the spatial fire map (Figure 3.3), the number of fires occurring in each 25 km grid over the forest region from 2003 to 2021 was counted. Then, these values were divided by the number of years to calculate the average annual fire count per grid.

In the temporal analysis, all fires occurring within each zone were aggregated for each year. These values were then averaged monthly for the seasonal analysis of fire count totals in each zone. Annual total fire counts were also calculated for each zone to assess the existence of a trend in fire occurrences in the period 2003-2021.

3.4.1 Spatial Signature of fire events in forest zones

The spatial variability of fire occurrences across Indian forests is uneven, with higher fire activity observed in specific regions such as the NE, northern WG, and southern CEN zones (Figure 3.3). The NE zone experiences the highest annual fire counts, with concentrations up to 250 fires per year in some grids. This high-fire activity can be attributed to the prevalence of shifting cultivation practices, also known as *jhum*, which involve deliberate burning for agricultural purposes (Heinimann et al., 2017). The high fire frequency in this region is also because the forests are subject to frequent ignitions due to both anthropogenic activities and the regional climate. WG is the zone with the second-highest number of fires. This zone, particularly the northern part, has annual counts ranging between 50 to 100. The semi-evergreen and semi-deciduous forests are subjected to periodic fires, which are often started by human activities such as land clearing and accidental ignitions (Renard et al., 2012). The combination of steep terrain and dry conditions during pre-monsoon contributes to the start and spread of fires. The southern part of Central India, encompassing forest areas of Maharashtra and Andhra Pradesh states, also exhibits high fire activity. These areas, dominated by mixed deciduous and tropical thorn forests, experience annual fire counts ranging from 50 to 150. The hot and dry weather conditions that prevail during most of the pre-summer and

summer periods in this part of the zone help dry biomass accumulate. This contributes to the high fire frequency in this part.

Overall, these patterns highlight the spatial variability of fire occurrences across different forest zones in India. Because of these variabilities, all the analyses were done by treating each zone separately in this study. Differences in climate, forest types, and anthropogenic factors influence fire patterns considerably. The most effective way to account for these variabilities in our study is to model them independently, allowing for more accurate and region-specific fire risk assessments.

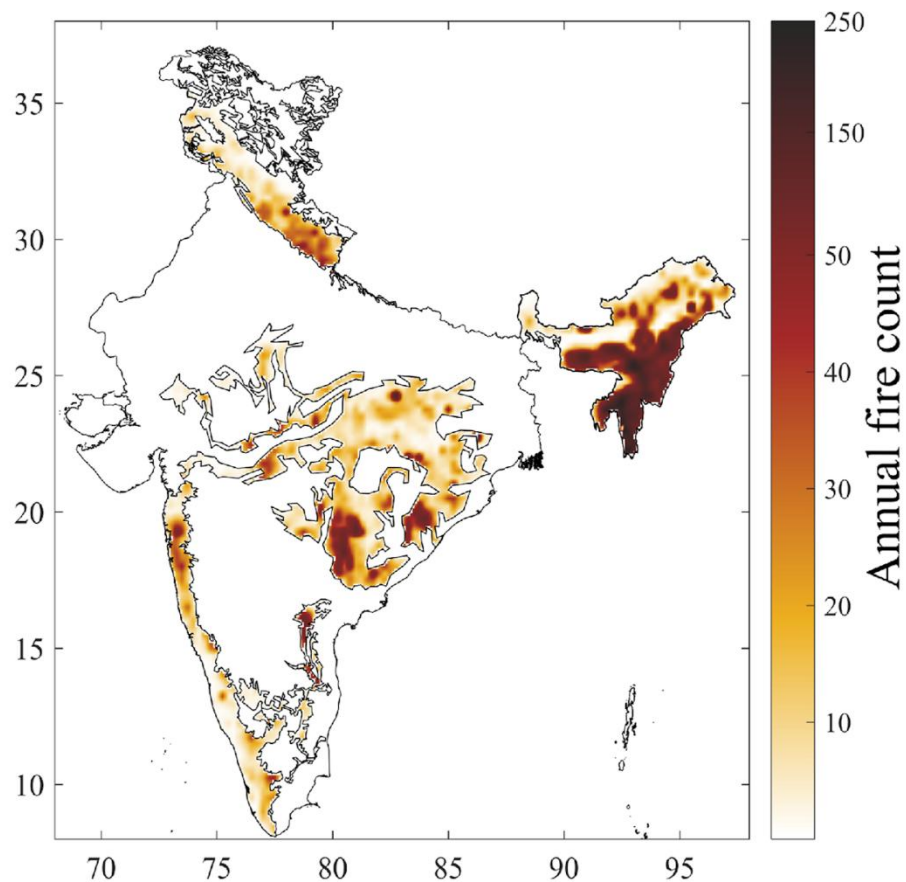


Figure 3.3: Annual fire count data in a 25km grid over forest zones of India

3.4.2 Temporal signatures of fire events in forest zones

This section looks at the temporal patterns of fire occurrences by analyzing two aspects. First, the seasonal variation will be used to identify the months with high fire activity and see how these patterns differ across zones. Second, check the trend for any pattern in fire occurrences over time.

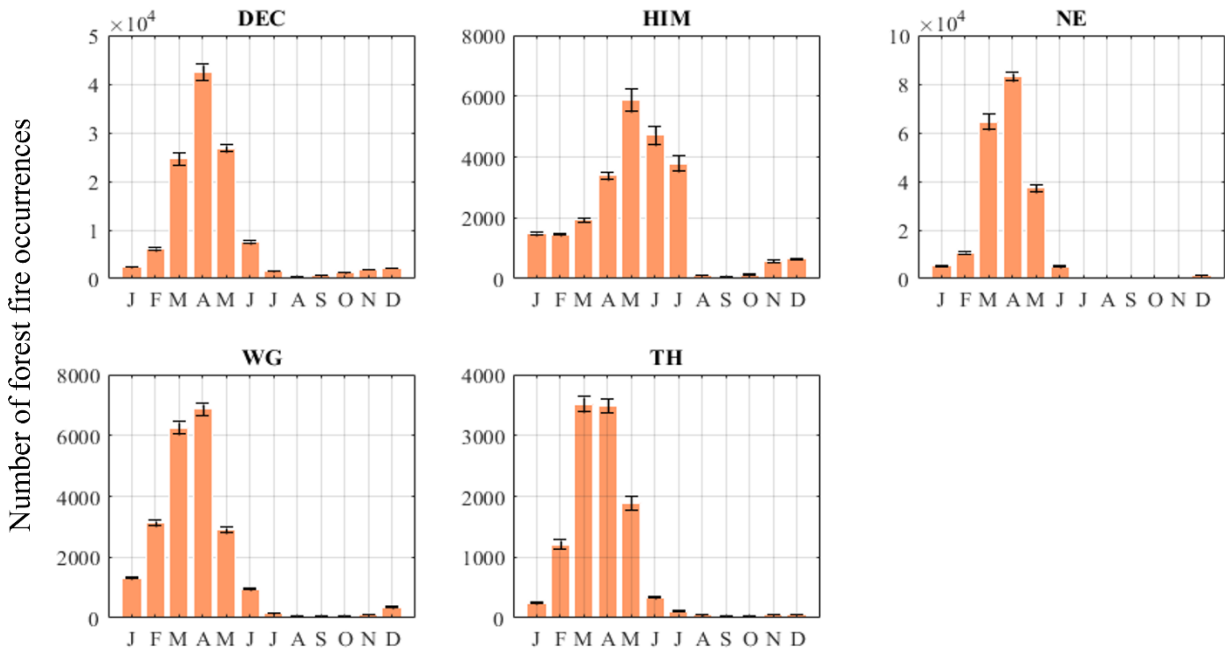


Figure 3.4: Monthly sum of forest fire occurrences over Indian forest zones during the period 2006 -2015. The standard deviation bars in the figure highlight the variability in fire occurrences.

Figure 3.4 illustrates the seasonal distribution of forest fire occurrences across different forest zones in India. A clear pattern of high-fire events in specific months can be observed across all zones. However, the period when this peak of fire occurs differs from zone to zone. In the DEC, fire occurrences peak sharply in March, April and May. This

period is the dry pre-monsoon season in all parts of this zone. Extreme heat and low humidity make the weather conducive to fires. The deciduous forests also become most susceptible to ignition in this period due to increased human activities such as agricultural residue burning. The fire occurrence pattern in the HIM region shows a similar but less intense peak during the late spring and early summer months of March to June. This pattern can be attributed to the complete melting of snow during this period, which exposes the underlying vegetation to atmospheric conditions. As temperatures rise and winds intensify, the dry subtropical pine forests, especially dominated by Chir Pine (*Pinus roxburghii*), become increasingly susceptible to fires.

Additionally, human activities like tourism and controlled burning are prevalent in this zone. An increase in such activities during the pre-summer months further elevates fire occurrences (Sharma, 2020; S. Singh & Suresh Babu, 2021). This region also experiences a considerable number of fires from January to March. These fires are primarily concentrated in the foothills. There is no snow cover in these parts, and prolonged drought periods following the monsoon make the dry vegetation more prone to ignition. The accumulation of highly flammable Chir Pine needles on the forest floor significantly contributes to the fire frequency (R. D. Singh et al., 2016). The North-East (NE) zone exhibits the highest fire counts, particularly in March and April. Among other zones, NE has the most prominent forest fire season during this period. This intense fire activity is mainly attributed to the widespread practice of shifting cultivation, known as *jhum*, where large forest areas are cleared and burned to prepare land for agriculture. In addition, this zone has dense forest cover, making it more susceptible to uncontrolled

fires once the weather becomes favourable. In the months of June-September, high humidity and persistent wetness during the southwest monsoon decrease the fire activity in this zone. The rainfall in the monsoon season effectively suppresses fire occurrences, making it nearly impossible for fires to ignite and spread in such conditions. Studies have shown that the high humidity levels, often exceeding 80% during the monsoon and post-monsoon periods, play a crucial role in preventing fire outbreaks in this region (Murthy et al., 2019). During the winter months, this region is subjected to the North-East monsoon. This, combined with cooler temperatures, further enhances the moisture content in the vegetation and lowers the fire activity during this period. The stark contrast between the pre-monsoon fire season and the near absence of fires during the southwest and northeast monsoon is a key characteristic of this zone. The Western Ghats (WG) and the tropical thorn forests (TH) exhibit similar fire seasons, primarily in March and April, typically the hot and dry pre-monsoon season in both zones. This similarity in fire season is due to their geographic proximity and similar climatic conditions during the pre-monsoon period. Despite the Western Ghats being known for their humid climate, the accumulation of dry leaf litter and the reduction in moisture content during this period increases fire occurrences. Ignition is majorly driven by anthropogenic factors such as forest clearing, firewood collection, and agricultural expansion (Kodandapani et al., 2004). The TH zone is characterised by thorn forests and scrublands, and fire activity peaks in March and April, though at a lower intensity.

The standard deviation bars in the figure highlight the variability in fire occurrences. Even though the timing of peak fire season is consistent, the number of fires varies significantly from year to year. This variability is due to inter-annual climatic fluctuations, such as pre-

monsoon rainfall and temperature variations, and the random pattern in human activities that impact the ignition.

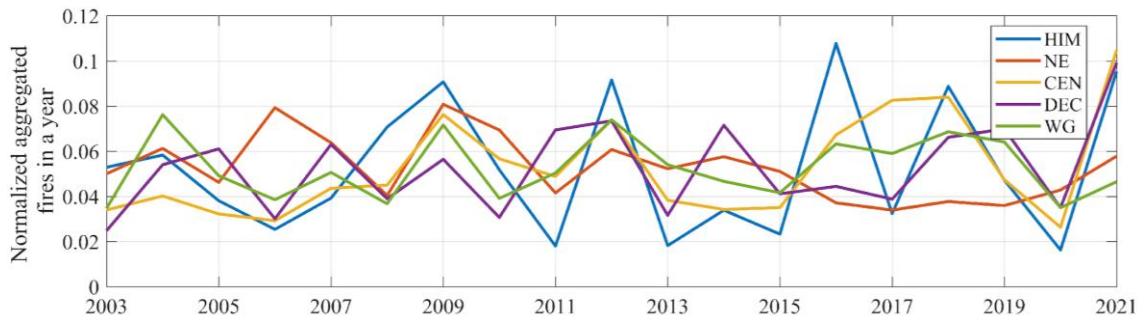


Figure 3.5: Time series of aggregated fire over a year in a zone

The trend was analysed using the time series of normalised aggregated fire occurrences across various forest zones in India from 2003 to 2021 (Figure 3.5). The analysis shows significant inter-annual variability with no clear long-term trend. The normalisation process adjusts fire counts to account for differences in area and helps to compare across zones. This lack of a consistent trend over the 20-year period suggests that such a timeframe may be too short to detect significant trend patterns in fire activity.

Many factors, like inter-annual weather variability, ignition sources, and regional ecological conditions, influence the inter-annual variability in fire occurrences. Years with comparatively higher temperatures during the fire season, drought, and extended dry spells have spikes in fire activity. Meanwhile, years with favourable monsoon seasons or fewer human-induced ignitions may result in lower fire counts. The randomness of ignition events due to human activities like shifting cultivation, forest clearing, and accidental fires further cause these variabilities.

No significant trend in fire occurrences was observed from 2003 to 2021. This indicates that projecting future fire regimes requires more than just extrapolating historical trends. Fire activity is strongly influenced by climatic parameters, which are expected to change in non-linear ways under climate change. Therefore, relying on climate model outputs becomes essential for understanding potential shifts in fire weather and patterns under various future scenarios. This approach allows for a more accurate assessment of fire risks in a changing climate where linear extrapolation methods are insufficient.

This approach also involves models that simulate fire weather with climate data inputs. In this study, the CFFDRS-FWI was employed for fire weather projections. The next chapter evaluates the applicability of CFFDRS-FWI to our study area, providing a framework for assessing climate hazards to fire regimes in response to future climate change.

Chapter 4

A robust Fire Danger Rating System (FDRS) for Indian forests

4.1 Application of CFFDRS-FWI in Indian climate

4.1.1 Coding the algorithm to function with gridded data

The CFFDRS-FWI algorithm was implemented using MATLAB based on the equations described by Wagner (1987). Existing tools to compute the CFFDRS-FWI, such as the R package *cffdrs* and other available implementations, were designed primarily to manage point data or station data. However, using them for gridded data requires external utilities to process one grid at a time. The MATLAB code developed uses matrix operations and allows all grids to be processed at the same time. During development, the code was tested repeatedly to ensure it ran quickly and efficiently. This makes it suitable for high-resolution studies on a regional or national scale.

To address the limitations in the existing modules, the CFFDRS-FWI algorithm was rewritten in MATLAB. This made the algorithm integrate seamlessly into the workflow for analysis with downscaled climate data as input. This code is archived in the GitHub open-access repository (https://github.com/anasuya993/CFFDRS-FWI_India/blob/main/CFFDRS_FWI_year_ABiitd.m).

The equations of the CFFDRS-FWI system and the danger thresholds were designed primarily for use in the Canadian climate. The following calibration steps were applied to implement this system in India.

- The FFMC index, which represents the fuel load of the topmost layer directly in contact with the near-surface atmosphere, depends heavily on meteorological variations. Hence, it does not need any adjustment.
- DMC and DC need adjustment because these computations are influenced by the daylight factor that depends upon the region's latitude and the date-of-year values. For our simulations, the latitude value at every grid point was considered to compute the corresponding day lengths.
- In potential evapotranspiration (PET) computation for DC, two assumptions were made: (1) The latitudes close to the equator (<20 in the northern hemisphere) receive consistent heating throughout the year, and (2) the PET in the higher latitudes is dependent on the month of calculation.

For this chapter, the evaluation studies were performed with daily and climatological FWI. The meteorological inputs to this algorithm for daily FWI were provided from the gridded (25km) ERA5 dataset. The variables were 12 noon IST values of 2 m temperature, relative humidity, wind speed, and 12 noon IST—12 noon IST accumulated precipitation.

4.1.2 Spin-up of FWI

Sensitivity experiments were conducted to deduce the spin-up required by the algorithm to provide stable and reliable outputs. The FFMC, DMC, and DC of a particular day depend on the values of these indices from the previous day. Typically, the first day of the simulation is started by initialising the FFMC, DMC and DC with the default values of 85, 6 and 15 respectively. Since the typical values of these indices are much higher in the

tropical regions, 12 experiments (Table 4.1) were performed in three sets to determine the time required by the system to produce stable FFMC, DMC and DC values.

Table 4.1 Sensitivity experiment sets to determine FFMC, DMC, and DC initialization.

Experiment Set	FFMC Initialization	DMC Initialization	DC Initialization	Experiment Duration
Set 1	75, 80, 85, 90	6 (default)	15 (default)	3 years
Set 2	85 (default)	6, 50, 100, 150	15 (default)	3 years
Set 3	85 (default)	6 (default)	15, 50, 100, 150	3 years

In all these experiments, different combinations of initialisation values of FFMC, DMC, and DC were provided on the 1st of January of the first year. In the second and third years, the simulated values of FFMC, DMC and DC of 31st December in the previous year were provided as initialisation. The model was provided with daily climatology values of meteorological inputs for all years.

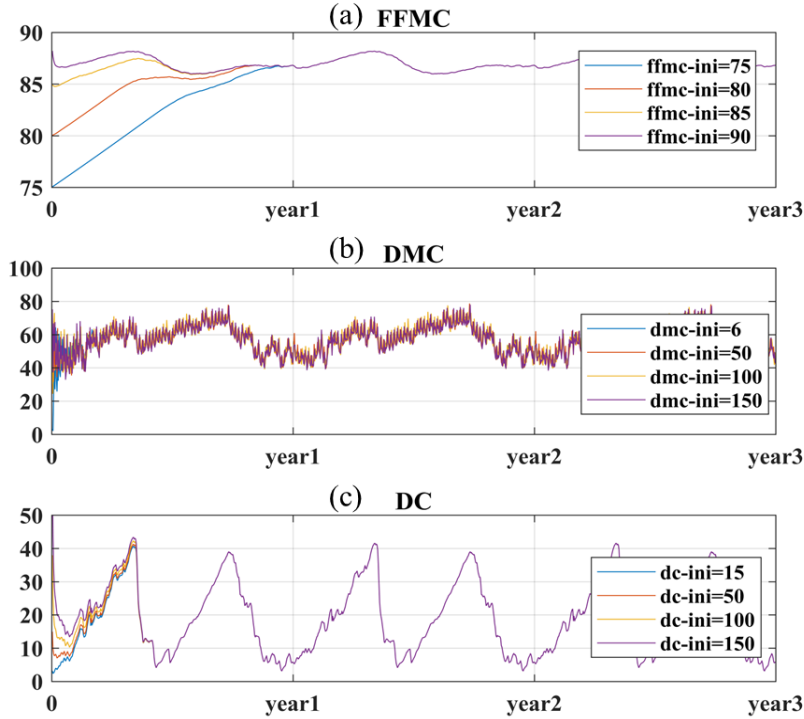


Figure 4.1: Spin-up simulation for (a) FFMFC, (b) DMC, and (c) DC

In all experiments, it was observed that intra-annual variability in DMC is the most pronounced, followed by DC, with the lowest variability observed in FFMFC. From the first set of experiments, it is observed that irrespective of the initialisation value of FFMFC, the curve stabilises after year 1 (Figure 4.1.a). For DMC (Figure 4.1.b), curves with different initialisation values start to converge from day 70, although they do not perfectly align. In the case of DC, a bimodal signature is observed annually, and the curves with different DC initialisations converge around day 150 of year 1. Overall, all three intermediate indices converge by year 1, leading us to conservatively conclude that the CFFDRS FWI consistently produces stable output irrespective of the initial values of FFMFC, DMC, and DC. In summary, regardless of the input meteorological dataset and the initial values, the CFFDRs should be spun up for at least a year for reliable outputs.

4.1.3 Evaluation of CFFDRS-FWI in Indian climate

The CFFDRS was originally developed for use in the Canadian climate, which differs significantly from the climatic and meteorological conditions in India. While numerous studies have applied this algorithm in various locations outside of Canada, it was important to test the applicability of the system to the Indian context before its implementation. Indian weather has distinct patterns like seasonal and latitudinal variations in temperatures, humidity, wind patterns and reversing monsoon winds leading to variations in precipitation patterns. A series of sensitivity experiments were performed to test the CFFDRS under various combinations of weather patterns. These experiments aimed to evaluate how well the CFFDRS could operate under Indian meteorological conditions. The ideal behaviour of the system was compared to the realistic behaviour of the system with actual meteorological conditions over India.

For idealized experiments, the model was provided with some gradually increasing values of one meteorological variable while keeping the other parameters at constant values. These experiments are listed in table 4.2. For all the three a, b, and c sets, the experiments were done for two rainfall conditions: precipitation = 0mm and precipitation = 10mm. The outputs of these idealistic sensitivity experiments were compared to the FWI calculated when the CFFDRS was forced with realistic ERA5 data over India. For this, the ERA5-forced simulated FWIs were segregated into conditions similar to the idealistic experiments. FWI computed from the ideal and realistic experiments were

plotted as the function of the corresponding meteorological input varied in that experiment and compared.

Table 4.2: Sensitivity experiments for assessing ideal CFFDRS behaviour

	2m Temperature	Relative Humidity	Wind speed	Precipitation
Experiment set (a)	(i) Varying from 0-100°C	20, 40, 60, 80, 100%	10 km/hr	prec=0
	(ii) Varying from 0-100°C	20, 40, 60, 80, 100%	10 km/hr	prec=10 mm
Experiment set (b)	(ii) 10, 20, 30, 40, 50°C	Varying from 0-100%	10 km/hr	prec=0
	(ii) 10, 20, 30, 40, 50°C	Varying from 0-100%	10 km/hr	prec=10 mm
Experiment set (c)	(ii) 10, 20, 30, 40, 50°C	10%	Varying from 0-50 km/hr	prec=0
	(ii) 10, 20, 30, 40, 50°C	10%	Varying from 0-50 km/hr	prec=10 mm

The families of curves (Figure 4.2) representing the idealistic behaviour of the FWI model identify the sensitivity of the varying weather parameters on the index.

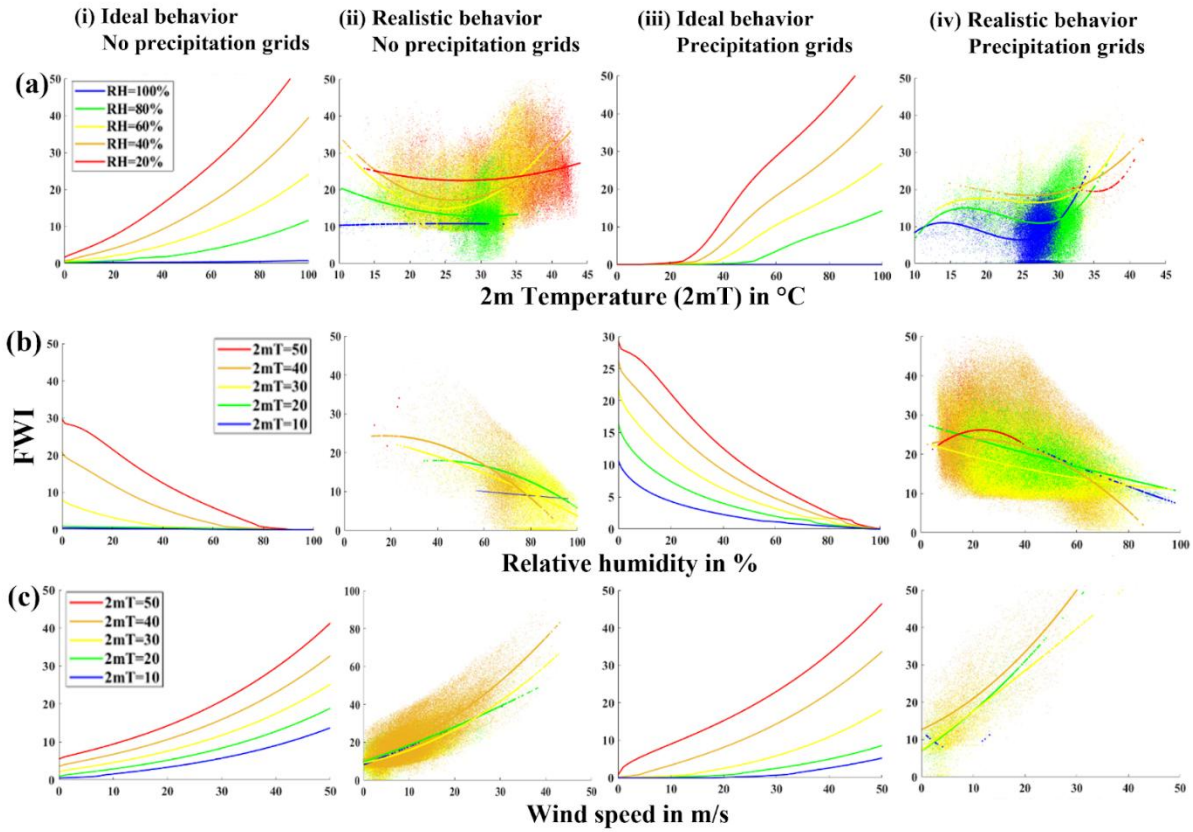


Figure 4.2: Idealistic (i and iii) and realistic (ii and iv) model performance with Indian Climate for varying (a) temperature, (b) relative humidity, and (c) wind speed for (i and ii) no precipitation grids and (iii and iv) precipitation occurring grids respectively.

FWI increases with an increase in temperature and wind speed, whereas the relative humidity parameter has an inverse effect on the index (Figure 4.2 i(a), i(b), i(c), iii(a), iii(b), iii(c)). A warm atmosphere helps ignite and burn fuel faster as less heat energy would be used to raise the fuels to their ignition temperature (Flannigan et al., 2000;

Wotton & Flannigan, 1993). At lower relative humidity, a steeper curve of FWI increasing with increasing temperature is observed. The rise in temperature also contributes to a decrease in relative humidity. Hence, the FWI is affected by the individual variables and their interdependence (Countryman, 1972). Unshaded fuels experiencing warmer and drier atmospheres are more susceptible to causing more intense fires if ignited (Scheiter et al., 2015). At very high relative humidity or when precipitation occurs, the available fuel becomes saturated with moisture (Dimitrakopoulos & Papaioannou, 2001), and under such conditions, FWI is very low and does not change with any change in temperature. With steadily increasing relative humidity, the evaporation rate of moisture from the fuel surface is affected, thus increasing the fuel moisture and decreasing FWI values. Drier atmospheres lead to conditions where a fire is likely to ignite easily and burn more vigorously (Cruz et al., 2012). Wind speed primarily affects the FFMC and ISI indices (Arnell et al., 2021; Field, 2020). Increased wind leads to more evaporation from damp surfaces by carrying away moist air and bringing in dryer air. When the fire is ignited, the wind increases the oxygen supply and facilitates the combustion process (Santoso et al., 2019). In the ideal experiments, it was observed that with uniformly increasing wind speed, FWI increases, and warmer and drier conditions increase the slope of this variation. These characteristic patterns were observed even when the FWI was computed with ERA5 forcing over India (Figure 4.2 column (ii) and (iv)).

The sensitivity experiments tested the applicability of the CFFDRS for simulating fire weather in Indian climatic conditions. The results showed that the idealized behavior - derived under controlled variations of meteorological parameters - corresponded well with the FWI computed using realistic ERA5 meteorological inputs over India. The

experiments also highlighted that FWI in India is highly sensitive to variations in temperature, relative humidity, and wind speed.

4.2 Association between FWI and fire frequency

The relationship between fire occurrences and FWI was required to be tested to ensure that FWI is suitable as a proxy for fire activity. It is important that high (low) FWI values are observed in areas with high (low) fire occurrences. This would make the index meaningful to be used in studying fire hazard. To test the association between MODIS fire data and the ERA5-based daily FWI over the period 2003-2021, multiple approaches were used.

First, three non-parametric statistical tests like the Chi-square test of association/independence (McHugh, 2013), Yule's correlation (Yule, 1897) and Fisher's exact test (Upton, 1992) were used to test the association between the raw MODIS active fire data and the FWI values of the grid where the fire occurred. These tests are best applied over nominal or ordinal variables. Hence, the FWI was converted to a nominal variable by introducing percentile data bins. FWI values lesser than the 40th percentile were considered to be zero, and the rest values to be 1. This threshold of the 40th percentile was chosen based on the observation that the curve of the percentile ranks showed maximum change in slope, with 97.9% of fires occurring beyond this threshold. The fire presence and absence were denoted as 1 and 0, respectively.

1. The Chi-square test of association/ independence tests the existence of a significant relationship between the datasets. The Chi-square test of association/ independence test returns a value of 8968.6, which is greater than the critical decisive test value. Thus, the null hypothesis was rejected, and the association between the two variables was established at a 95% significance level.

2. Yule's correlation tests the strength of the association between FWI and fire count. Yule's coefficient gives a correlation parameter between 0 and 1, with higher values signifying a stronger relationship. For computing Yule's correlation (Q), the concordant cells consist of two favourable scenarios wherein low FWI and high FWI correspond to no fire and fire scenarios, respectively. The discordant pair consists of unfavourable outcomes for FWI and fire datasets. Q yields a value of 0.803, indicating a strong positive association.

3. Fisher's exact test also tests the strength of the association between the datasets. Fisher's odds ratio is a measure of the relative odds of the occurrence of the outcome of interest, which, in our case, is more fire-counted and associated with higher FWI values. Fisher's exact test over FWI and fire data yields a value of $h=1$ at a 95% significance level and an odds ratio of 9.18 (8.54-9.87). This test also suggests a significant non-random association between the fire occurrence and its corresponding FWI value. The odds ratio of 9.18 indicates that the odds are 9.18 times higher that a fire will occur at low FWI values than at high FWI.

These non-parametric statistical tests suggest consistent results, indicating a significant association between FWI and fire occurrences.

The Chi-square goodness of fit test (Cochran, 1952) returns a decision $h=1$ (null hypothesis for FWI) and $h=0$ for fire occurrences, which denotes that the FWI dataset belongs to a normal distribution, whereas the fire count does not. Hence, using Pearson's correlation coefficient and simple linear regression between the two variables is inappropriate as they assume a normal distribution. In addition, a higher FWI does not necessarily ensure a high number of fires. The number of fires depends on other factors, such as ignition. A fire occurrence, however, would generally translate to comparatively high severity of fire favourable conditions and hence higher FWI.

Next, the percentiles of annual mean FWI were compared with the MODIS observed annual fire count by pixel with spatial plots. A scatterplot of FWI percentile bins vs. the count of fire events corresponding to those percentile values was also plotted. The percentile bins were computed from the daily FWI dataset at all grid cells within a particular zone. Even the fire count was aggregated from the daily fire count for 10 years between the percentile bins. These curves showed us how the fire counts are spread across various percentile levels of FWI. Also, the best-fit curves were computed and plotted to determine the nature of the curve and the coefficient of determination.

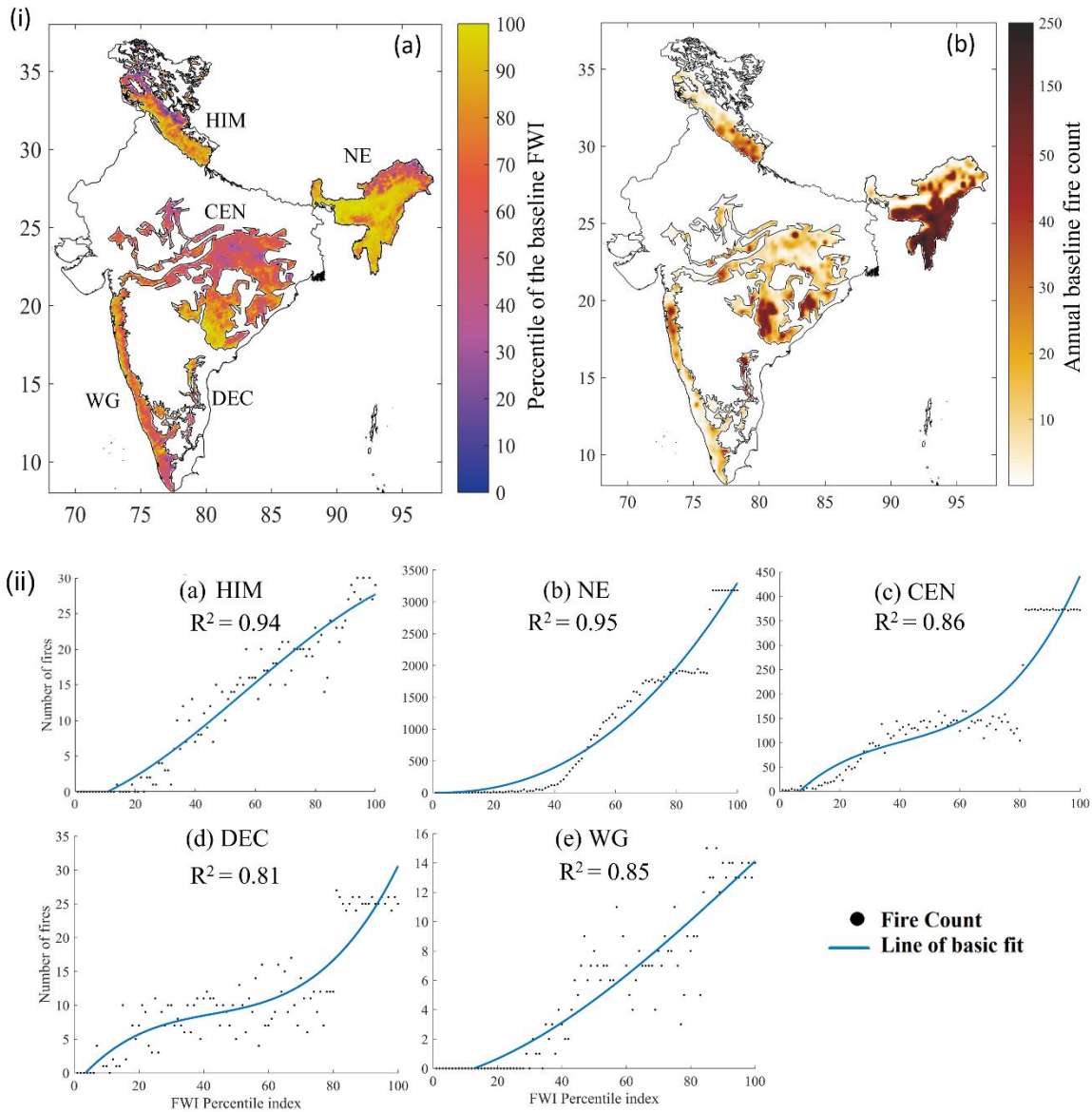


Figure 4.3: Relationship between fire counts and percentiles of FWI. (i) Spatial map of percentiles of annual mean FWI and b MODIS observed annual fire count and (ii) scatterplot of fire count for each FWI percentile bin for a HIM, b NE, c CEN, d DEC, and e WG FWI zones for the baseline period (2006–2015). R^2 represents the coefficient of determination.

The maps of the annual mean FWI percentile for the baseline case and the observed MODIS fire count for the same period (Figure. 4.3.i) show that there is a spatial correspondence between fire count and FWI. Grid cells with high fire counts have higher (above the 40 percentile) FWI values. For example, NE has a high FWI and extremely high fire count due to high anthropogenic ignition from the prevalence of shifting cultivation practices (Bedia et al., 2015) also reported a high correlation between burned area and FWI averaged over the fire season in this region. Similar signatures of higher FWI and corresponding high fire occurrence can be observed in HIM, southern CEN, northern WG, and DEC.

To further study the association between FWI and fire count, a scatterplot of fire count vs. the FWI percentile values corresponding to the fire events was plotted (Figure. 4.3.ii). This is slightly different from the spatial map, where overall FWI values were averaged irrespective of whether a fire occurred or not. It was observed that there is a strong relationship between FWI and fire count, with more (less) fire events at high (low) FWI values for all the forest zones (Figure. 4.3). However, the nature of the relationship varies by forest zones. The best-fit curves with the highest values of coefficient of determination show that the relationship is exponential in the case of the NE zone (Figure. 4.3.ii.b) but cubic in the HIM, CEN, DEC, and WG zones (Figure. 4.3.ii.a and c-e). As discussed later, this difference has implications for developing FWI thresholds for fire severity classes for different forest zones. Overall,

In the third approach, the Epanechnikov Kernel Density Estimations (KDE; Epanechnikov, 1969; Samiuddin & El-Sayyad, 1990) was plotted to compare the distribution of FWI values corresponding to fire and no-fire events (Figure 4.4). This approach demonstrated the distinct differences in FWI spread, affirming its effectiveness as a metric for identifying conditions conducive to fire occurrence.

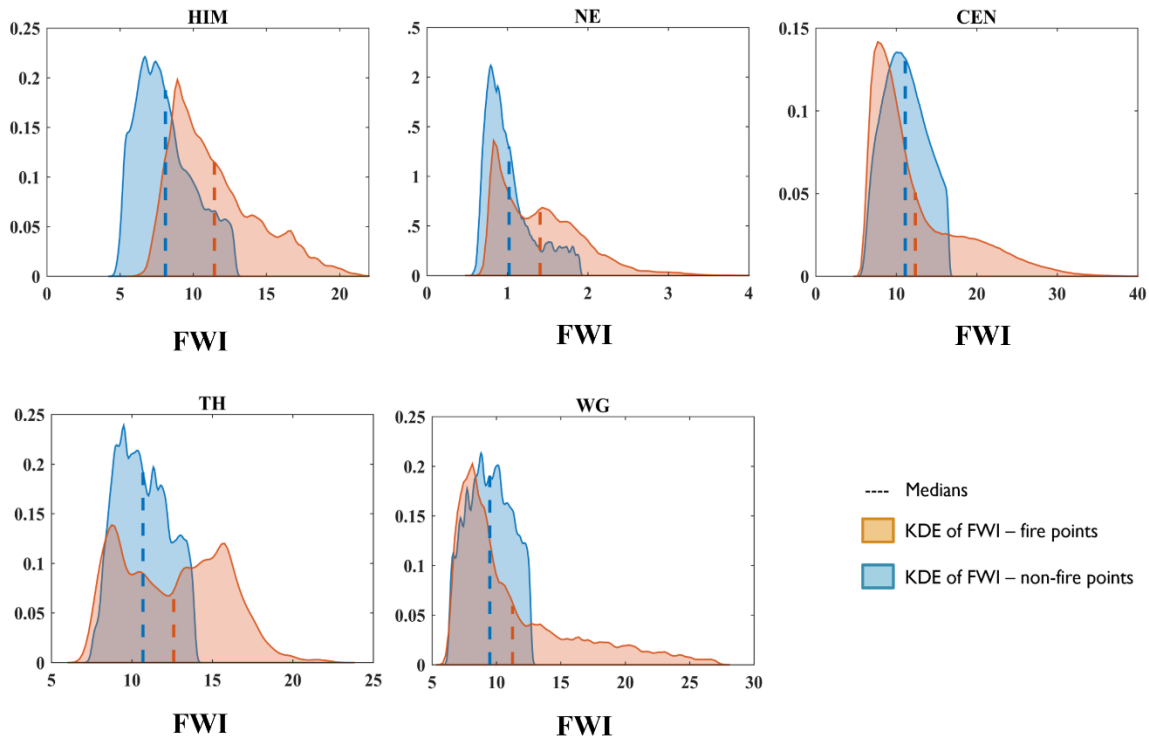


Figure 4.4: Kernel Density Estimation of FWI corresponding to that of fire-occurring grids and non-fire grids for different zones.

It was observed that in all the zones, the FWI corresponding to the fire points spread towards higher values. The peak of FWI spread corresponding to no-fire points occurs at comparatively lower FWI values. Also, in all the zones, the median of FWI at the fire points curve is at a higher value than that of no-fire points. This affirms that fire occurrences are

accompanied by comparatively higher FWIs. This difference between the KDE curves is prominent in HIM, NE and DEC regions. In the CEN and WG regions, although the FWI in fire points extends towards higher values, there is also a notable peak of fire point FWIs at lower values. This can be attributed to the higher fragmentation of forests in these regions, with some grids exhibiting as low as 20-30% forest cover. Consequently, a grid with lower forest cover may exhibit fewer fires than a grid with higher forest cover despite the latter having a lower FWI.

Overall, this analysis shows that FWI is a robust indicator of fire weather hazard.

4.3 Fire danger rating system

Fire danger rating is a necessary tool for the quantitative assessment of fire danger in a systematic way (Stocks et al., 1989; Vasilakos et al., 2007). It is a tool to communicate with the public and fire agencies about potential threats. Five classes, Low, Medium, High, Very high, and Extreme, were chosen as they adequately represent the FWI spread over the zones. These classes show the increasing degree of fire hazard and also make it easier to communicate the hazard. For this, FWI was computed using the CFFDRS-FWI MATLAB code with ERA5 meteorological inputs on a climatological scale. Daily climatologies of maximum 2m temperature and averages of relative humidity and wind speed were computed over the period 2003-2021 from the hourly ERA5 single-level reanalysis dataset at a 0.25° resolution. For operational fire danger assessments, the values of these variables at 12 noon local time are used as inputs to the CFFDRS-FWI.

However, for climatological evaluations, daily maximum temperature, average or minimum relative humidity, and average wind speed are preferable. This approach ensures that the assessments are less sensitive to short-term fluctuations in weather conditions at specific hours of the day, providing a more statistically robust assessment of fire hazard over extended periods.

Regarding relative humidity, an ongoing debate exists about whether daily minimum or daily mean values are more appropriate for use in the CFFDRS. However, a global study by (Quilcaille et al., 2023) indicates that using mean or minimum relative humidity does not significantly affect the outcomes. In this study, daily minimum relative humidity was used. Daily climatology of precipitation was obtained by averaging the daily 24-hour accumulated precipitation from the ERA5-Land dataset at a 0.1° resolution over 2003-2021 and aggregated to a 0.25° resolution.

The default approach to calculate the fire danger class thresholds is to define the lower limit for the Extreme class using the FWI dataset. If this value is considered to be the 99th percentile of FWI in each zone, and geometric progression is used to define the limits of other danger classes, the conditional probability of fires occurring beyond High and Very High classes in a few zones saturate at 1. This defeats the purpose of developing different classes to denote different fire danger levels. Hence, to compute these upper FWI thresholds for the danger classes, an ensemble of 4 different methods was selected and evaluated. These four statistical methods are based on logistic regression, percentile-based, percentage of fire-based and K-means clustering (Figure 2.5). Machine learning

techniques were also introduced within these methods to reduce subjective decision-making and finally computed modified thresholds in terms of percentiles. As the range of FWIs varied across zones, these thresholds were calculated separately for each zone. Following is a detailed description of the methods.

1. Percentile based

This is a popular method used by various operational fire management services such as the U.S. Forestry Services. Initially, 22nd, 45th, 90, and 97th percentile FWI thresholds are considered as the upper threshold values for Low, Medium, High, and Very high danger classes respectively. Then, to further refine these thresholds, the Receiver Operating Characteristics (ROC) curve was plotted in these intervals for all the zones (Figure 4.5). The ROC curve is a tool used to find the best classifier in categorical problems. In a given interval, it plots a curve between the True Positive Rate (TPR) and the False Positive Rate (FPR) at varying decision thresholds. The point in the curve closest to the (1,0) point marks the best operating point. In this case, the interval between the 0th and 22nd percentile was first selected. Considering all consecutive values between 0-22 as the decision threshold, the ROC curve was plotted, and the best operating point was determined. This was the threshold value of that interval. This was then repeated for the other intervals and all the zones. Thus, instead of the threshold values at the 22nd, 45th, 90th, and 97th percentile, the best classifier percentile values in that interval were selected using the ROC curve.

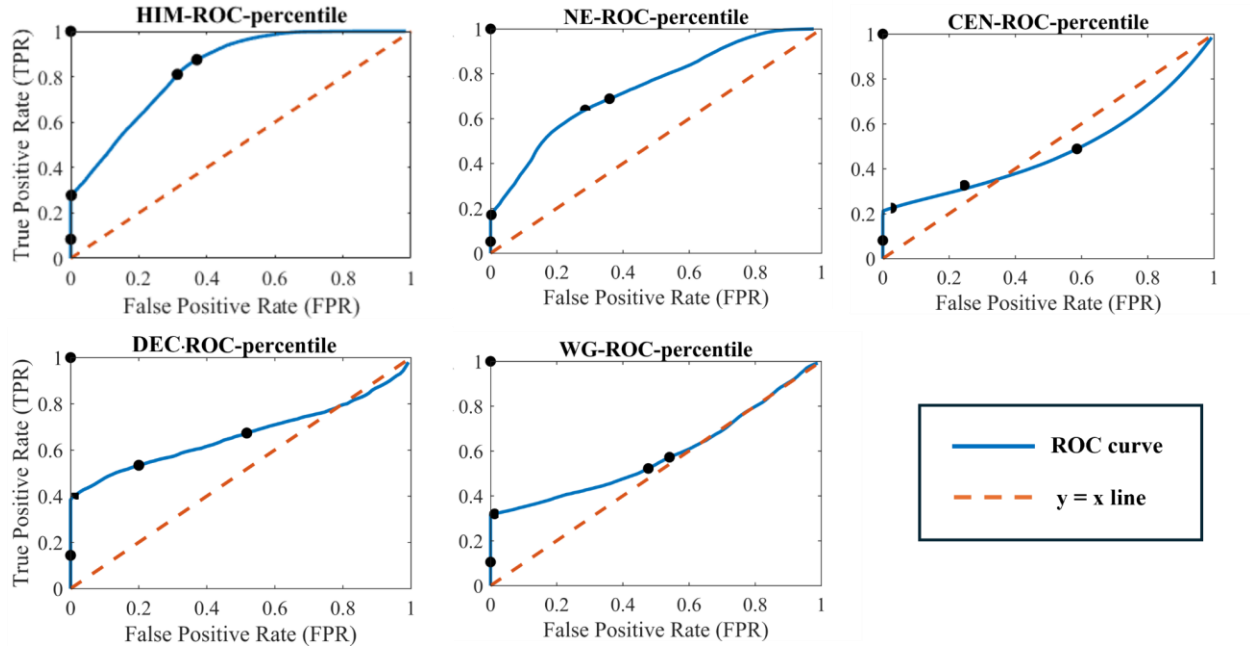


Figure 4.5: Graphical illustration of ROC curves of the percentile-based method for every zone

2. Percentage of fire events based

In this method, the percentage of fires occurring beyond every percentile index (PI) of FWI was computed and hierarchical clustering was applied to classify the dataset into 5 clusters. Hierarchical clustering (Nielsen, 2016) is an unsupervised learning method that is used to divide data points based on similar attributes and patterns. Here, agglomerative hierarchical clustering was used, where data points start as individual clusters and are successively merged to form larger clusters. Hierarchical clustering is implemented by calculating distances between data points, which in our case is the percentage of fires corresponding to each PI (blue curve in Figure 4.6). Then, it iteratively merges clusters based on these distances. The process continues until a desired level of detail or structure is achieved. The highest value of the percentage of fires was computed in the 5 clusters,

and the corresponding FWI and PI were computed as thresholds for each class (Figure 4.6).

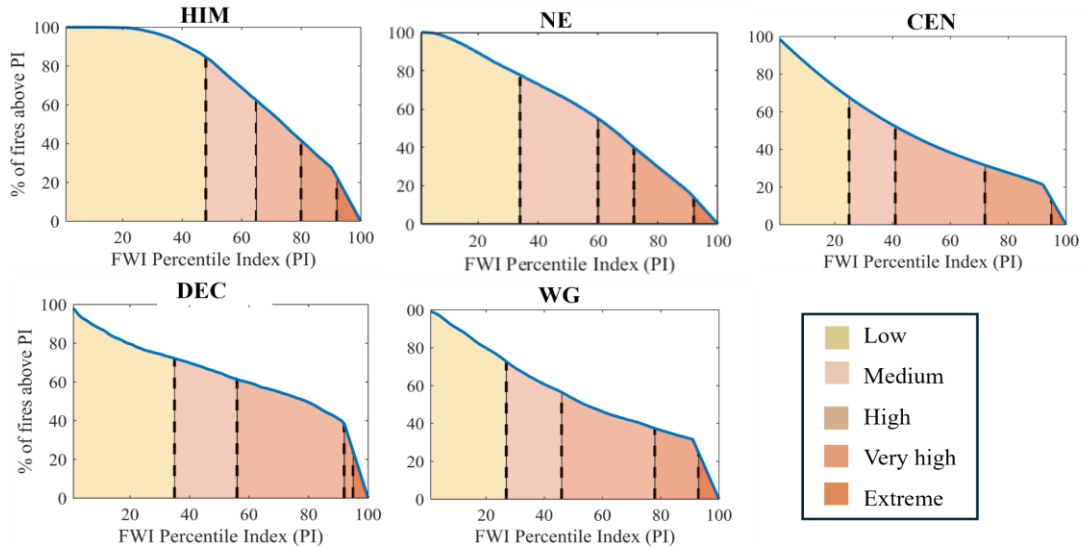


Figure 4.6: Graphical illustration of classes developed using percentage of fires beyond PI and hierarchical clustering for every zone

3. Logistic regression based

Logistic regression is another method that computes the probability of occurrence in problems with two possible outcomes (DeMaris, 1995). It is particularly useful in scenarios where the dependent variable is categorical or dichotomous, such as the occurrence or non-occurrence of a fire. The logistic regression model estimates the probability of the outcome occurring based on one or more predictor variables.

The basic equation for logistic regression is:

$$y = 1 / (1 + \exp(\beta_0 + \beta_1 x)) \quad (\text{Eq.1})$$

Where y is the predictand, x is the predictor variable, and β_0 and β_1 are the regression coefficients. The logistic function, also known as the sigmoid function, maps the linear

combination of predictors to a probability value between 0 and 1. In this study, logistic regression was used to model the probability of fire occurrence based on the FWI values. The fire data was first converted into a nominal variable, representing the binary outcome (fire occurrence or no fire). Each data point in this dataset corresponds to a specific grid cell. The converted binary fire information and the corresponding FWI values of each grid cell were provided as inputs to the logistic regression model. The FWI value served as the predictor variable, while the binary fire data served as the response variable, and fire occurrence probability was computed as a function for both. Initially, The FWI values corresponding to fire probabilities of 0.2, 0.5, 0.7, and 0.9 were considered to be thresholds for the classes. These thresholds were further optimized by using hierarchical clustering between the classes and computing the highest value of likelihood in each cluster (Figure 4.7).

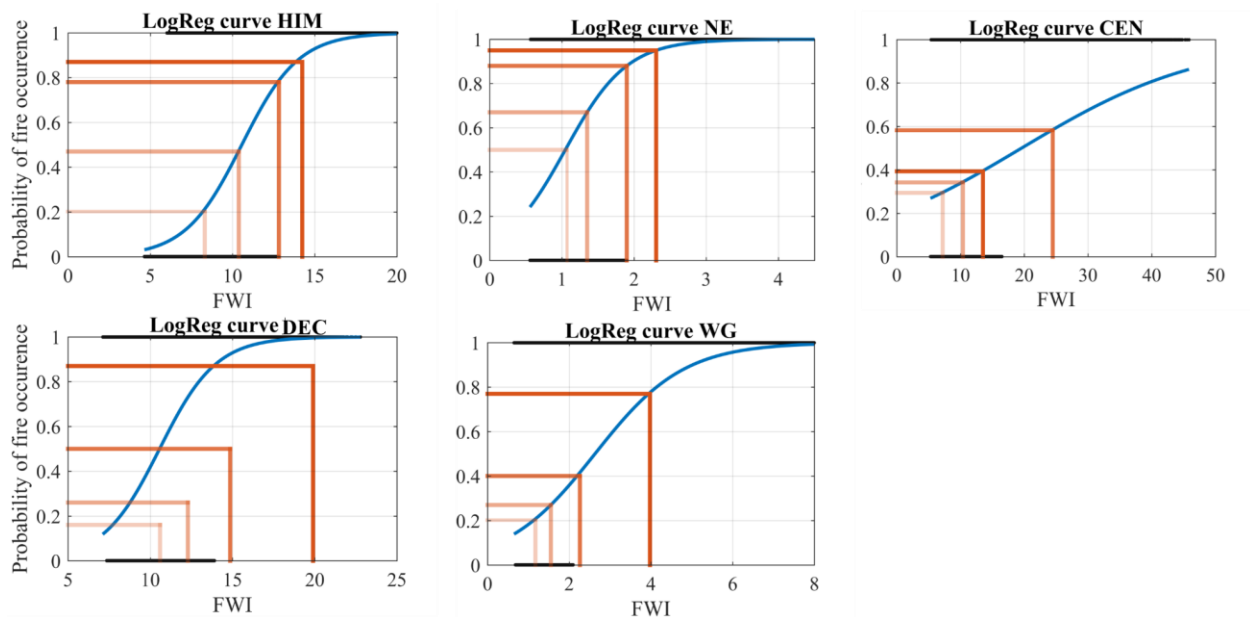


Figure 4.7: Graphical illustration of classes developed using logistic regression probabilities and hierarchical clustering for every zone

4. K-means clustering

K-means clustering is a machine learning-based clustering technique. This unsupervised learning method is effective in identifying patterns and grouping similar data points based on their features. The K-means algorithm operates through a process of initialization, assignment, and update until convergence. Initially, k centroids are randomly selected from the dataset. Each data point is then assigned to the nearest centroid by calculating the Euclidean distance between the data points and the centroids. The centroid of each cluster is recomputed by taking the mean of all data points assigned to that cluster. This process of assignment and update is repeated until the centroids no longer change significantly or a maximum number of iterations is reached, resulting in the data points being grouped into k clusters characterized by their centroids.

K-means clustering was applied to the fire count per percentile bin of the FWI dataset for every grid point (Figure 4.8). This fire count per PI was clustered into five danger class clusters and their corresponding FWI PI values were considered as the thresholds. It took 10^6 iterations to get the results to converge.

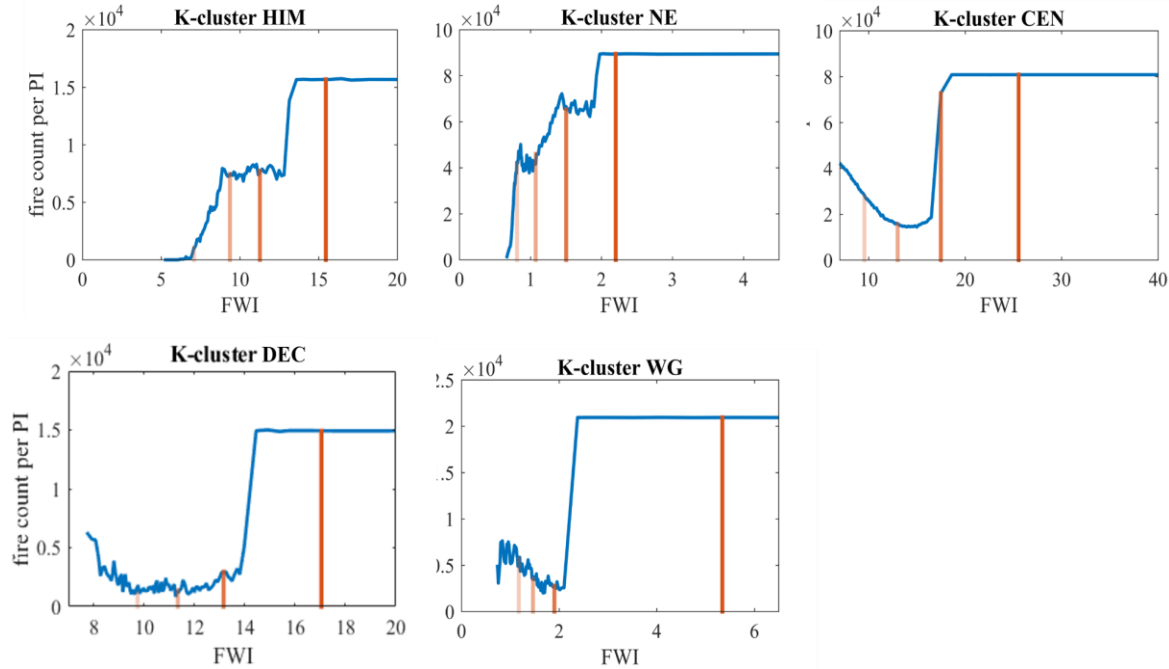


Figure 4.8: Graphical illustration of classes developed using K-means clustering for every zone

The highest value in each threshold class computed from the above five methods were averaged. These characterized the limiting values of each fire danger class in terms of percentiles (Table 4.3). By expressing the thresholds in terms of percentiles, they become adaptable for use with any dataset, gridded or station data, facilitating a more versatile and operationally relevant threshold classification. This approach makes the thresholds applicable across different forest regions, time periods, and FWI datasets, contributing to a robust fire danger assessment framework. The range of thresholds in terms of percentiles in all the zones is similar with the Low class threshold ranging around the 40th percentile to the Extreme class beyond the 95th percentile.

Table 4.3: Upper thresholds of fire danger classes in percentiles of FWI for the different zones

Fire danger classes	HIM	NE	CEN	DEC	WG
Low	40	36	38	40	34
Medium	61	57	65	66	58
High	85	82	87	90	87
Very high	95	96	97	98	98
Extreme	>95	>96	>97	>98	>98

4.4 Evaluation of FDRS

To ensure the robustness of our developed thresholds, three key criteria were implemented.

1. Minimum overlap between the classes when considering different methods.

It was ensured that there was no overlap between classes. For example, if the low threshold in method 1 surpasses the medium threshold of method 2, then there would be an overlap, and it would be inappropriate to use the methods in an ensemble threshold computation. To assess this, the spread of FWI was observed in each class for different methods using a violin plot (Figure 4.9).

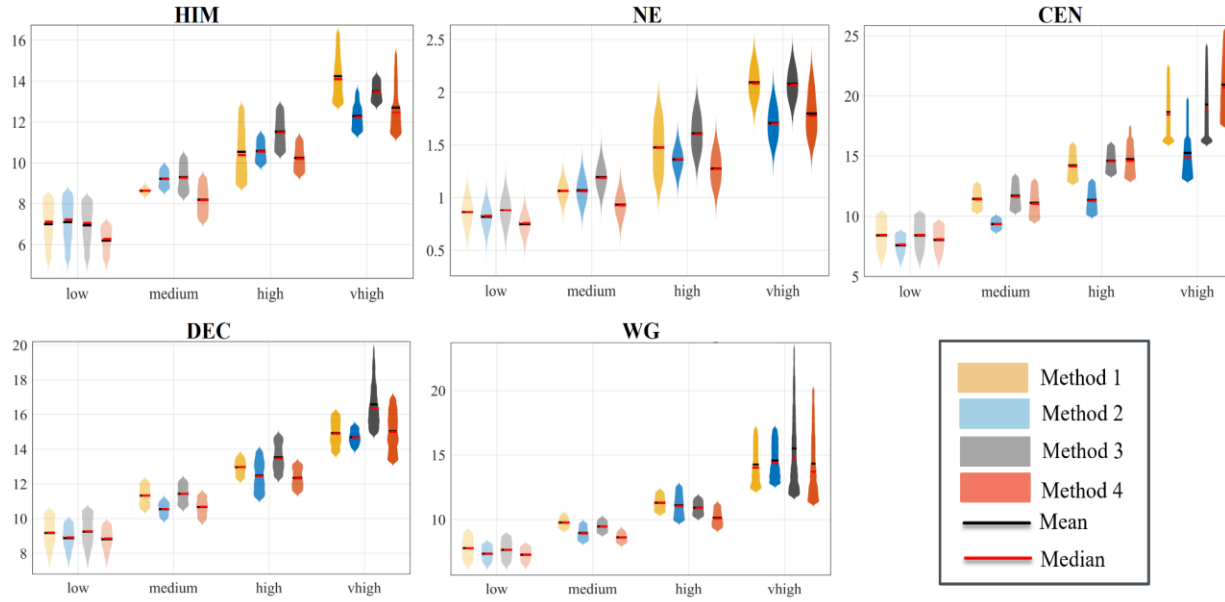


Figure 4.9: Violin plots for danger class thresholds developed using different methods along with the mean and median for different zones

This plot combines the aspects of a box plot and a kernel density curve and displays the distribution of data across different categories or groups. The violin shapes convey information about the kernel density of the data in the category, highlighting characteristics such as skewness and multimodality. The black and the red lines indicate the mean and the median of data in that category, which provides measures of central tendency.

From this, it is observed that the mean and median thresholds in each method consistently do not overlap with the thresholds of the previous class. This also shows agreement between the methods in threshold development, which is essential for their ensemble use. Also, the pattern of kernel densities, including the shape of the kernel density curve, skewness, and relative frequency magnitudes, are in agreement across

the chosen methods. This uniformity also shows coherence within the methods and develops confidence in our approach. Another observation is that the spread of kernel densities is more pronounced in the very high class in all the zones. This ensures a broad range of values in the class denoting high fire danger, effectively minimizing the occurrence of true negatives. This strategic emphasis on a comprehensive range in the Very High class enhances the sensitivity of our fire danger thresholds, which is crucial for accurate risk assessment and management strategies. The observed skewness in the distribution of some methods towards lower values can be attributed to the lower prevalence of highly fire-conducive conditions compared to moderate fire weather conditions. In some zones, the kernel densities in the Low class exhibited skewness towards higher values.

2. Increase in the fire occurrence probability with each class.

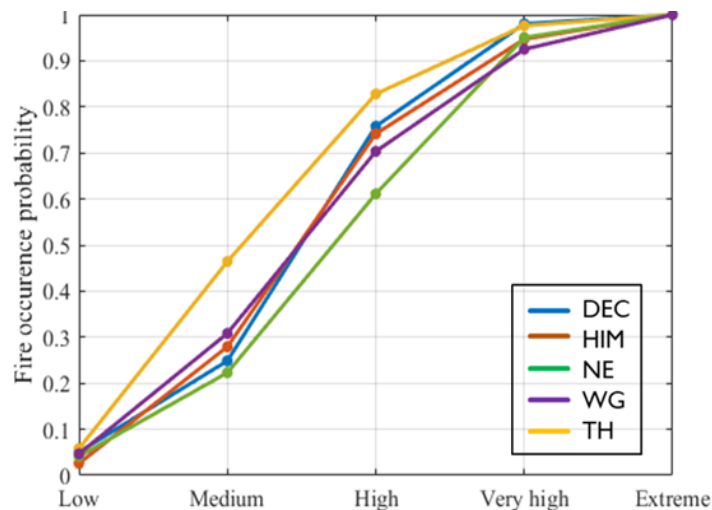


Figure 4.10: Fire occurrence probability at fire danger classes for different zones

The second criterion is to ensure that the probability of fire occurrence within each danger class increases in comparison to its previous class (Figure 4.10). The probability was computed as the ratio of favorable events—in this case, instances of fire occurrence—to the total number of events in each class. As anticipated, the results show that lower fire danger classes exhibit a correspondingly lower fire probability, and the higher fire danger classes demonstrate a higher fire probability. The significance of this probability criterion lies in its role in ensuring the reliability of the established danger classes. If, for instance, a high fire danger class were associated with a low fire probability, it would introduce a contradiction and diminish the practical utility of the thresholds. Therefore, incorporating this probability criterion is essential for developing thresholds that make the delineated danger classes acceptable. Moreover, the violin plot in Figure 4.9 also illustrates a clear progression of thresholds, showing the increase in the spread of FWI values from low to high classes in all the methods. This alignment between fire danger classes and the associated fire occurrence likelihood provides a robust foundation for the developed thresholds.

3. Coherent values of evaluative parameters like critical success rate (CSI; Schaefer, 1990), probability of detection (hit rate), and false alarm ratio (FAR; Schaefer, 1990), hits due to chance and correct rejection. These parameters were calculated using the following equations:

1. Critical Success Index (CSI):

$$CSI = Hits / (Hits + Misses + False\ alarms)$$

2. Probability of Detection (Hit Rate):

$$\text{Hit Rate} = \text{Hits}/(\text{Hits} + \text{Misses})$$

3. False Alarm Ratio (FAR):

$$\text{FAR} = (\text{False alarms})/(\text{False alarms} + \text{Correct rejections})$$

4. Hits due to Chance:

$$\text{Hits due to chance} = (\text{Total events} \times \text{Total Hits})/(\text{Total observation}^2)$$

5. Correct Rejection:

$$\text{Correct rejection} = (\text{Correct rejections})/(\text{Correct rejections} + \text{False alarms})$$

To assess these parameters, the Low danger class threshold was considered as a benchmark for the confusion matrices for each zone. The results reveal a consistently high hit rate across all zones, with the highest value in HIM. This high hit rate indicates that the danger classes defined in this study are effective in capturing true positive events. Hits due to chance are consistently low across all zones. This ensures that the observed hits are not merely coincidental but are due to the model's ability to accurately predict fire occurrences. Correct rejection rates vary within the range of 15-35% across zones, representing the proportion of instances where the model correctly identifies non-fire events. The moderate values in this parameter indicate a balanced classification performance. An interesting observation is the relatively high False Alarm Ratio (FAR), especially in CEN, DEC, and WG zones. This metric is the ratio of false alarms to the total positive predictions. Within these zones, the prevalence of hot and dry conditions during

the pre-summer monsoon months contributes to a large number of days having high FWI. However, the presence of high FWI does not necessarily result in fires unless there is an ignition source. Despite the elevated FAR in these zones, the overall classification remains acceptable as it does not compromise the accurate identification of true negatives. The comprehensive CSI combines various performance measures and indicates high values in HIM and NE. In other zones, the CSI is comparatively lower because of high false alarms. In summary, the defined danger classes demonstrate coherent values for evaluative parameters, with a consistently high hit rate, low hits due to chance, moderate correct rejections, and an acceptable FAR. The rigorous evaluation of these thresholds makes the designed danger classes suitable for operational fire management use.

Table 4.4: Evaluative parameters to test the skill of the developed system in fire prediction

	HIM	NE	CEN	DEC	WG
Critical success rate (CSR)	0.52	0.56	0.26	0.22	0.18
Probability of detection/ hit rate	0.92	0.76	0.56	0.7	0.56
False alarm ratio (FAR)	0.45	0.31	0.67	0.75	0.78
Hits due to chance	0.22	0.36	0.23	0.12	0.13
Correct rejection	0.25	0.15	0.24	0.32	0.33

These thresholds were also compared with the thresholds developed without integrating the ROC curve and clustering techniques. The thresholds without machine learning relied on subjective threshold numbers and were tailored to specific regions and applications. This limits their usage as potential thresholds for operational usage for India with all kinds of datasets. To ensure the robustness of these danger classes, recalibration of the initially chosen numerical thresholds was undertaken. The incorporation of clustering and ROC curves provided a more adaptive and data-driven framework for threshold computation. The metric CSI was used to compare these new thresholds with the previous ones. CSI is a comprehensive metric that factors in true positives, false positives, and false negatives. This approach gauges the effectiveness of our thresholds, considering both accurate predictions and false negatives.

The results show consistently higher CSI values for the thresholds derived from machine learning methods (Figure 4.11). This suggests an improvement in the classification to predict fire danger accurately. An overall improvement of 30-50% was observed in the CSI in all the zones except WG where it was observed that Low and Medium class thresholds show no significant improvement. However, there is a 23% improvement in the CSI of the Very high danger class. The highest improvement is in the DEC zone followed by CEN with CSI increasing by 49.5% and 43% respectively in the newer thresholds than the older ones. In the Low and Medium classes, the most significant improvement was observed in the NE zone. In higher danger classes, DEC and CEN zones show maximum improvement. In summary, the overall CSI of new thresholds shows an increase of 28% across all classes and zones in Indian forests. This evaluation

shows that the inclusion of objective decision-making approaches significantly influences the overall performance of the resulting fire danger threshold computation.

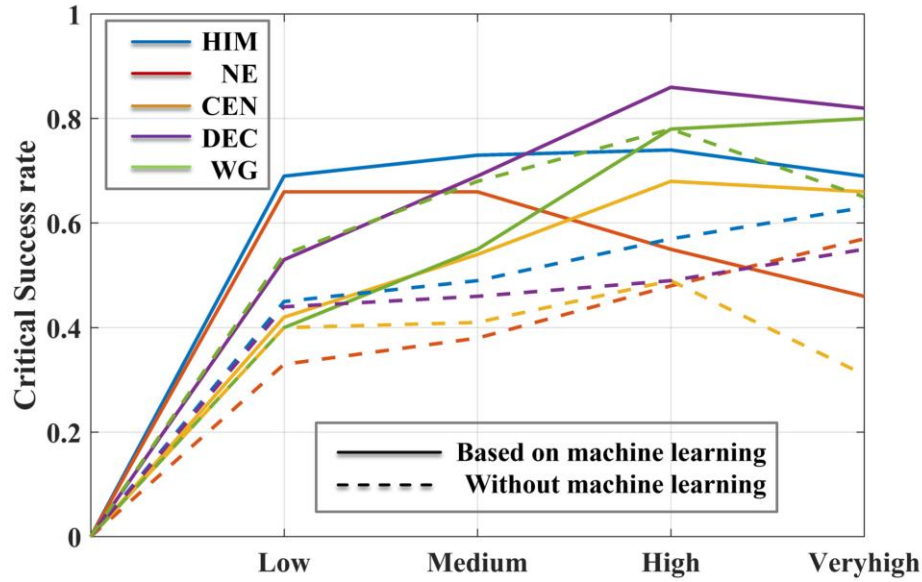


Figure 4.11: Critical Success Rate (CSR) of thresholds for each danger class developed without machine learning (dashed lines) and with machine learning (solid lines) for different zones.

4.5 Summary

In this chapter, a comprehensive approach to developing a robust fire danger rating system (FDRS) was presented. The CFFDRS-FWI algorithm was implemented in MATLAB to adapt to work with high-resolution gridded climate data, aligning with the objectives of this thesis. This code is archived on GitHub. It was determined that a minimum spin-up period of 365 days is required for stable and reliable outputs. Analysis shows that this algorithm provides reliable outputs if spun up properly, even with Indian climate conditions. The ERA5 weather data was used as input for the CFFDRS-FWI to

produce fire weather conditions that demonstrated a statistically significant relationship with MODIS fire count data. This established that the FWI is a reliable metric for assessing potential fire occurrences.

Then, a systematic FDRS was developed, classifying FWI values into five classes—low, medium, high, very high, and extreme—in different forest zones in India. Classical methods were integrated with machine learning approaches to ensure that the system is adaptable to a wide range of inputs and applicable to regions with similar weather patterns like that of the five zones. The evaluation of threshold values confirmed that the methods used are consistent, and the thresholds robustly reflect fire occurrence patterns across the zones.

With this revised version of the CFFDRS-FWI algorithm and the developed FDRS, the FWI was simulated using high-resolution climate data for baseline (2006-2015) and end-century (2091-2100) periods. This will help in analyzing the potential impacts of climate change on fire danger across India's forest zones. The subsequent chapter details the development of this high-resolution climate data through the dynamical downscaling of GCM outputs.

Chapter 5

High-resolution climate scenarios

5.1 Introduction

In this chapter, the dynamical downscaling of the bias-corrected CESMv1 (Hurrell et al., 2013) climate projections from the CMIP5 project for the RCP 8.5 scenario is discussed.

The CFFDRS requires accurate climate projections as input to estimate fire danger indices like the FWI under climate change scenarios. However, the coarse spatial resolution of GCMs, ranging from 100 to 600 km, limits their ability to capture localized climatic variations necessary for high-resolution fire weather assessments. Downscaling is a technique to refine GCM outputs to higher spatial resolutions. Local climatic processes, such as convective activity and terrain influences, are not well captured by GCM outputs. These processes are crucial for accurately estimating high-resolution values of temperature, humidity, wind speed, and precipitation. These meteorological factors, in turn, are essential for calculating fire weather indices at high resolution. Downscaling helps overcome this limitation by providing detailed regional climate projections that account for these local processes.

Two primary approaches exist for downscaling climate projections: statistical and dynamical (Trzaska & Schnarr, 2014). The statistical approach, which is computationally efficient, involves deriving empirical relationships between large-scale predictors and local climate variables using observational data (Navarro-Racines et al., 2020; N. S. Patil & Laddimath, 2021). Conversely, the dynamical approach uses high-resolution Regional Climate Models (RCMs) to simulate local climate conditions driven by large-scale atmospheric features from GCM projections while incorporating the effects of local drivers such as topography and land cover (Trzaska & Schnarr, 2014). However, biases and uncertainties inherent in GCM outputs may be transferred to RCM simulations, making preprocessing methods like bias correction necessary

before downscaling (Xu & Yang, 2012). Although computationally expensive, dynamic downscaling at optimized spatial and temporal scales offers a robust method for simulating locally relevant phenomena under changing climate conditions (Wood et al., 2004; Xu & Yang, 2012).

The selection of a GCM for downscaling required careful consideration of how well the primary climate model performs over the Indian region. For accurate fire weather predictions, the model needed to capture the distinct climatic patterns that influence fire activity across India's diverse forest landscapes. The CESM was selected based on its established performance in simulating climate processes over India. CESM is a widely used model and is validated in various studies for the Indian subcontinent. Its inclusion in numerous regional climate assessments further shows its reliability in capturing the meteorological variables required for fire weather estimation. Additionally, CESM projections were available in a bias-corrected form, which is useful for minimizing model errors and aligning the simulations with observed climate data. This correction enhances the credibility of using CESM output for further downscaling. This ensures that the downscaled results are both accurate and suitable for regional-level analyses. While CMIP6 data has recently become available, bias-corrected outputs are not yet widely accessible. This further justified the use of CESM from CMIP5 for our study, as it offers a validated, bias-corrected dataset that supports the high-resolution downscaling needed for fire weather computations in the Indian context (Hurrell et al., 2013; van Vuuren et al., 2011). Thus, CESM was chosen to provide a robust foundation for producing downscaled climate data and reliable FWI projections over the Indian forest zones.

This coarse resolution CESMv1 climate dataset was downscaled by a popular mesoscale RCM, the WRF model (et al. Skamarock WC, 2008), to produce a high-resolution input dataset to CFFDRS-FWI at 10 km spatial resolution for the current (2006-2015) and end century (2091-2100) time periods. The 10 km spatial resolution was selected to enable detailed analyses of climate impacts and for informed decision-making on forest fires at the district level for India. With a 10 km grid spacing, as per sampling theory, the dataset will be able to resolve processes at $20\text{ km} \times 20\text{ km}$ ($= 400\text{ km}^2$). Since more than 96% of Indian districts have an area larger than 400 km^2 , this resolution was considered sufficient to skillfully represent climate variability at the district scale across most regions. While higher resolutions, such as 1-2 kilometers, could provide more accurate representation of convective processes over forest zones, it would be computationally expensive. The chosen 10 km resolution offers a cost-effective and skillful compromise, with finer details beyond this resolution appropriately addressed through parameterization. Since the performance of the WRF model is sensitive to various physical parameterizations such as cumulus, planetary boundary layer (PBL), surface layer, and radiation schemes (Gunwani et al., 2021; Gunwani & Mohan, 2017; Rai & Pattnaik, 2019), eight sensitivity experiments were conducted to find the appropriate parameterization combination over the study region. The combination that performed the best compared to reanalysis data from the ERA5 and IMDAA were selected for the downscaling.

5.2 WRF model configuration

The downscaling simulations in this study were performed using a nested grid system in the WRF model to refine the resolution of the simulations over India. In this case, the finest grid, or domain (d03), has a resolution of 10 km and covered an area of 3700

km x 3700 km (Figure 5.1). This grid was “nested” within two larger grids: the second domain (d02) with a resolution of 30 km and the largest domain (d01) with a 90 km resolution.

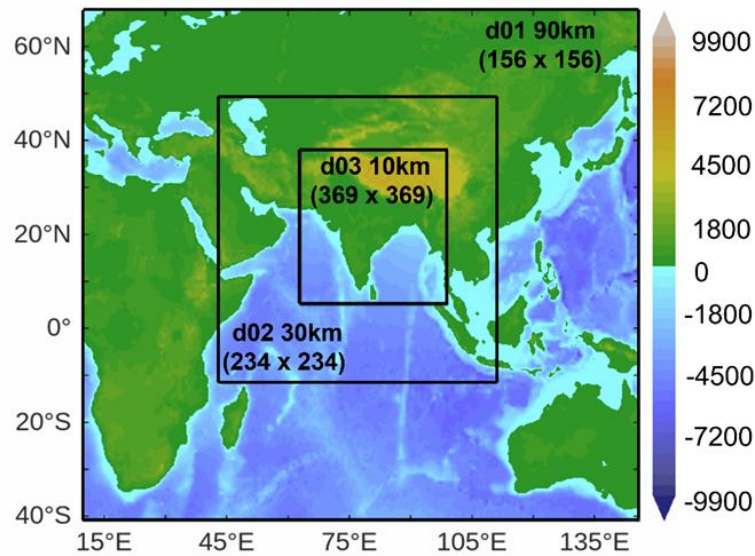


Figure 5.1: WRF simulation domains showing the topography and bathymetry (in m with respect to mean sea level) and three nested grids d01, d02 and d03 at resolutions 90 km, 30 km, and 10 km, respectively

Table 5.1: Nested Grid Configuration in WRF Simulations

Domain Name	Resolution	Time Step
d01	90 km	270 seconds
d02	30 km	90 seconds
d03	10 km	30 seconds

Nesting allows the model to focus computational power on smaller areas while still capturing large-scale atmospheric patterns from the outer grids. The simulation's time steps were adjusted for each grid to ensure numerical stability and accuracy. Time steps were set at 270 seconds (d01), 90 seconds (d02), and 30 seconds (d03), with shorter intervals for finer grids because of their higher resolution. Shorter time steps

reduce numerical errors by ensuring the calculations between each model step account for rapid atmospheric changes in higher-resolution areas.

The initial and boundary conditions, which are the starting atmospheric states and the external conditions influencing the model, were provided by a coarser-resolution climate model, the CESM bias-corrected dataset. These inputs were updated every six hours to keep the simulations aligned with the GCM data. This method ensures that the smaller grids (d03) receive the necessary large-scale information from the coarser grids to simulate the local atmosphere more accurately.

Hourly values of downscaled atmospheric parameters were saved as output to capture detailed, high-resolution data. Saving data at hourly intervals provides a fine temporal resolution, allowing for a more thorough analysis of weather and climate patterns, which is critical for studying short-term variations and extreme events.

5.3 Sensitivity analysis to select parameterization schemes

Parameterization is crucial in numerical weather prediction models like the WRF model because it represents the physical processes that occur at scales smaller than the model's grid resolution. These processes include cloud formation, radiation transfer, surface-atmosphere interactions, and more. The WRF model offers a variety of parameterization schemes to represent different physical processes. These include microphysics, cumulus convection, planetary boundary layer (PBL), surface layer, radiation, and land surface schemes. Each scheme has its own set of assumptions and formulations that influence how specific processes are simulated. A literature survey was conducted to identify parameterization schemes that have been successfully used in simulations over the Indian region. Based on this, the WRF model was configured using these schemes:

Radiation Schemes:

The Dudhia scheme (Dudhia, 1989) was used to simulate shortwave radiation transfer. The Rapid Radiative Transfer Model (RRTM) (Mlawer et al., 1997) was employed for longwave radiation transfer. These radiation schemes have been found to effectively simulate the sensitivity of Indian meteorological features, particularly the summer monsoon (Andraju et al., 2019; R. Patil & Kumar, 2016; Ratnam et al., 2017).

Land Surface Scheme:

The NOAH-MP land surface scheme (Niu et al., 2011) was selected to provide the bottom boundary conditions to the atmosphere. NOAH-MP is a multi-parameterization scheme that includes advanced canopy and soil moisture computations, enhancing the simulation of surface fluxes and soil moisture (Niu et al., 2011; Reddy et al., 2020). This scheme has shown better performance in simulating precipitation over the core monsoon area in India (Attada et al., 2018).

Surface Layer Scheme:

The MM5 surface layer scheme (Paulson, 1970), which uses the Monin-Obukhov similarity theory to compute surface exchange coefficients for heat, moisture, and momentum, was utilized. This scheme has provided satisfactory results in simulations over India (R. Patil & Kumar, 2016)

In addition to the above-mentioned parameterization schemes used for the dynamic downscaling of CESMv1, the WRF model also requires schemes to simulate atmospheric microphysics, planetary boundary layer (PBL) transport and cumulus convection. However, there is no consensus in the literature about the best possible schemes for these processes over the Indian region. Past works over this region have

used The Yonsei University Scheme (YSU) non-local scheme (Hong et al., 2006) and Mellor-Yamada-Janjic (MYJ) local closure scheme (Janjić, 2000) to simulate PBL dynamics (Andraju et al., 2019; Ratnam et al., 2017), WSM6 (Hong et al., 2006) and Thompson (Thompson et al., 2008) schemes to simulate microphysics (Andraju et al., 2019; Rajeevan et al., 2010; Ratnam et al., 2017), and Betts Miller Janjic (BMJ) (Janjic, 2002) and Kain–Fritsch (KF) (Kain & Kain, 2004) schemes to simulate cumulus convective processes (Rajeevan et al., 2010; Ratnam et al., 2017; Reddy et al., 2020; Srinivas et al., 2013) over India. Sensitivity experiments (Table 5.1) were conducted using various combinations of these physical parameterizations to identify the ideal model configuration over our domain.

Table 5.2: Physics parameterization combinations for the sensitivity experiments

Sr. No.	PBL Scheme	Microphysics Scheme	Cumulus Scheme
SET 1	YSU	WSM6	BMJ
SET 2	YSU	WSM6	KF
SET 3	YSU	Thompson	BMJ
SET 4	YSU	Thompson	KF

SET 5	MYJ	WSM6	BMJ
SET 6	MYJ	WSM6	KF
SET 7	MYJ	Thompson	BMJ
SET 8	MYJ	Thompson	KF

WRF downscaling simulations are typically conducted by initializing the model and running it continuously for the desired time period. Some studies show that continuous month-long runs can lead to model drift (Qian et al., 2003; Tian et al., 2020; Xia et al., 2017). In contrast, other studies have found that WRF downscaling for a month-long continuous run is the optimal choice for their area of interest (Tian et al., 2020). To test the performance of these two approaches, each of the eight test simulations (Table 2) was performed by two methods:

1. Reinitialization approach where the model is initialized at 00 UTC of each day and run for 24 hours. Outputs from 30 consecutive day-long runs are concatenated to generate a month-long downscaled dataset.
2. Continuous approach where the model is initialized at 00 UTC of the first day of the month and run for 30 days straight to generate a month-long downscaled dataset.

The sensitivity simulations were conducted for the months of January (dry season) and July (wet season) for the normal monsoon year 2006, which was wetter than the usual year 2007 and drier than the usual year 2009. With eight parameterization combinations and two types of initializations for 2 months in 3 different years led to a total of 96 month-long simulations.

To test the performance of the model, the January and July simulated 2m Temperature (T2m) and July Precipitation for the three years were compared with the IMDAA reanalysis data. The IMDAA reanalysis dataset accurately captures Indian weather patterns, particularly monsoon variability (Ashrit et al., 2020; Singh et al., 2021). Hence, it was used to evaluate the different experiments. The simulated data was regridded from 10 km to 12km resolution to match the IMDAA resolution. The area outside the geographical boundaries of India was masked out, and grid-to-grid monthly average T2m and monthly accumulated precipitation were statistically compared against the respective IMDAA grid values. The Pearson's correlation coefficient (R), root mean square error (RMSE), and standard deviation (ρ) of each simulated dataset compared with the IMDAA data were computed and depicted in a Taylor diagram.

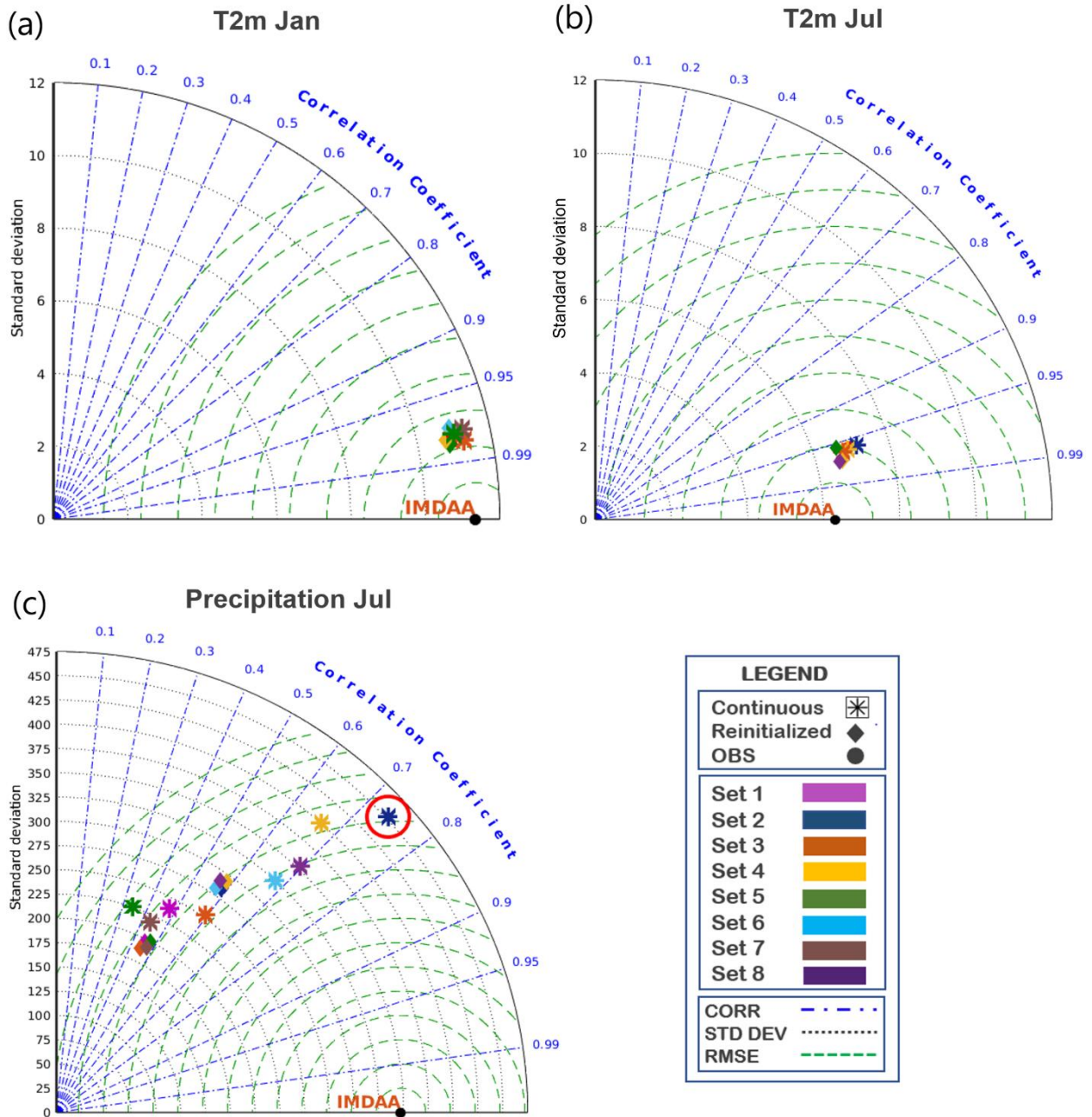


Figure 5. 2: Taylor Diagram of sensitivity experiments vs IMDAA reanalysis dataset of monthly mean 2m-temperature for (a) January and (b) July, and (c) total monthly precipitation for July.

Taylor diagrams are widely used for comparing the performance of multiple models or experiments against observations. This is a well-suited method to determine the best performing experiment statistically. In these diagrams, the pixel-by-pixel similarity in

patterns between the simulated and observed variables is represented by the correlation coefficient (R), shown by the azimuthal angle. The observed value is always positioned on the x-axis, where the azimuthal angle is 0, corresponding to $R=1$. The root mean square error (RMSE) is indicated by the distance between the model and observation points. At the same time, the standard deviation (ρ) is depicted by the radial distance from the origin. Therefore, the model value closest to the observed value is the best performer, as it exhibits high correlation, low RMSE, and similar ρ to the observation.

The results in Figure 5.2 indicate that for a 2-meter temperature, all experiments produced similar outcomes for both winter (January) and monsoon (July) seasons. In each case, the correlation was high, the RMSE was low, and the standard deviations were close to those of the IMDAA data. This shows that all experiments successfully simulated daily temperature patterns. For precipitation, the RMSE values were within a similar range across all combinations. The differences in standard deviation compared to IMDAA were also similarly distributed. Based on this, the Set 2 was selected, which had the highest correlation value ($R = 0.74$). This set used the YSU scheme for PBL, WSM6 for microphysics, and KF for cumulus parameterization.

The results also demonstrated that the reinitialization approach did not offer any significant advantage over continuous simulations for the domain and resolutions used. Additionally, the reinitialization approach was found to be slightly more computationally expensive than the continuous method. Therefore, the continuous approach using Set 2 was chosen for the downscaling simulations.

5.4 Evaluation of downscaled data

Using the model configuration described above, the bias-corrected CESM data was downscaled for the two study periods - baseline and end-century. The DSCESM data are provided at an hourly frequency in UTC hours. These UTC outputs were converted to Indian Standard Time (IST) as for FWI estimation, temperature, wind speed and relative humidity is required at 12 noon of the local time. Daily time series (TS), monthly TS, and monthly climatology for eight variables (as listed in Table 5.3) were computed for the current and future ten-year periods. These variables include minimum and maximum temperature, wind speed, relative humidity, precipitation, downward shortwave flux at the ground surface, outgoing longwave radiation, mean surface sensible and latent heat fluxes. Standardized formats of these variables are archived in the dataset repository. For this, the maximum and minimum temperatures are estimated by taking the highest and lowest values, respectively, from the 24-hour IST data. Daily total precipitation was computed by aggregating the 24-hour rainfall values. These daily values were added (for total precipitation) or averaged (for other variables) over a month to obtain the monthly TS, and mean values for each month were calculated to obtain the monthly climatology dataset. These standardised variables are evaluated against reanalysis and station data.

Table 5.3: List of variables in the DSCESM dataset

Variable short name	Variable long name	Variable Description	Dataset Description			Units
			Daily TS Dataset	Monthly TS dataset	Monthly climatology dataset	

t2m_mean	Mean 2m Temperature	Air temperature at 2m above land surface	Daily average of 24hrs (00IST-00IST) 2m air temperature	Monthly average of 2m air temperature	Monthly climatology of 2m air temperature	K
t2m_max	Maximum 2m Temperature	The highest temperature of the air at 2m above land surface since the time it was last archived	Daily highest (00IST-00IST) 2m air temperature documented	Monthly average of highest 2m air temperatures documented for each day.	Monthly climatology of highest 2m air temperatures	K
t2m_min	Minimum 2m Temperature	Lowest temperature of air at 2m above land surface since the time it was last archived	Daily lowest (00IST-00IST) 2m air temperature documented	Monthly average of lowest 2m air temperatures documented for each day.	Monthly climatology of lowest 2m air temperatures	K
precip	Total Precipitation	Combined large-scale and convective rainfall	Daily Accumulated (00IST-00IST) total precipitation	Monthly aggregated total precipitation	Monthly climatology of aggregated total precipitation	mm
rh	Relative Humidity	Water vapor pressure expressed as percentage of value at which air begins to get saturated	Daily average of 24hrs (00IST-00IST) relative humidity	Monthly average of relative humidity	Monthly climatology of relative humidity	%

wspd	Wind Speed	The magnitude of wind computed from the zonal and meridional components at 10m above land surface	Daily average of 24hrs (00IST-00IST) wind speed	Monthly average of wind speed	Monthly climatology of wind speed computed for 10 years	m s-1
sw	Downward shortwave flux at ground surface	Amount of solar radiation that reaches a model grid box at the surface of the Earth	Daily average of 24hrs (00IST-00IST) surface shortwave radiation	Monthly average of surface shortwave radiation	Monthly climatology of surface shortwave radiation computed for 10 years	W m-2 (Positive values denote downward fluxes)
lw	TOA outgoing longwave radiation (OLR)	The thermal/longwave radiation emitted to space at the top of the atmosphere (TOA)	Daily average of 24hrs (00IST-00IST) surface OLR	Monthly average of surface OLR	Monthly climatology of surface OLR computed for 10 years	W m-2 (Positive values denote outgoing fluxes)

shf	Mean surface sensible heat flux	Transfer of heat between land and atmosphere due to turbulent motion	Daily average of 24hrs (00IST-00IST) surface sensible heat flux	Monthly average of surface sensible heat flux	Monthly climatology of surface sensible heat flux computed for 10 years	W m-2 (Positive values denote downward fluxes)
lhf	Mean surface latent heat flux	Transfer of latent heat between land and atmosphere due to water phase change	Daily average of 24hrs (00IST-00IST) surface latent heat flux	Monthly average of surface latent heat flux	Monthly climatology of surface latent heat flux computed for 10 years	W m-2 (Positive values denote downward fluxes)

For evaluation, the DSCESM variables were statistically evaluated against the IMDAA and ERA5 reanalyses as well as GSOD observations for the period 2006-2015 on various temporal frequencies. The metrics used to assess the performance of the dataset are Pearson's correlation coefficient (r), standard deviation (p), Root Mean Square Error (RMSE), and bias. The p , RMSE, and bias statistics were normalized by dividing their values with corresponding annual mean so the performance of different variables can be compared. These statistics were plotted in Taylor diagrams (Figure 5.3 (a)).

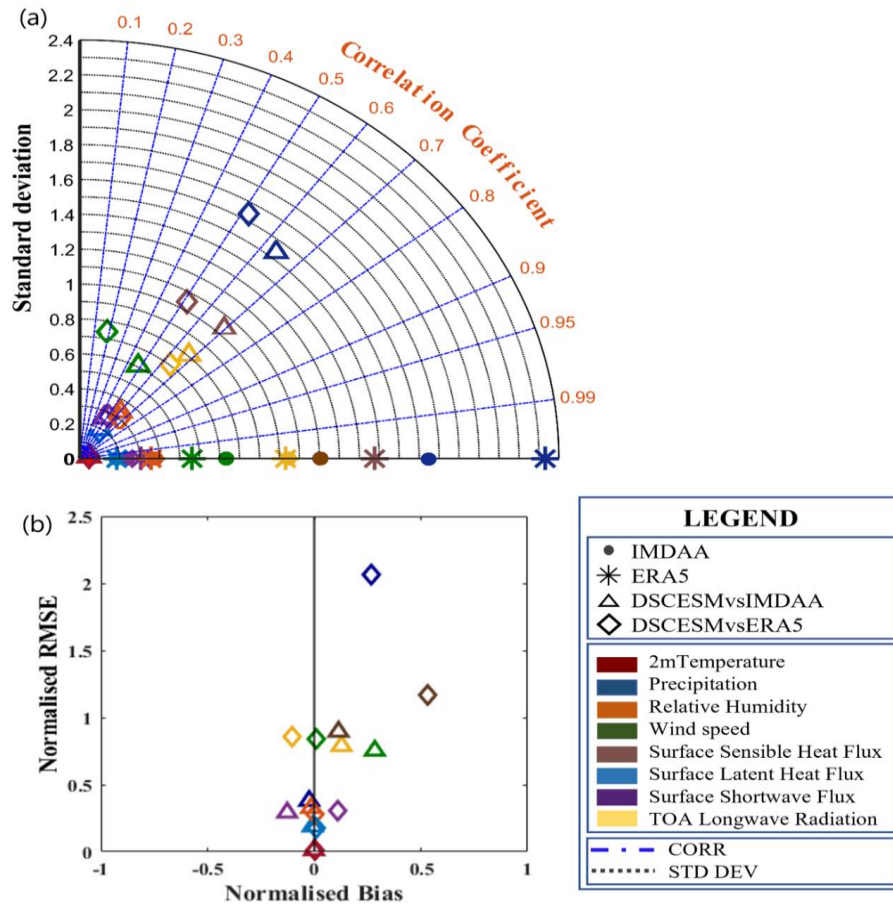


Figure 5.3: (a) Taylor Diagram and (b) the RMSE vs BIAS diagram of DSCESM daily variables against IMDAA and ERA5 reanalysis variables.

Also, the RMSE and bias were plotted against each other (panel b). Then, the RMSE of monthly averages of all DSCESM variables were compared to IMDAA and ERA5 at every grid point in the domain (Figure 5.4). These maps give us an idea of the spatial pattern of the performance of the downscaled variables.

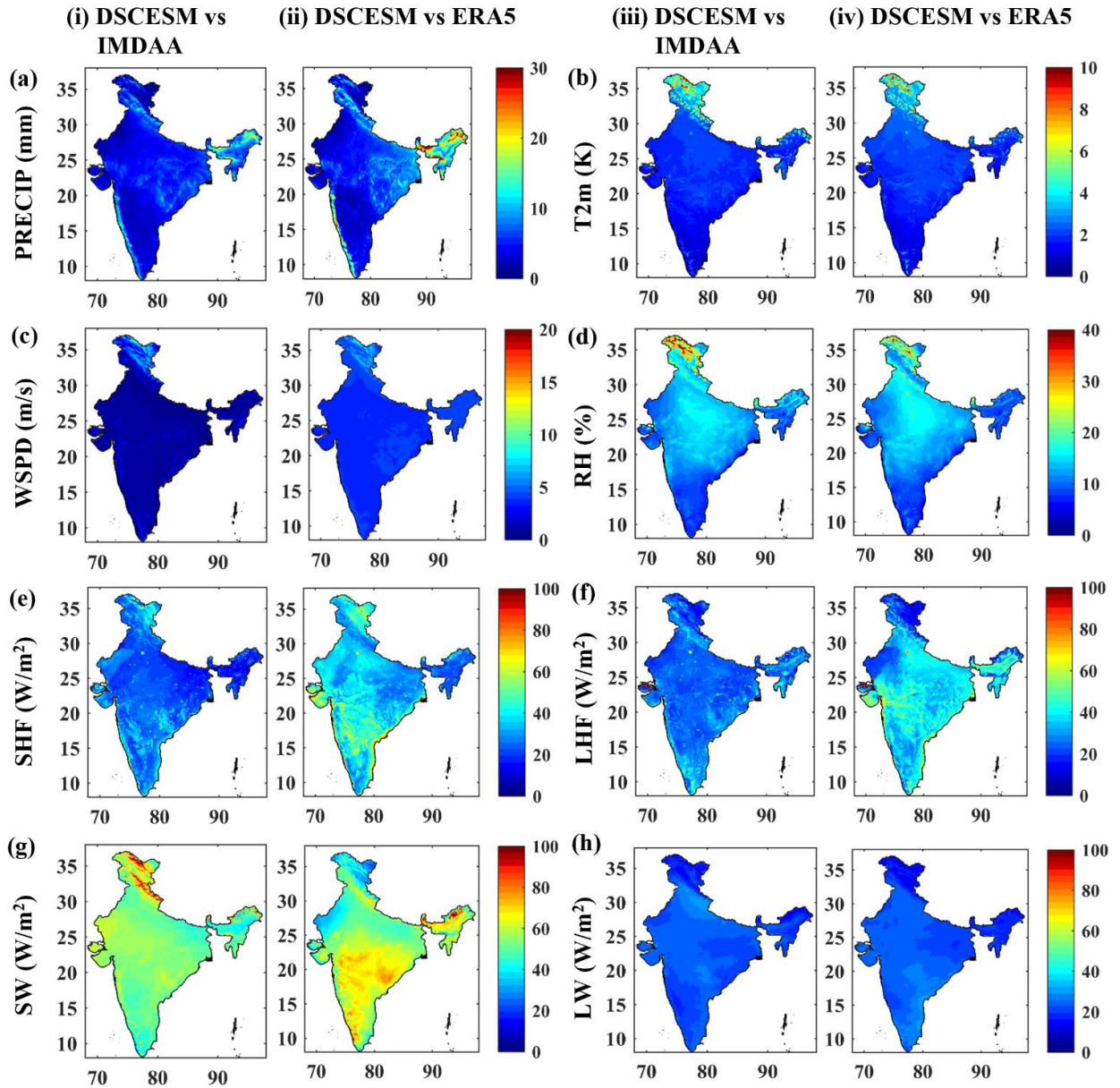


Figure 5.4: RMSE of (a) monthly accumulated precipitation and monthly means of (b) 2m temperature (K), (c) wind speed (m/s), (d) relative humidity (%), (e) sensible heat flux (W/m^2), (f) latent heat flux (W/m^2), (g) downward surface shortwave radiation (W/m^2) and (h) outgoing long wave radiation (W/m^2) with respect to IMDAA (column i and iii) and ERA5 (column ii and iv) reanalyses.

Then, the monthly climatology of the downscaled DSCESM variables was compared with the reanalysis datasets (Figure 5.5).

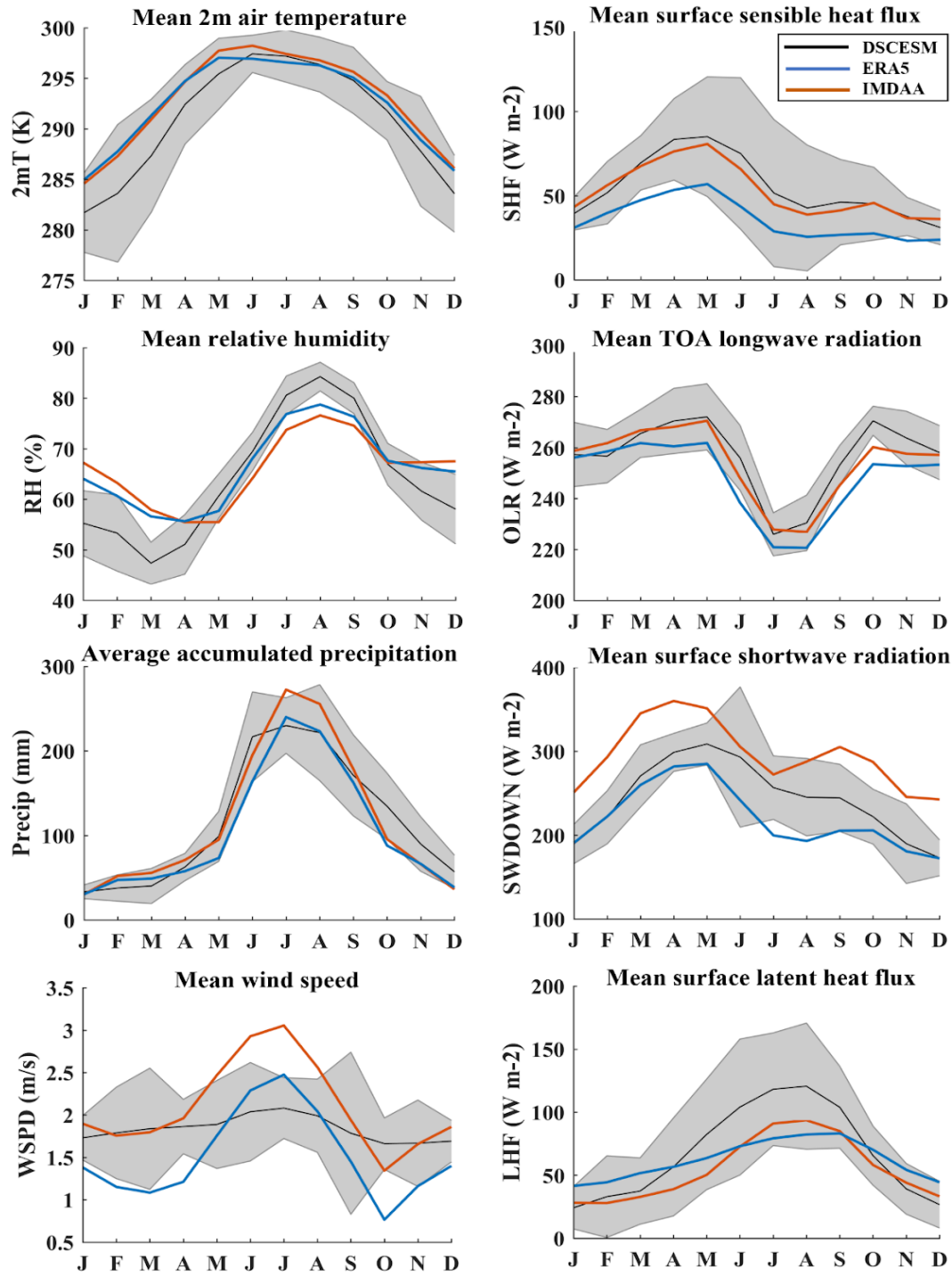


Figure 5.5: Seasonal cycle of DSCESM variables (black) in comparison with the IMDAA (orange) and ERA5 (blue). The grey shaded area represents the DSCESM uncertainty (one standard deviation).

The Probability Density Functions (PDFs) of the DSCESM monthly climatology variables at every grid cell were also computed and plotted against the PDFs of reanalysis datasets. PDFs are particularly useful to understand how well a model simulated data captures the distribution of observed values. Moreover, the PDFs are sensitive to localized differences. This allows us to analyze if the model can represent both mean and extreme events.

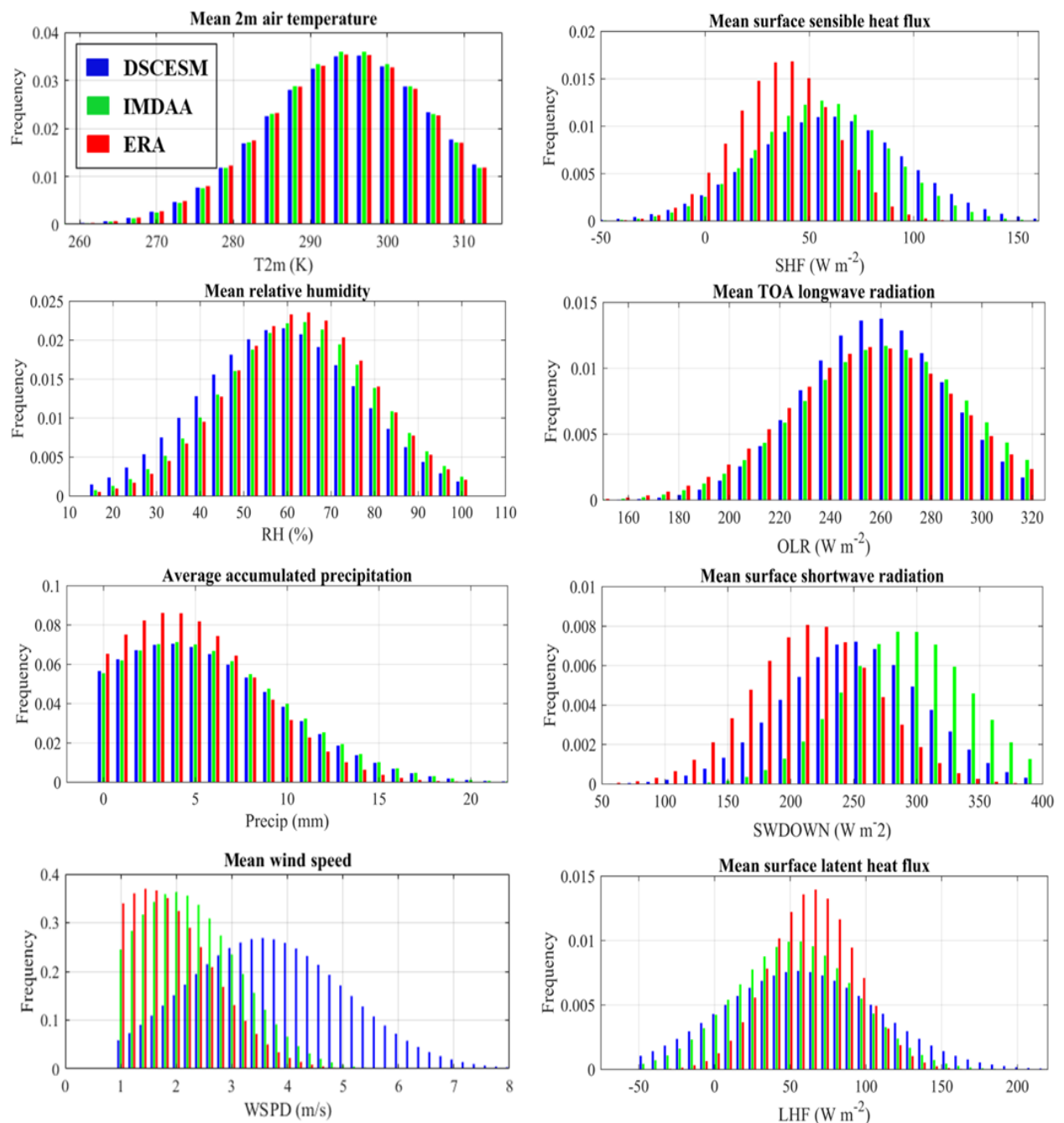


Figure 5.6: Probability distribution functions (PDFs) of the 10-year average values of DSCESM variables (blue), IMDAA (Green) and ERA5 (red).

Temperature, relative humidity, wind speed and precipitation for the period 2006-2015 from the raw CESMv1 and DSCESM were retrieved at all the 60 GSOD station locations within India. Correlation of daily climatology of these datasets and GSOD observations were computed and plotted (Figure 5.7).

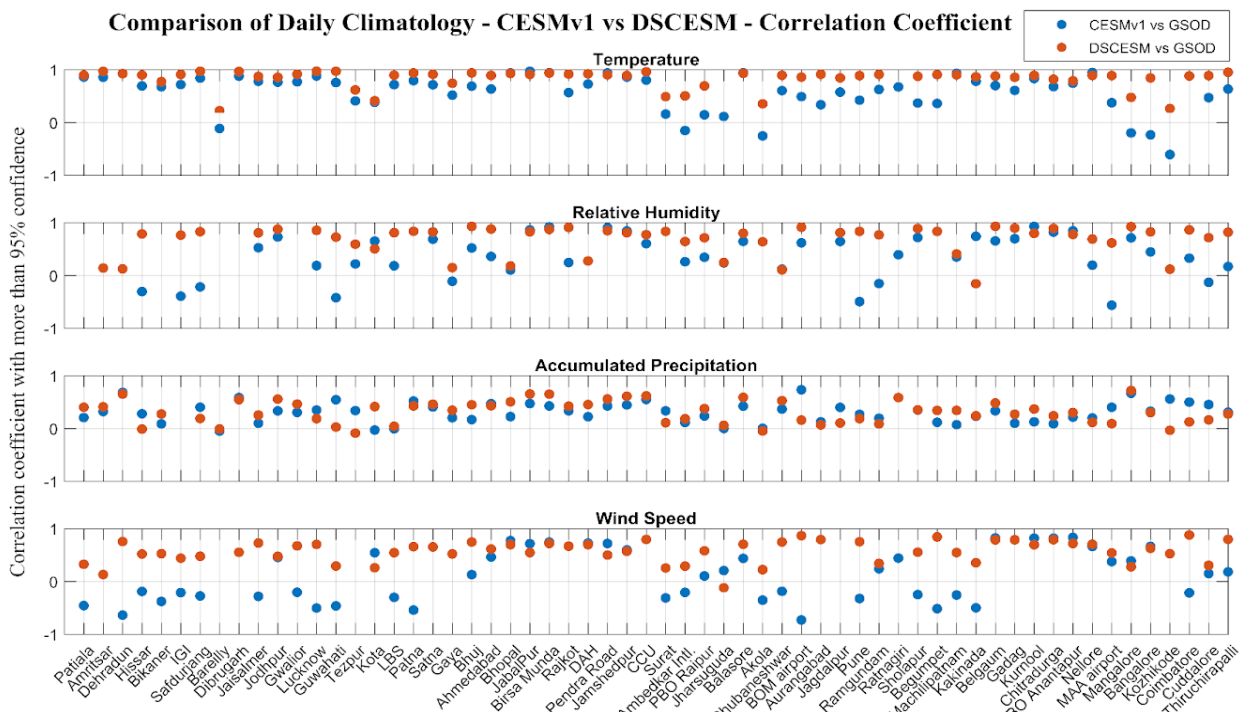


Figure 5.7: Location wise Pearson's correlation coefficients for daily climatology of CESMv1 and DSCESM against GSOD station observations from 2006-2015

Figures 5.3a and 5.3b show the Taylor diagram and the RMSE-bias plot for the DSCESM data, respectively. The 2m Temperature shows reasonably good performance with high R (~0.97) and almost equal DSCESM and reanalysis p. The overall R values of other variables are above 0.5, and their ps are comparable to that

of the corresponding reanalyses. In Figure 5.3b it can be observed that 2m temperature depicts negligible bias as well as RMSE with both the reanalyses. The performance of the DSCESM relative humidity and latent heat flux fares well against the reanalyses, suggesting reliable future estimates of the variables. The mean surface latent heat and the shortwave radiation fluxes show positive and negative biases for IMDAA and ERA5, respectively, denoting the slight underestimation of the variables compared to IMDAA and overestimation compared to ERA5.

Figure 5.4 shows the RMSE of monthly accumulated precipitation as well as monthly averages of other DSCESM variables compared to IMDAA and ERA5 at every grid point in the domain. These maps give us an idea of the spatial pattern of the performance of the downscaled variables. Accurate simulation of daily precipitation characteristics over the Indian region has been a challenge for the scientific community. The coarse-resolution uncorrected CESM1 outputs are known to have shortcomings, such as underestimation of rainfall over Northern India and the Bay of Bengal and poor prediction of the rainfall extremes over the region (Xia et al., 2017). The chances of transmission of these systematic errors in precipitation have been reduced by the bias correction prior to downscaling. Though the RMSE of precipitation remains low throughout the country with a value of about ~5-10 mm, the error is comparatively higher in the complex terrains of the Northeast and Western Ghats along the west coast of India (Figure 5.4a). Overall DSCESM precipitation can satisfactorily capture the rainfall pattern over India. Hence, the downscaled mid and end century precipitation can be used to study various rainfall-based processes in the future scenario at high resolution.

The RMSE values of monthly DSCESM 2m temperature is consistent at about 1 K throughout the country with slightly larger errors 4-6° K over the Northern Himalayan

region (Figure 5.4b). As observed from Figure 4c, monthly averaged DSCESM wind speed performs better against IMDAA as compared to ERA5, with very consistent RMSE throughout the country. Relative humidity estimates fare better in the coastal, Southern and Northeast India (Figure 5.4d). The error in the heat flux variables is low at about 10% of their maximum values as compared to the IMDAA dataset. However, higher error values are observed at the urban clusters (Figure 5.4e, 5.4f). Outgoing Longwave Radiation (OLR) estimates are better with lower RMSE values, about 5% of maximum values (Figure 5.4h), than those of shortwave estimates, which are about 20% of the maximum values (Figure 5.4g). Consistent with all the variables, the high-resolution estimates show an overall low RMSE with IMDAA reanalysis as compared to ERA5.

In Figure 5.5, the monthly climatology of the downscaled DSCESM variables with the reanalysis datasets (ERA5 and IMDAA) was compared. This assesses how well the DSCESM captures the seasonal variations of different climate variables. For each variable, the solid lines represent the datasets, while the shading indicates the spread of downscaled data.

It was observed that the DSCESM 2m air temperature captures the general seasonal trend, showing a peak during the pre-monsoon months of May and June. However, DSCESM tends to underestimate temperatures slightly compared to ERA5 and IMD, particularly during the pre-monsoon period. The alignment between the datasets is closer during the post-monsoon and winter months, where the temperature differences become minimal. In the case of average accumulated precipitation, DSCESM matches more closely with ERA5 than with IMDAA. However, both the reanalyses curves lie within the spread of the DSCESM data, indicating that the downscaled data successfully captures the range of precipitation variability. This suggests that

DSCESM is able to reproduce the general seasonal pattern and intensity of precipitation over India. In the case of mean wind speed, DSCESM shows less pronounced seasonal variation compared to both ERA5 and IMDAA. While the reanalyses show a strong increase in wind speeds during the pre-monsoon season, DSCESM maintains more consistent values throughout the year. This indicates that the downscaled model may smooth out some of the seasonal extremes present in the reanalysis data. For relative humidity, DSCESM aligns well with ERA5 and IMDAA, showing lower humidity levels before the monsoon and a significant increase during the monsoon. However, seasonal dynamics are more pronounced in DSCESM, especially in the pre and post-monsoon seasons.

Other variables, including surface sensible heat flux and latent heat flux, show good agreement between DSCESM and the reanalyses, with some variations during the pre-monsoon period. Shortwave radiation and TOA longwave radiation follow similar seasonal cycles in all datasets. Overall, DSCESM demonstrates a strong ability to capture seasonal variations, particularly in temperature and precipitation, while showing some smoothing of wind speed seasonal patterns. Its spread encompasses both the reanalyses signatures. This shows the reliability of the downscaled variables.

Overall, the results show that the seasonal variability pattern of the downscaled variables is similar to the IMDAA and ERA5 seasonality. The reanalyses monthly climatology values are within one standard deviation of the DSCESM values for most cases.

From the PDF analysis (Figure 5.6), it was understood how well a model simulated data captures the distribution of observed values. Moreover, the PDFs are sensitive to localized differences. This allows us to analyze if the model can represent both

mean and extreme events. It was observed that the distribution of DSCESM 2m temperature, relative humidity and longwave were in agreement with those of ERA5 and IMDAA. In the case of precipitation and sensible heat flux, the DSCESM frequencies match more with IMDAA than ERA. For latent heat flux and shortwave, the DSCESM frequencies are in between those of ERA and IMDAA. The downscaled output overestimates the spread of wind speed as compared to the reanalyses, which is also clear from the monthly climatological mean in Figure 5.5. Corrective measure was taken prior to using the DSCESM wind speed in FWI calculations as explained in section 5.6.

In Figure 5.7, temperature, relative humidity, wind speed and precipitation for the period 2006-2015 from the raw CESMv1 and DSCESM were retrieved at all the 60 GSOD station locations within India, and Pearson's correlation coefficient of daily climatology of these variables and GSOD observations were plotted. It was observed that in most of the stations, the downscaled variables are in better agreement with the station observations compared to the raw data. Out of the 55 stations where the correlation coefficient is statistically significant for temperature, 45 stations show improved correlation after downscaling, and the rest of the stations show almost negligible change. For relative humidity, out of the 48 statistically significant stations, 33 stations show a significant improvement in correlation, and about eight stations depict similar r values. Thirty-three stations show that the precipitation amount simulated by DSCESM is a better estimate of the variable as compared to raw CESM, with some stations in Northeast India and along the Western Ghats having not much improvement in the r . In almost all these station locations, wind speed shows considerable improvement in correlation.

The monthly mean temperature and accumulated precipitation of DSCESM was also compared with the Coordinated Regional Climate Downscaling Experiment-South Asia (CORDEX-SA) against GSOD station observations over India for 2006-2015. For this, the monthly mean temperature and precipitation data were retrieved from both CORDEX-SA and DSCESM datasets for the period 2006-2015 at GSOD locations and correlation coefficient values were computed. The DSCESM dataset, which uses a finer 10 km resolution, showed a significantly better correlation with the GSOD observations compared to the coarser CORDEX-SA dataset (Figure 5.8). This indicates that the DSCESM dataset provides a more accurate representation of local climate conditions, demonstrating its added value for detailed climate impact studies and for this study.

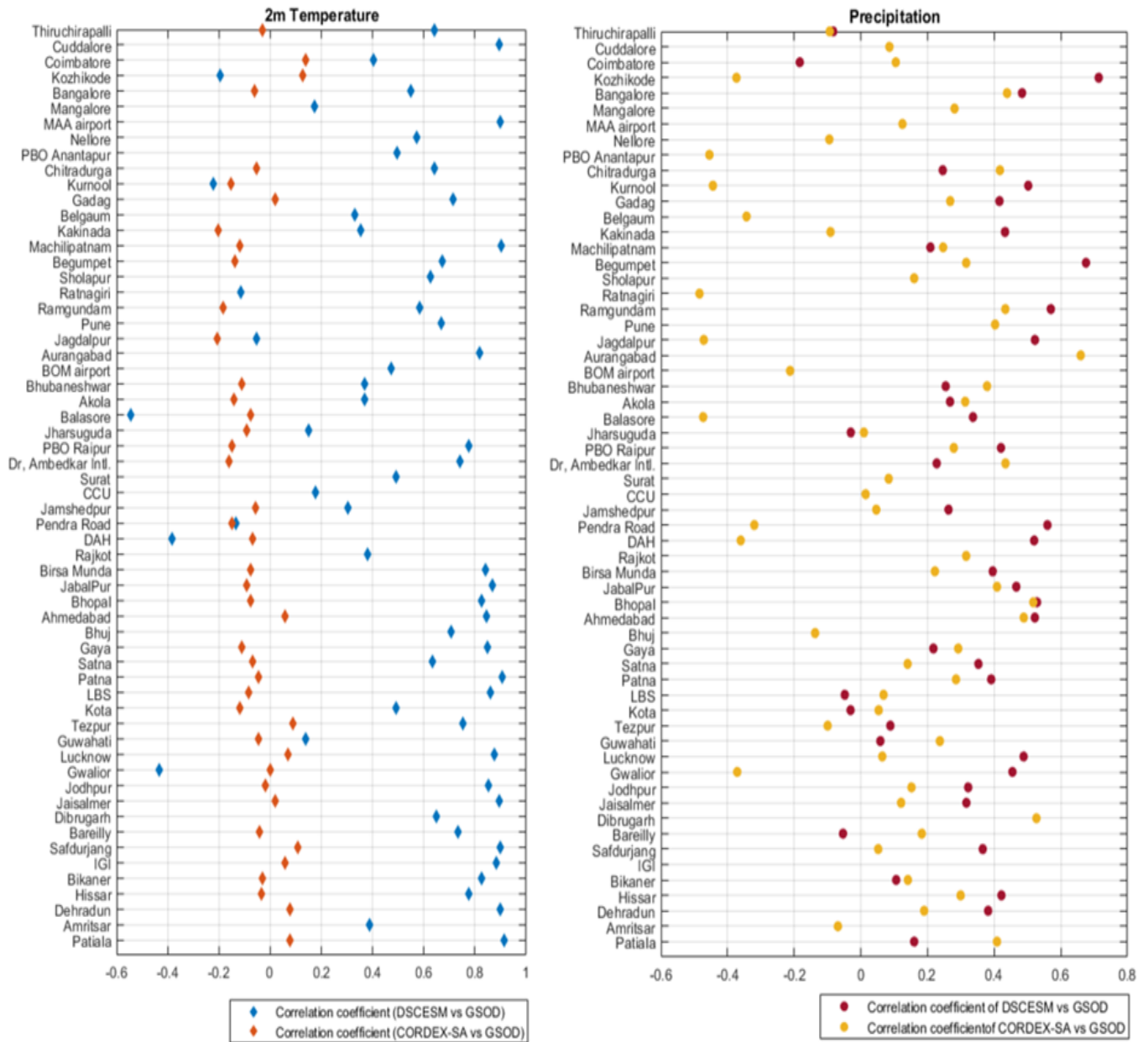


Figure 5.8: Comparison of correlation coefficients of GSOD observations with DSCESM and CORDEX-SA for monthly mean 2m temperature and monthly accumulated precipitation.

Overall, the performance of the downscaling is satisfactory as the DSCESM variables adequately match the GSOD observations as well as IMDAA and ERA5 reanalysis daily, monthly and climatology patterns.

5.5 DSCESM data archival with DKRZ

The DSCESM dataset (https://doi.org/10.26050/WDCC/WRF10km_wbc_C5_forc_oIndia and https://doi.org/10.26050/WDCC/WRF10_wbc_C5_forcIndia_MC_V2) (Barik et al., 2021) provides climate projections for three time periods: current (2006-2015), mid-century (2041-2050), and end-century (2091-2100), based on the RCP8.5 scenario over India. These projections were generated by dynamically downscaling bias-corrected CESM1 output using the WRF model at a 10 km spatial resolution. The dataset spans the Indian region on a 369 x 369 grid, with areas outside India masked out. Data is offered at three temporal resolutions: daily, monthly, and monthly climatology, across 10 meteorological variables (see Table 2), along with latitude, longitude, and time details. The dataset is structured into 90 NetCDF files (10 variables x 3 temporal resolutions x 3 periods), with daily, monthly, and climatology files containing 369x369x3650, 369x369x30, and 369x369x12 data points, respectively, totalling approximately 120 GB in size. Detailed metadata about the files is included with the dataset. The file naming convention follows:

2006-2015: Current_XXX_YYY.nc

2041-2050: MidCenturyRCP85_XXX_YYY.nc

2091-2100: EndCenturyRCP85_XXX_YYY.nc

Here, "XXX" indicates the temporal resolution and "YYY" represents the variable short name as defined in Table 5.2. The WRF-ARW source codes and tutorials are provided

as an open-source model, accessible on NCAR's website (https://www2.mmm.ucar.edu/wrf/users/download/get_sources.html). The WRF model configurations, specified in the namelist, can be found in the WRF_namelist.pdf file available on GitHub (https://github.com/anasuya993/postprocessing_DSCEM). The WRF codes were compiled and executed on Linux servers, which required licensed compilers and libraries, such as NetCDF and Jasper.

Postprocessing of the downscaled data was done using MATLAB. The scripts for converting hourly WRF outputs from UTC to IST, generating daily and monthly time series, and creating NetCDF files for monthly climatology are provided in the same Github repository in the form of self-explanatory *.m MATLAB codes. Further details are available in the repository's readme file.

5.6 Bias correction of DSCEM wind speed

To check for biases in variables, all four variables of DSCEM dataset (averaged over India) was compared with the mean of 35 GSOD station data (both averaged over 2006-2015). A consistent bias in wind speed was observed (Figure 5.9), but the biases in other variables are well within limits. The downscaled output overestimates the spread of wind speed as compared to the GSOD and also the reanalyses, which is clear from the monthly climatological mean in Figure 5.5. Thus, suitable corrections prior to using the DSCEM wind speed are recommended. The downscaled wind speed from the DSCEM dataset was bias-corrected for the baseline period against the GSOD observations. All the 35 GSOD stations within our FWI zones with continuous wind speed data for our baseline period were selected. Then, the correction was computed using two popular methods: linear scaling and variance scaling. For the linear scaling method, a linear correction value by subtracting the

monthly mean value of DSCESM wind speed extracted at the GSOD station locations from their respective monthly mean values of GSOD wind speed for each of the 12 months was computed.

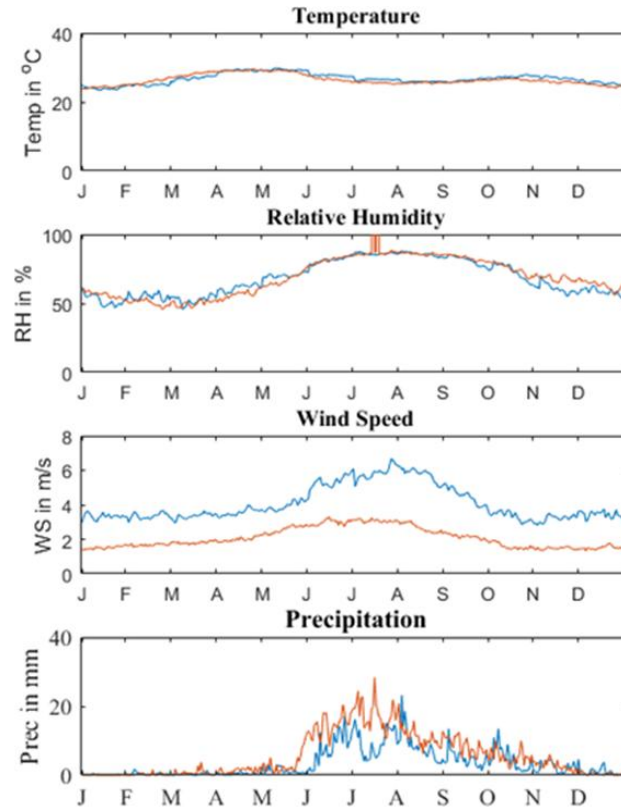


Figure 5.9: Bias of DSCESM climatology with GSOD station data observations

This correction value was applied to the DSCESM daily wind speed value at all grid points (eq. A1).

$$WS_{baseline}^* = WS_{baseline} + \mu_m WS_{GSOD} - \mu_m WS_{baseline} , \quad (eq. A1)$$

The correction value in the variance scaling method is computed using both the mean and variance of the daily wind speed dataset. In this approach, first, the daily linear scaled correction value for all stations is calculated (Eq. A2). The mean of this daily dataset is then subtracted to shift the values to a zero mean (Eq. A3). This zero-mean

dataset is subsequently scaled by applying the ratio of the standard deviations between the GSOD dataset and the dataset's own standard deviation (Eq. A4). Finally, the mean value, which was previously subtracted, is added back to the scaled values (Eq. A5).

$$WS_{baseline}^{*1} = WS_{baseline} + \mu_d WS_{GSOD} - \mu_d WS_{baseline} , \quad (\text{eq. A2})$$

$$WS_{baseline}^{*2} = WS_{baseline}^{*1} - (\mu_d WS_{baseline}^{*1}), \quad (\text{eq. A3})$$

$$WS_{baseline}^{*3} = WS_{baseline}^{*2} \times (\sigma_d WS_{GSOD} / \sigma_d WS_{baseline}^{*1}), \quad (\text{eq. A4})$$

$$WS_{baseline}^{*} = WS_{baseline}^{*3} + (\mu_d WS_{baseline}^{*1}) \quad (\text{eq. A5})$$

When the two bias-corrected outputs were compared, it was observed that the statistically linear scaling approach performed better than the variance scaling approach. The quantile-quantile map of linear scaling bias-corrected, and variance scaling bias corrected wind speeds were also plotted, each with daily ERA5 reanalysis wind speed for the period 2006-2015 (Figure 5.9). In the linear scaling approach, the fitted distribution closely follows the reference line (Figure 5.9(a)). It shows the distribution of linear scaling bias corrected DSCESM follow that of ERA5. In the variance scaling approach (Figure 5.9(b)), at the higher values of wind speed, the fitted distribution deviates to the left from the reference line, indicating an overestimation of the bias-corrected data. Thus, a linear scaling approach was selected to bias correct the daily baseline as well as end-century wind speeds.

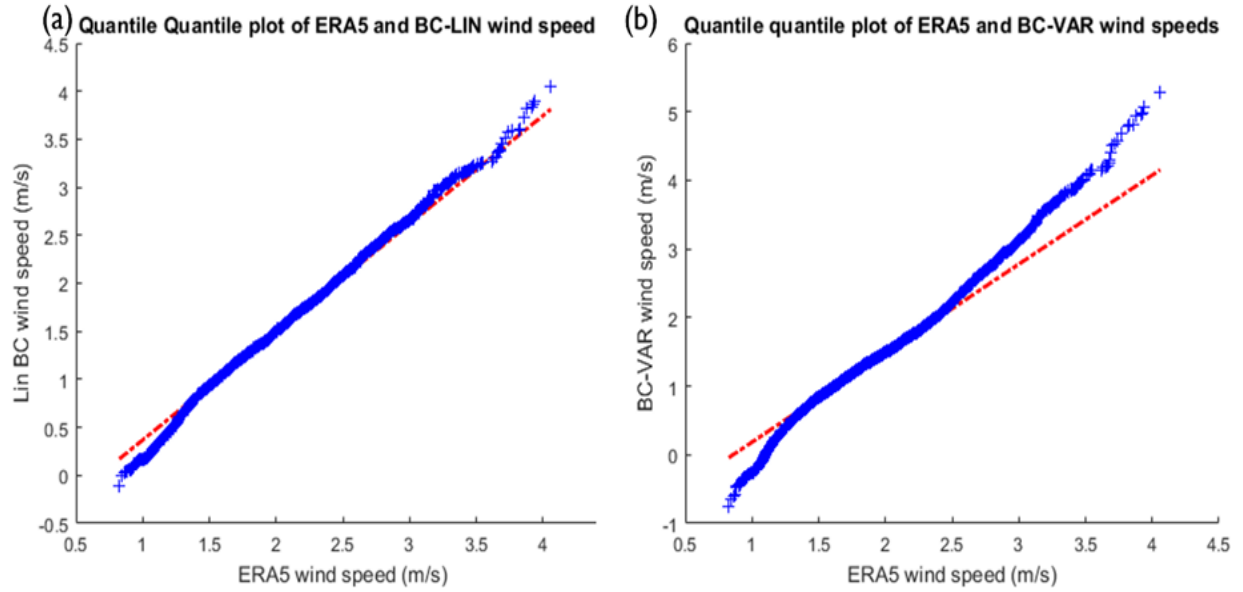


Figure 5.10: Quantile-quantile plot of daily ERA5 wind speed with (a) linear scaling bias corrected wind speed and (b) variance scaling bias corrected wind speed. The dotted red line denotes the normal reference line, and the blue markers denote the quantile of x quantity plotted against the quantiles of y quantity.

After the application of the linear correction values, the bias at all 35 GSOD stations were recomputed. The bias-corrected wind speed, when compared at every grid point against the ERA5 reanalyses, also showed considerable improvement (Figure 5.10).

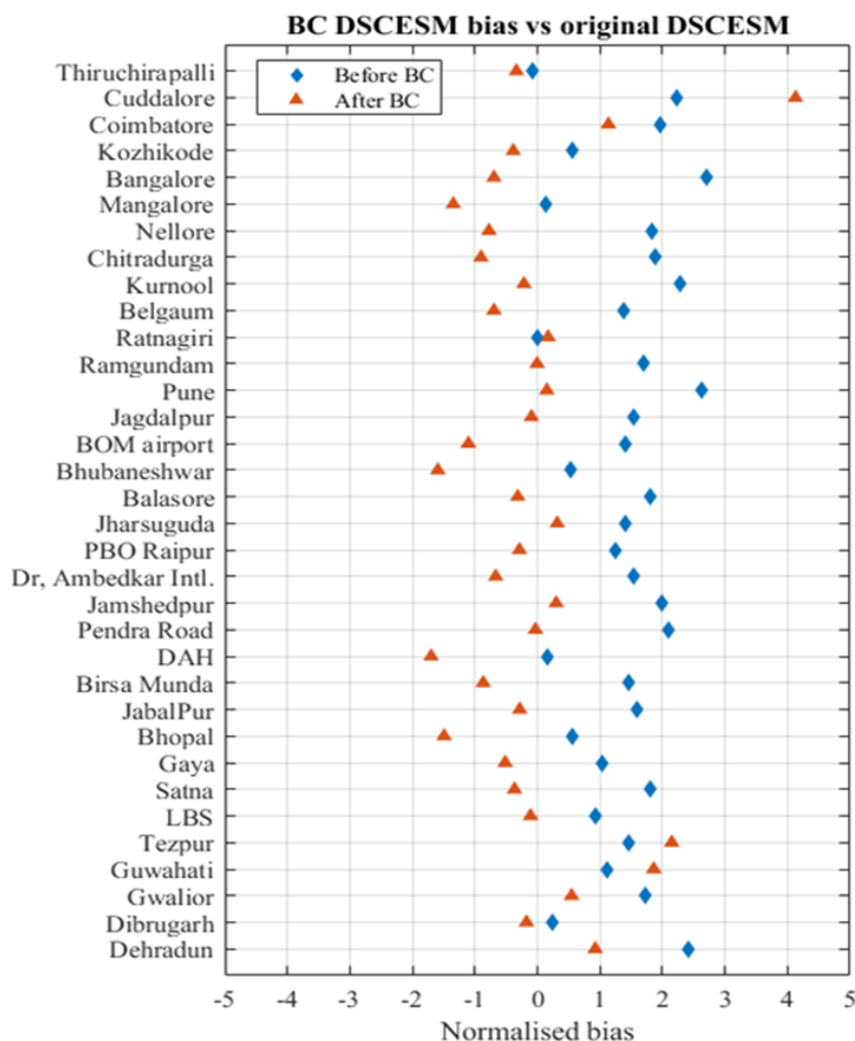


Figure 5.11: Comparison of correlation coefficients of GSOD observations with DSCESM and CORDEX-SA for monthly mean 2m temperature and monthly accumulated precipitation.

Then, the linear correction was assumed to be consistent for the entire analysis period and hence applied to the baseline as well as end-century daily wind speed at every grid point (Eq. no. A6).

$$WS_{\text{endcentury}}^* = WS_{\text{endcentury}} + \mu WS_{\text{GSOD}} - \mu WS_{\text{baseline}}, \quad (\text{eq. A6})$$

Overall, the performance of the downscaling was found to be satisfactory, as the DSCESM variables show a strong match with GSOD observations, as well as the

IMDAA and ERA5 reanalysis for daily, monthly, and climatology patterns. The results from the extensive evaluation suggest that downscaling improves the quality of climate projections at finer spatial scales. This enhanced granularity allows for a more detailed understanding of regional climate dynamics.

In this study, multiple precautions were taken to ensure the reliability of the downscaled product. The WRF model, known for its strong performance in the Indian region, was chosen for the downscaling process. Sensitivity experiments were conducted to fine-tune the model to align the simulated data more towards the observational data. Rigorous validation was carried out to assess the downscaling performance, and parameterization schemes were selected based on their effectiveness over the specific domain. The DSCESM results demonstrate a closer match to historical observations compared to the raw CESM outputs. Thus, confidence in the robustness of the downscaling approach and tool is high. Using different GCMs and RCMs might yield varying results and provide a range of climate projections. However, such an endeavour would be computationally expensive.

In conclusion, the downscaled high-resolution DSCESM is a reliable product, and it can be effectively utilized to assess climate change impacts on fire weather in India.

Chapter 6

Effect of climate change on fire weather index

6.1 Introduction

This chapter explores the impact of climate change on the FWI in India by using data from the dynamically downscaled DSCESM dataset and the extensively evaluated CFFDRS-FWI algorithm. The FWI was computed across the study area of 3680 km x 3680 km, centered around India. The domain was discretized into a 10 km grid, matching the DSCESM data resolution. Simulations were conducted with a daily timestep for two distinct time slices: the baseline period (2006-2015) and the end-century period (2091-2100) under the RCP8.5 climate change scenario.

In this chapter, the changes in end-century FWI as compared with baseline values are analysed. This end-century minus baseline approach is a widely used and effective method for assessing changes in fire weather. It provides a direct measure of how fire risk evolves under future climate conditions relative to the present. The changes in mean annual FWI are evaluated, and the primary meteorological drivers of these changes are identified. Additionally, the chapter investigates changes in the number of severe fire weather days, the fire weather danger season, and the Seasonal Severity Rating (SSR) resulting from climate change. By computing changes at various temporal resolutions—daily, seasonal, and annual—different patterns of fire behavior and risk are analysed. While seasonal and annual assessments help in understanding long-term shifts in fire danger and developing broader fire management strategies, change in number of days with severe fire weather captures changes in extreme fire weather signatures. This multi-temporal analysis ensures that strategies can be tailored effectively to different time scales and levels of risk.

6.2 FWI computation for baseline and end-century

All components of the Fire Weather Index (FWI) system were computed using the CFFDRS-FWI module with DSCESM meteorological input for the baseline period (2006–2015) and the end-century period (2091–2100). As per the requirement of the CFFDRS-FWI model, 12 noon IST values of 2 m temperature and relative humidity were retrieved from the hourly output of raw DSCESM. The 12-noon values of wind speed were bias corrected using the linear bias correction method discussed in Section 5.6, and 12 noon IST—12 noon IST accumulated precipitation was computed from the hourly raw DSCESM outputs. For both periods, the system was initialized with default FFMC, DMC, and DC values of 85, 6, and 15, respectively, for every forested grid cell and run for 5 years. Even though the spin-up period required is much less for the system to produce stable outputs, a spin-up of 5 years ensured the reliability of the actual simulations used in the analysis. The FFMC, DMC, and DC values for each forest grid cell at the end of the spin-up simulation were used to initialize that grid cell for the actual 10-year simulations for the baseline and future scenarios. The final output FWI dataset was created at a daily temporal resolution and a spatial resolution of 10×10 km for both periods.

6.3 Change in mean annual FWI by end-century

The climatological change in FWI was computed by subtracting the baseline 10-year average from the end-century 10-year average. Out of the four variables of temperature, relative humidity, precipitation, and wind speed, four sensitivity experiments were

conducted to identify the major contributors to the climatological change in FWI. Each experiment used end-century values for one variable while retaining baseline values for other variables. This approach separated the individual impacts of each variable on future FWI changes. For each spatial pixel, the variable with the highest sensitivity relative to baseline FWI was identified as the major contributor to future FWI change. A modified scale based on De Martonne's aridity index (Martonne, 1923; Ullah et al., 2022) was used to classify the forest grids into arid, intermediate, and humid categories. Pixels with index values less than 20 were classified as arid, those with values between 20 and 35 as intermediate, and those with values greater than 35 as humid. All the contributor variables were then analyzed against this modified aridity index.

A non-parametric probability density estimation of daily FWI was performed within each FWI zone using Epanechnikov KDE with an optimally computed bandwidth for both the baseline and end-century periods. The Epanechnikov KDE is often preferred over other types, such as the Gaussian KDE, due to its advantages regarding the bias and variance trade-off, which is critical in FWI studies. It minimizes mean integrated squared error, resulting in lower variance and controlled bias, which is crucial for precise density estimation of fire weather indices. Its robustness to outliers further enhances its suitability for comparing FWI in two-time slices. The shift in average daily FWI for each zone was calculated using the Bootstrap confidence interval for the mean parameter at a $p < 0.05$. This bootstrapping method optimizes the length of the confidence interval and is less conservative compared to the asymptotic method. This approach ensured that changes in fire weather danger by the end-century were not underestimated. The number of days

exceeding thresholds of Medium, High, and Very High fire danger was also computed for both periods. The baseline values and the difference between the end-century and baseline severe fire weather days were plotted spatially, and changes observed were analysed.

The projected change in annual mean FWI was analyzed by comparing the end-century average FWI with the baseline (Figure. 6.1 (a)). It was observed that fire weather is projected to show a mixed signal of increase and decrease across different forest zones of India. FWI is projected to increase in the northern CEN zone, southern WG, NE, and most of the HIM zone. Conversely, a decrease in mean projected FWI is seen in western CEN and northern WG. To understand the underlying reasons for these changes, a map was plotted to show which variable contributes most to the FWI change for each pixel (Figure. 6.1 (i)(b)). The information regarding the dominant contributor was then compared with a modified de Martonne's aridity index for each pixel. In arid and intermediate regions, temperature was identified as the major contributor to the projected change in FWI (Figure. 6.1 (i)(c,d)). However, in humid regions, precipitation and/or relative humidity were found to play a more significant role than temperature (Figure. 6.1 (i)(e)). For instance, in the humid NE zone, a major decrease in climatological FWI is expected due to an increase in annual precipitation. In contrast, the decrease in climatological FWI in the humid northern WG region is primarily governed by an increase in relative humidity. Temperature is recognized as the dominant factor driving the change in future FWI in the arid and intermediate regions of CEN, southern WG, and DEC.

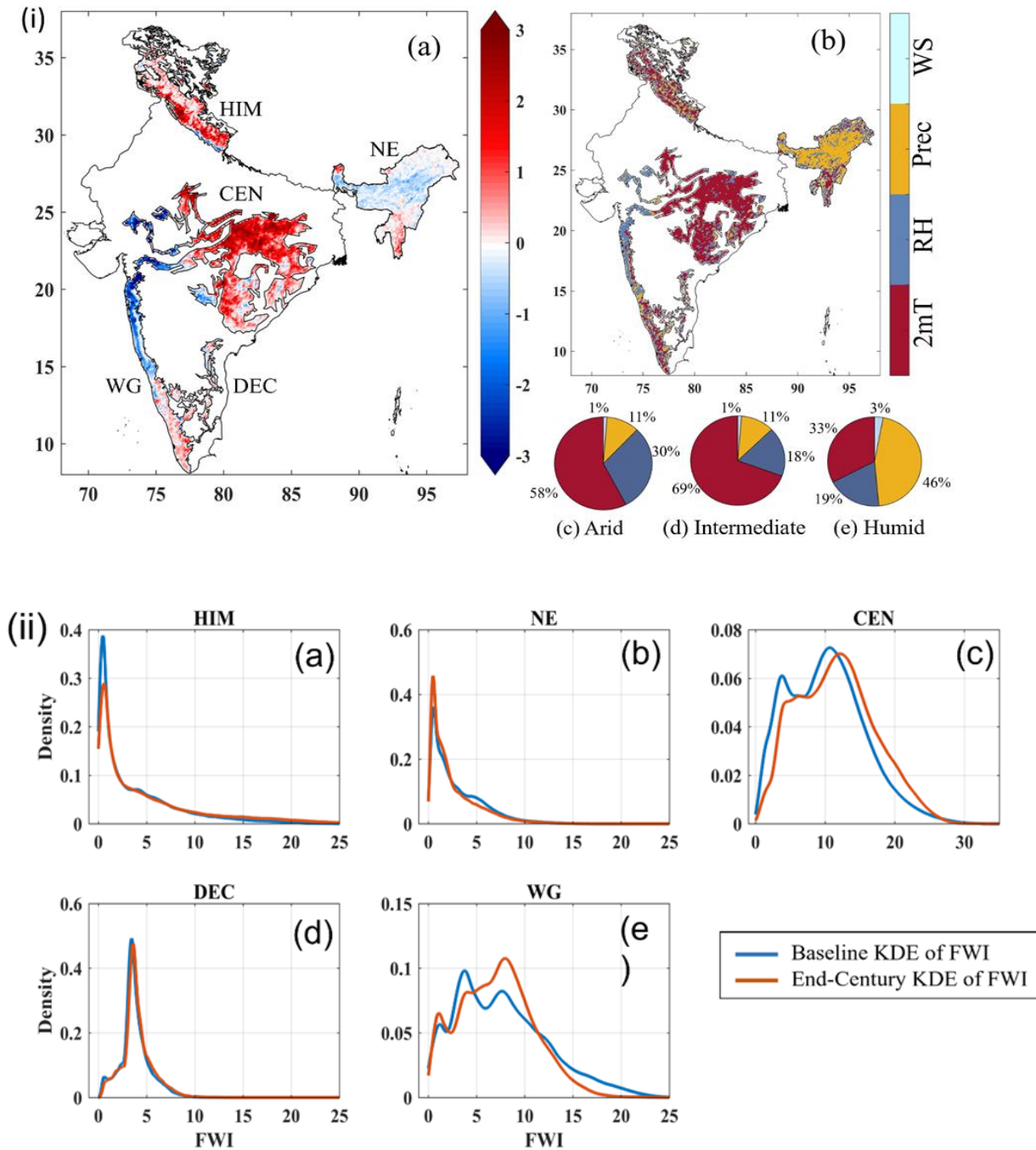


Figure 6.1: (i)(a) Spatial map of the change in mean annual FWI between baseline and end-century, (b) variable contribution resulting in this change, pie charts of dominant contributor in (c) arid, (d) intermediate, and (e) humid regions and (ii) Kernel density estimation (KDE) for baseline and future daily FWI for different FWI zones

To analyze the expected change in the mean annual shift in FWI by the end-century, the Kernel Density Estimation (KDE) distribution of mean FWI was computed for different forest zones for both time slices. The KDE distribution curves in all zones were found to be multimodal (Figure. 4(ii)). In the CEN zone, where a hot and arid climate persists for most of the year, the distribution curve is skewed toward higher FWI values (Peel et al., 2007). Conversely, in the NE and HIM regions, the values are skewed primarily to the left, indicating comparatively lower overall FWI values. This can be attributed to the relatively colder temperate temperatures in HIM. In NE, the lower FWI values are mainly due to the wetter tropical monsoon climate. Although NE has a distinct peak in KDE at low FWI values, the frequency and severity of fires in these regions remain high due to factors such as terrain, species composition, and ignition sources (Badarinath et al., 2007; Fulé et al., 2021). This observation justifies the necessity for a lower danger threshold in this region.

In WG, several peaks in KDE are observed. The peaks corresponding to low FWI values can be linked to the humid climate prevailing in that zone during the southwest monsoon season. Heavy precipitation during this period inhibits fire occurrences. The minimal fire activity during low FWI periods maintains a higher fire danger threshold compared to NE.

The KDE curves for the end-century shift toward the right from the baseline, with a significance level of $p > 0.05$ in all forest zones. This indicates that, overall, higher FWI values are expected in the end-century compared to the baseline for a particular value of probability density. To quantify the extent of the shift in FWI by the end-century,

bootstrapped mean values of the kernel distributions at 95% significance were computed. The results show an overall increase of 5-10% in mean FWI by the end-century. The CEN region exhibits the maximum difference of about 0.54, while the least difference is found in the NE zone at about 0.09 FWI. Additionally, some parts of the KDE curve in NE and WG (Figure. 6.1 (ii)(a,c)) indicate that the end-century curve shifts to the right, signifying lower future FWI in those areas.

6.4 Change in spatial pattern of severe FWI days

In this section, the spatial pattern of expected changes in severe fire weather days by end-century was analysed. The analysis of the number of days exceeding thresholds, as developed in the FDRS system, focuses on the frequency of extreme fire danger conditions. This provides insights into how often severe fire weather is likely to occur in baseline and how this frequency would change in the future. This differs from the mean change in FWI analysis, which reflects overall shifts in average fire weather conditions. While mean, FWI gives a general sense of long-term changes; the threshold-based analysis highlights potential increases in the intensity and frequency of extreme fire hazard events.

Maps were plotted to show the number of days per grid cell where FWI values exceeded Medium, High, and Very High thresholds under baseline conditions, along with projections for changes by the end of the century (Figure. 6.2). The results indicate considerable variation both between and within different forest zones. Currently, large areas of the CEN, NE, and WG forests are subject to Medium, High, and Very High fire weather for

more than 150, 50, and 30 days per year, respectively, while the HIM forests experience the lowest fire weather danger.

The most vulnerable regions include the dry deciduous forests in western CEN, moist deciduous forests in NE and northern WG, and semi-evergreen forests in southern NE (ISFR, 2021). Satellite and ground-based observations confirm that tropical dry deciduous forests in India experience the most fire events, closely followed by tropical evergreen forests (ISFR, 2021; Srivastava & Garg, 2013; Vadrevu et al., 2013; Verma et al., 2017). Similar trends are observed in tropical evergreen forests in Indonesia (Herawati & Santoso, 2011).

By the end of the century, a significant portion of forested areas is expected to experience an increase in the number of days with severe fire weather. Increases across all three danger classes are projected for moist deciduous forests in the Himalayan foothills (HIM) and southern NE, dry deciduous forests in eastern CEN and DEC, and tropical evergreen forests in northern WG. A 20-60% rise in severe FWI days is anticipated. Areas of greatest concern, where the number of extreme fire weather days may increase by 30-50 days per year, include the Cachar semi-evergreen and mixed moist deciduous forests in Tripura and Mizoram, Chir pine and Sal forests in the Himalayan foothills, northern moist evergreen forests in the Western Ghats, and southern mixed deciduous forests in Orissa and Andhra Pradesh. Similar increases in fire disturbance have been observed in the northwestern USA (Halofsky et al., 2020), projected for Canada (Augustin et al., 2022), and predicted for various regions globally (Bedia et al., 2015; Liu et al., 2010; Quilcaille et al., 2023; Scholze et al., 2006).

Certain forest areas are expected to experience a decrease in severe fire weather days. Opposite signals are noted within some forest zones, such as NE, CEN, and WG. For instance, the western part of CEN is likely to show a decrease in High and Very High FWI days by the end of the century, while the eastern part is projected to experience an increase. This is different from the signal of climatological change in FWI (Figure 6.1 i(a)). In northern CEN, although mean FWI is expected to increase in the future, the number of severe fire weather days will decrease. This reduction is attributed to the increase in temperature in the region (Figure 6.1 i(b)). However, the DSCESM precipitation projections show that the daily rainfall amounts would increase in 70% of the days in the future. More number of wetter days in an extended monsoon season would result in higher fuel moisture content and hence, fewer days with severe FWI in the future.

In WG, the northern part shows an increase in high FWI days, while the central and southern parts are expected to decrease. This contrast is explained by different variables influencing the change. In southern WG, the projected $\sim 2.1^{\circ}\text{C}$ increase in mean annual temperature drives the rise in mean FWI, while in northern WG, a 40% increase in relative humidity lowers the future FWI. However, the number of high FWI days is primarily driven by projected increases in precipitation events, which are stronger in the south than in the northern WG. In central NE, a decrease in days exceeding all three danger thresholds is expected. This is primarily due to increased mean annual rainfall, identified as the key contributor variable in that region (Figure 6.1 i(b)).

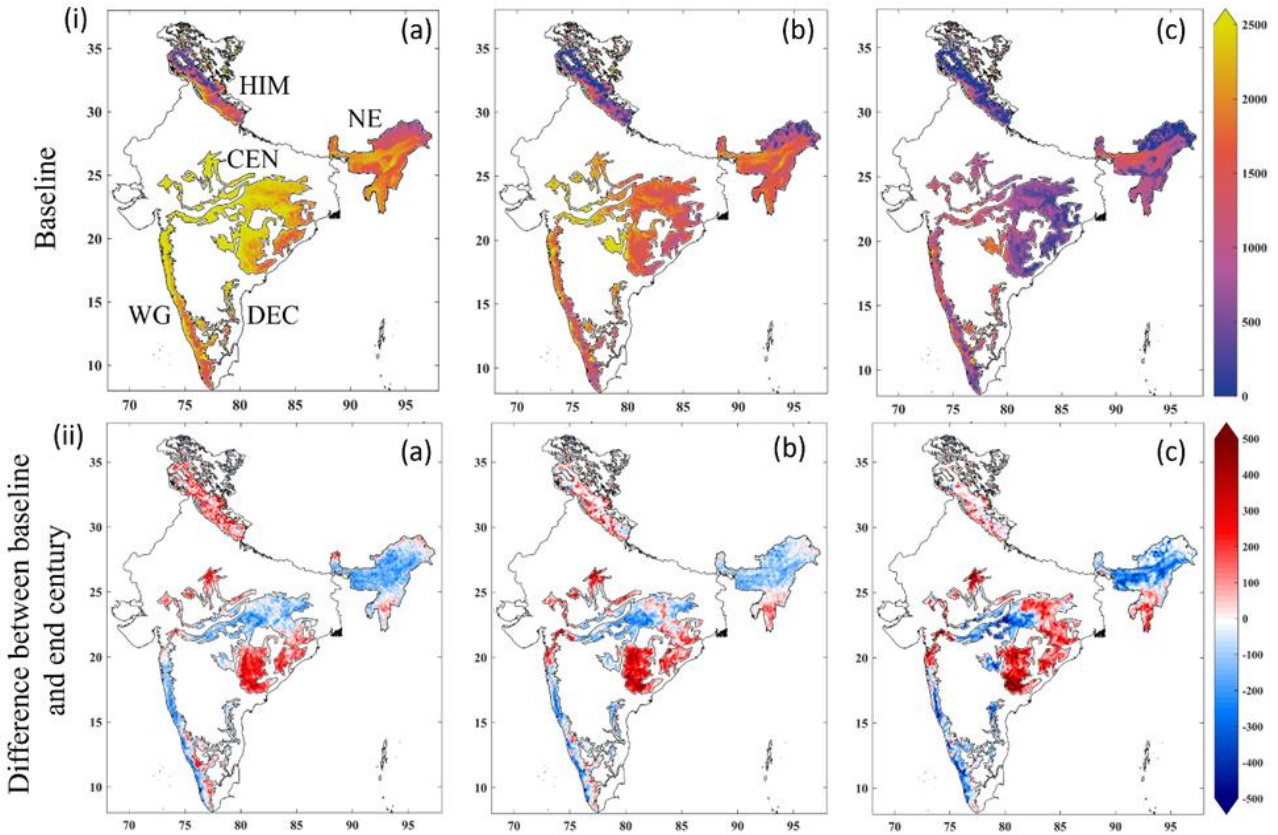


Figure 6.2: Number of days per year exceeding (a) Medium, (b) High, and (c) Very High thresholds of FWI for (i) the baseline period and (ii) change in these numbers of days expected by end-century.

6.5 Change in seasonal pattern of fire weather severity

The Seasonal Severity Rating (SSR) was used to examine the seasonal pattern of fire weather severity and its potential changes under future climate conditions. SSR, a numerical index derived from FWI, represents the level of difficulty in controlling fire events on a seasonal scale. In addition to the mean change in FWI and extreme fire weather days, the SSR offers detailed insights into how fire danger fluctuates throughout the year in baseline as well as in future. This is aimed to help in understanding the

seasonality of fire weather hazards, identifying critical periods of heightened fire risk, and developing more precise seasonal fire management strategies.

The Daily Severity Rating (DSR), an additional component of the FWI system, is a numeric measure of the difficulty of controlling fires. It is based on the FWI and represents the expected effort required for fire suppression.

$$DSR = 0.0272 * FWI^{1.77} \quad (\text{Eq.6.1})$$

Higher FWI values are emphasised through the power relation. The DSR can be accumulated over time as the cumulative DSR or averaged over time as the Seasonal Severity Rating (SSR) as in Eq. 6.2

$$SSR = \sum_{i=1}^n [DSR_i / n] \quad (\text{Eq.6.2})$$

where DSR_i is the DSR value for day i , and n is the total number of days.

SSR was computed for the baseline and future periods to analyse seasonal changes in fire danger. These parameters were filtered using forest layer shapefiles and divided into zones. A 90th percentile SSR value in the baseline scenario was used as a threshold beyond which fire potential becomes severe. The SSR thresholds for the HIM, NE, CEN, DEC, and WG zones are 0.52, 0.3, 0.59, 0.8, and 0.62, respectively.

Figure 6.3 (i) shows that MAM experiences the most extreme fire weather. According to research using satellite and ground-based observation, the majority of forest fires in India happen during this season (ISFR, 2021). In this season, the SSR exceeds the 90th

percentile severity thresholds in areas such as the northern DEC and WG zones, the western CEN, and the foothills of the western Himalayas in HIM. It is interesting to note that even during the JJA monsoon season, there is a significant level of fire weather severity in the western CEN and DEC regions. This is because the month of June typically has a high SSR before the southwesterly monsoon reaches these inland areas. When the monsoon precipitation arrives in July and August, the fire weather severity significantly drops. The lowest SSR occurs during the post-monsoon season (SON). The WG, DEC, and southwest CEN forest zones have high SSR during the winter (DJF) season.

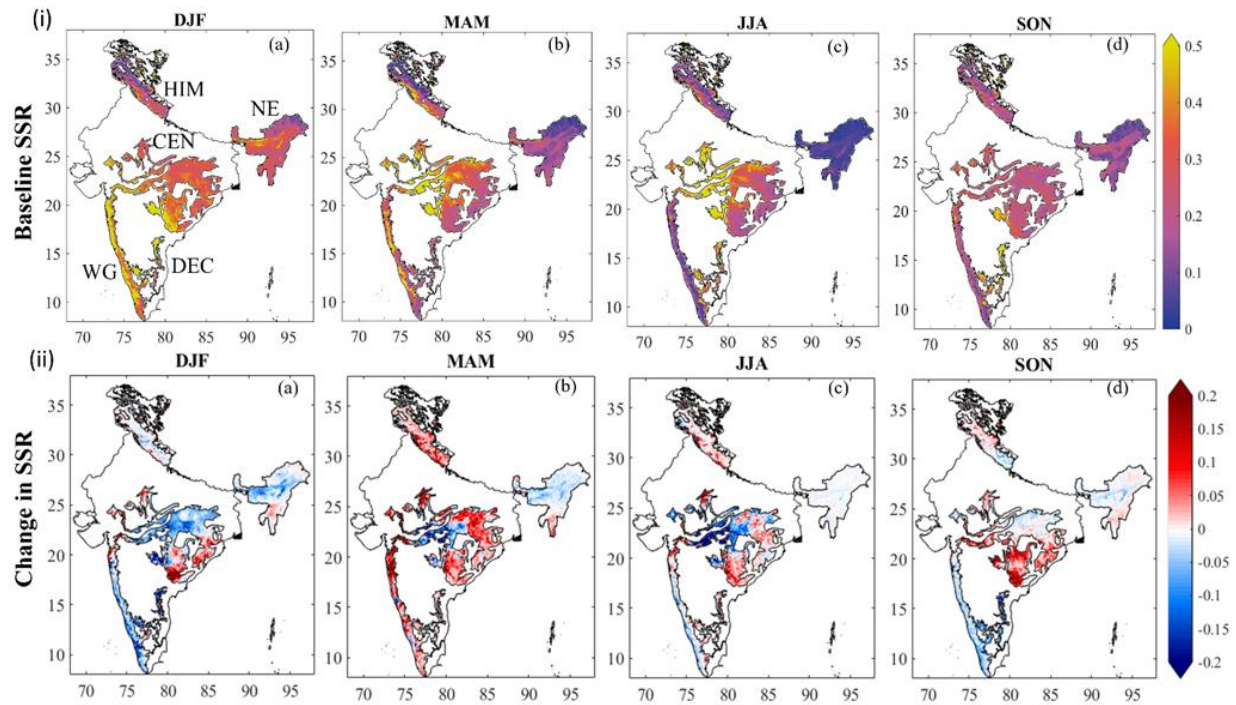


Figure 6. 3: Spatial Seasonal Severity Rating (SSR) of the (i) baseline and (ii) the difference between the end-century and baseline SSR for different seasons

The pattern of changes in end-century SSR change is mixed. Eastern CEN increases consistently throughout the year, though at different intensities (Figure. 6.3 (ii)). Only during the MAM season does the WG zone have an increasing signal; in other seasons, the signal decreases. A decrease in the number of High and Very High fire weather days is consistent with a decrease in the SSR during MAM, JJA, and DJF seasons in certain areas of the western CEN (Figure. 6.2 (ii)). By the end of the century, the most severe fire weather season of MAM can be expected to become more severe (Figure. 6.3 -iib). It is projected that the forest area whose SSR increases beyond the 90th percentile criteria will increase by approximately 34.5% compared to the baseline. A 3–5 °C increase in temperature in the western CEN will result in a 30% increase in SSR. We expect the HIM zone to become 8% drier and more than 5 °C hotter. Future temperature and RH fluctuations in this zone will likely have a combined impact on increasing the SSR in the future. The estimated ~3 °C warming in WG is expected to increase SSR. On the other hand, a 15% rise in RH and pre-monsoon precipitation will reduce the future SSR even though MAM is expected to be ~3°C warmer in the Northeast by the end-century.

In other seasons too, some interesting patterns were noticed. A 50% rise in future SSR in the HIM and eastern CEN regions and a 30% increase in DEC during the JJA monsoon season is expected (Figure. 6.3 (ii). c). This is primarily due to the fact that certain regions will see a higher increase in temperature in the future than other regions. The high SSR regions of western CEN will experience a decrease in the future. In the post-monsoon season of SON, southern parts of CEN show a high increase in SSR (Figure. 6ii(d)). This is because the southern part is projected to be drier and hotter than the northern CEN.

SSR would moderately increase by about 20-30% in some parts of HIM and NE and decrease moderately in the rest of the regions.

In DJF, forest areas exceeding the 90th percentile criteria would still experience a 26.5% increase in end-century SSR despite an estimated 20–50% decline in mean SSR across all the zones. The NE, northern WG, and western CEN zones show a significant decline in SSR in this season. Additionally, climate projections indicate that these areas will experience a 5–10% increase in precipitation by end-century. SSR is projected to increase in some parts of northern NE, eastern CEN, and the northernmost part of WG. These are the regions where projected future temperatures are higher than other regions. In general, temperature is the contributing variable in the increase in SSR throughout the year, while precipitation and RH are key contributors in decreasing the SSR. This finding is similar to the annual change signal in FWI discussed in the previous section.

6.6 Change in fire weather danger season

A 'fire weather danger season' was defined as the period when the probability of fire occurrence is elevated. This season was identified from the daily climatology curve when the FWI exceeded the Medium fire danger threshold in each zone. The fire weather danger season during the end-century period was compared with that of the baseline to assess potential increases, decreases, or shifts. It is important to distinguish the fire weather danger season from the 'fire season.' The fire season is defined as the period during which a high number of fire incidents are recorded, whereas the fire weather danger season is identified as the period when the likelihood of fire occurrence is high

due to favourable weather conditions, assuming the availability of ignition sources. Shifts in the fire weather season, driven by projections of weather variables, have significant implications in both policymaking and forest health. When the fire weather season extends into hotter months or starts earlier in the pre-monsoon period, the combination of higher temperatures and reduced humidity can lead to drier vegetation, increasing fuel availability. This creates conditions conducive to more intense and frequent fires, as drier fuels ignite more easily and spread more rapidly.

Understanding these shifts is important for developing fire management strategies. Early warning systems may need to be adjusted to alert authorities sooner in the season. Furthermore, understanding these shifts enables more accurate predictions of ecosystem responses. Extended fire seasons may disrupt forest ecosystems by increasing the frequency of fires, which can affect species that are not adapted to frequent burning. This could lead to changes in forest composition, with fire-resistant species outcompeting others. Additionally, extended seasons can cause soil degradation, reduced regeneration rates, and the loss of carbon storage capacity. This will further contribute to climate change.

In Figure. 6.4, the daily climatology of FWI for both the baseline and end-century periods is depicted, with shaded regions indicating uncertainty at a significance level of $p < 0.05$. Results demonstrate a strong periodicity in FWI across all forest zones. FWI generally peaks during the pre-monsoon season due to high temperatures and low humidity. This pattern is also observed in the SSR maps (Figure. 6.3 (i)) and observational studies. Post-monsoon, FWI declines as humidity rises. Despite this similar pattern, significant variability exists in the timing of peaks and troughs in different forest zones, making it

difficult to define a uniform fire weather danger season for all forest types. If the Medium FWI threshold is used to define the fire weather danger season, it generally begins between December and February and ends between June and September, depending on the forest zones. For example, in HIM forests, two distinct periods of high FWI are observed due to the dry pre-monsoon and winter seasons (Figure 6.4 (a)), while in DEC thorn forests, FWI peaks during the monsoon and drops sharply by late February (Figure 6.4 (d)).

Changes in the fire weather danger season are expected in the future. Figure. 6.4 shows that future FWI values are likely to increase during pre-monsoon months and decrease in winter months, a pattern consistent with the projected rise in SSR during MAM. Figure. 6.2 shows that some regions may experience an increase in Medium, High, and Very High FWI days, potentially extending the fire weather danger season. To quantify this change, the start and end days of the fire weather danger season were identified from FWI climatology (Table 1). The results show that the length of the fire weather danger season could increase by up to 61 days, with the largest increase occurring in the CEN forest zone, followed by HIM and NE zones. The nature of the change in fire weather danger season was also analysed. For example, in the CEN, HIM, and DEC zones, the season is expected to start earlier, while in NE, it would end later by approximately 15 days in April. In WG, the season would shift slightly by 5 days, maintaining almost the same length as the baseline period.

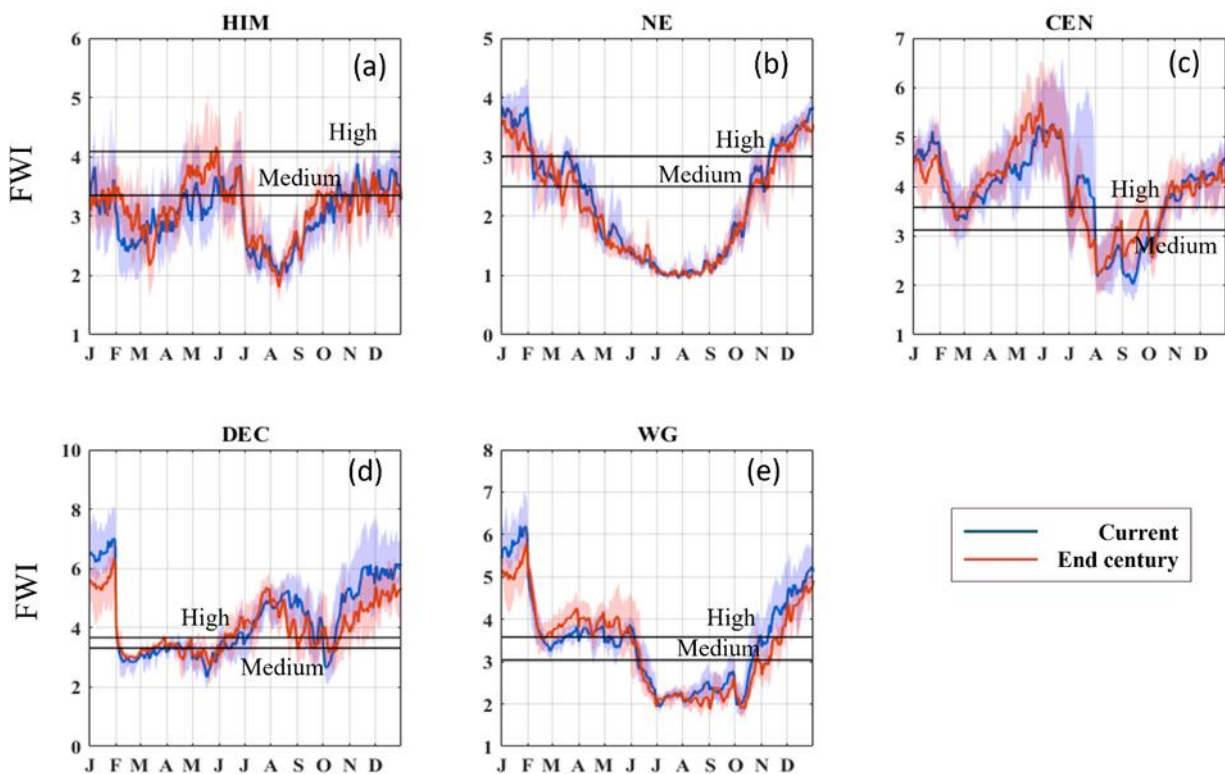


Figure 6.4: Daily FWI climatology for baseline (blue) and end-century (red) for (a) HIM, (b) NE, (c) CEN, (d) DEC, and (e) WG. The shaded region denotes the bootstrap uncertainty computed at 95% significance.

Table 6.1: Zone-wise severe fire weather danger season for baseline and end-century

Zones	Baseline severe season	Future severe season	Diff. in days	Remarks
HIM	15 th April - 25 th June	15 th April – 24 th June	33	Early start and extended end

	15 th October- 28 th January	20 th September – 10 th February		
NE	15 th October – 1 st April	15 th October – 15 th April	15	Extension of end
CEN	10 th October – 1 st August	20 th August – 20 th July	61	Early start
DEC	20 th June – 2 nd February	8 th June – 2 nd February	12	Early start
WG	15 th October – 8 th June	20 th October – 10 th June	3	Shift

Chapter 7

Conclusion and future work

Through an analysis using CFFDRS-FWI integrated with dynamically downscaled DSCESM climate projections, this work provides insights into the fire weather dynamics across India's diverse forest zones under baseline and projected end-century scenarios. By applying high-resolution land cover data, WRF modelling, and MODIS observation validation, the study ensured robust fire weather estimates. It also creates a foundation for a long-term fire hazard rating system. This chapter consolidates the main conclusions of the thesis and focuses on the novel features of the study, followed by future work recommendations.

This thesis is a comprehensive analysis of the impacts of climate change on forest fire weather in India. Most of the existing studies in the domain relating fire, weather, and climate across India are highly localized. They majorly focus on specific regions without providing a comprehensive picture of the entire country. Existing global studies, while broader in scope, generally lack the spatial resolution necessary to capture India's unique regional fire dynamics. Many such studies have generalized their inferences for the entire country. This lack of countrywide studies creates a gap in understanding fire-weather-climate interactions across India's diverse forest zones. Many forest zones are geographically distant, and their fire dynamics differ significantly. This thesis addresses this gap by using an optimal spatial resolution and by conducting analyses across defined forest zones. This approach enables a more comprehensive understanding of fire-weather-climate interactions specific to each zone. Also, countrywide meaningful insights into both current fire weather patterns and projected changes under future climate scenarios were derived.

This comprehensive approach not only fills a critical gap in understanding fire-weather dynamics across India but also establishes a foundation for future studies on analyzing fire weather behavior at both national and zonal scales. Some of the novel aspects of this thesis that contribute to advancing our knowledge in this domain are as follows:

- First, the analysis presented has an optimal spatial resolution for a countrywide analysis, which provides a unified view of fire behavior across India's diverse forest zones.
- Second, the use of the CFFDRS-FWI system was adapted for Indian forest conditions and evaluated extensively. This provides a basis for better understanding the fire-climate dynamics via a modelling approach.
- Third, this thesis developed and incorporated a high-resolution, dynamically downscaled climate dataset.
- Next, this study establishes, for the first time, a structured framework to develop an FDRS tailored for India. This framework is designed for operational use and can also support research into future fire projections.
- Finally, high-resolution projections of future fire weather were developed. Multiple approaches to quantify future fire hazards, such as fire weather danger days and mean and seasonal shifts, were analysed.

Summarizing, the introductory chapter provides a broad context, focusing on the prevalence of forest fires in India and the mechanism of how they are affected by climatic variables. A literature review establishes that a quantitative analysis of fire weather changes in a climate change context has not been adequately addressed for India. The chapter also identifies the need for high-resolution climate data and a country-wide FDRS,

establishing a research gap. These gaps lead to the formulation of the thesis objectives. In the second chapter, spatial and temporal patterns of forest fires in India based on satellite data were analysed. The key objective here was to map the distribution of forest fires across different forest zones and to determine the seasonal variations in fire occurrences. Using MODIS fire data and high-resolution land cover maps, this analysis shows significant heterogeneity in fire activity across forest types. Specific zones where fires are more frequent and high-frequency periods or major fire seasons during the year were identified. In Chapter 3, a robust fire danger rating system is developed specifically for Indian forests by adapting the CFFDRS and its FWI module. The results from the chapter indicate substantial regional variability in fire weather across India's forest zones. The fire weather indices varied significantly, with northeastern forests showing susceptibility to fire at lower FWI values than other regions, underscoring regional differences in fire danger thresholds. The main outcome of this chapter was the establishment of fire danger thresholds tailored to distinct forest types of India, setting up a foundational tool for understanding and managing fire risk in the Indian context.

Chapter 4 outlines the development of a high-resolution climate dataset by dynamically downscaling CESM projections using the WRF model. This dataset is at a 10-km resolution and meets the need for district-level climate data. This makes it a useful resource for detailed regional climate impact studies. Validation with ERA5 and GSOD observations confirms the accuracy of this dataset. This dataset provided climate data to drive the CFFDRS framework to analyze the effect of climate change on fire weather, which is discussed in detail in Chapter 5. This chapter reports that the mean FWI is expected to increase by approximately 5%, though the impact will differ from forest to

forest. Climate change will likely increase fire danger in the arid and intermediate forests, while humid forests may see a decrease in fire risk due to increased precipitation and humidity. Arid and intermediate zones will likely experience a 60% increase in days exceeding high-severity thresholds, driven by temperature shifts. Conversely, humid forest regions could see a decrease in fire danger days due to increased rainfall and relative humidity. The heterogeneity of the impacts highlights a non-uniform response to climate drivers, especially in regions where extreme rainfall may counterbalance the effects of warming. Additionally, the length of the fire season is projected to extend by up to two months in certain regions. Notably, the MAM pre-monsoon season holds the highest hazard with a projected extension of severe fire weather across several months, especially in central and eastern regions, covering around 55% of the country's forested area. These findings align with the global understanding that climate variability strongly governs fire regimes, as shown by Gincheva et al., (2024), who found that around 60% of interannual variability in burned areas is explained by climatic factors, with wetter regions being more responsive to same-season weather and arid regions to antecedent conditions. Similarly, (Turco et al., 2018, 2023) demonstrated the substantial influence of anthropogenic climate change on fire activity, notably attributing nearly all the observed fivefold increase in summer burned area in California since 1996 to human-induced climate change. While these studies collectively emphasize the dominant role of climate drivers in shaping fire regimes, the present findings suggest that in regions with high precipitation and humidity — such as India's humid forests — increases in these moisture-related variables under future climate scenarios may locally reduce fire danger, despite rising temperatures. Thus, context-specific assessments become important, as climate-

fire interactions can differ substantially between arid, intermediate, and humid ecosystems.

The spatial and seasonal variability of projected fire danger over India aligns with observed patterns of fire occurrence and vulnerability reported in existing studies. The most vulnerable regions are known to include the dry deciduous forests in western Central India, moist deciduous forests in the Northeast and northern Western Ghats, and semi-evergreen forests in southern Northeast India (ISFR, 2021). These areas, already prone to frequent fire events (Srivastava & Garg, 2013; Vadrevu et al., 2013; Verma et al., 2017), are projected to experience increased fire danger due to climate-induced shifts in temperature and humidity. Similar trends have been observed globally, where dry and intermediate forest ecosystems have exhibited heightened fire sensitivity under warming scenarios, as seen in Indonesia (Herawati & Santoso, 2011), the northwestern United States (Halofsky et al., 2020), and Canada (Augustin et al., 2022). Global model-based projections also report region-specific variations in fire danger, though with considerable inconsistencies over India (Bedia et al., 2015; Liu et al., 2010; Quilcaille et al., 2023; Scholze et al., 2006). The present findings, indicating an intensification of fire danger particularly during the pre-monsoon season and an extension of the fire season in parts of Central and Eastern India, provide high-resolution, India-specific evidence of these emerging risks. This reinforces the critical role of localized, ecosystem-specific fire management strategies in responding to the heterogeneous impacts of climate change on fire regimes.

One of the important outcomes of this research is the development of a 10-km high-resolution downscaled climate dataset - the DSCESM. This dataset bridges a critical gap in fine-scale climate information necessary for district-level analysis over India, addressing the diversity in climate and topography that is essential for understanding region-specific climate impacts. With this high-resolution product, the climate signal can be reliably modelled for over 96% of Indian districts, capturing processes down to approximately 400 km². Validation efforts confirmed that the downscaled dataset aligns well with GSOD and ERA5 reanalyses, reinforcing its suitability for robust climate impact studies. Although achieving finer resolutions could enhance detail, the 10-km scale balances accuracy and computational efficiency, making it practical for a range of applications, including climate adaptation planning and regional environmental assessments.

This thesis also advances scientific understanding by showing that fire weather in India is influenced by an interaction of multiple climatic factors, with precipitation and humidity moderating the impact of temperature increases, particularly in humid zones. Methodologically, the use of a 10-km spatial resolution and well validated DSCESM climate projection represents an enhancement over previous studies by providing granular insights suitable for district-level fire management. The elimination of non-forest fires from the analysis further strengthens the focus on forest-specific fire hazard. This is an advancement in accurately representing fire-climate relationships in complex forested landscapes. The development of a robust FDRS is an important advancement in the field of fire danger management across India. As India lacks a nationwide FDRS, this work

sets a foundation for a comprehensive fire danger classification, identifying high-risk areas and offering region-specific thresholds for action. The FDRS framework adapts to diverse climatic and vegetation zones. This system, integrated with climate data across forest zones, highlights the need for non-uniform fire danger thresholds to inform policymakers. Continued refinement of the FDRS based on high-resolution climate reanalysis data is expected to further support adaptive wildfire management.

Overall, this study also contributes significantly to understanding and managing fire weather in a changing climate. The methods and codes developed, including the CFFDRS MATLAB code and associated datasets, are made open access.

This study utilises a single climate model and one emission scenario to project future fire weather conditions. While the CESMv1 model was evaluated for its performance over India during 2006–2015 and the downscaled DSCESM product was validated against ERA5, IMDAA, and GSOD datasets, it is recognised that this represents only one possible future realisation. Although the model's satisfactory performance in the baseline period lends confidence to the projections, uncertainties remain regarding the range of possible climate responses. In the future, incorporating additional GCMs to achieve a more diversified and robust projection could considerably strengthen the FWI projections. Using multi-model, multi-scenario framework, would allow assessment of inter-model variability and scenario-based uncertainties. However, the computational demands of bias correction, dynamical downscaling, and FWI simulation across multiple models were beyond the present study's scope. In downscaling with RCM, each grid cell requires

detailed calculations based on various physical processes. Additionally, the downscaling process in this study incorporates sensitivity analyses and validation against observational data. Such procedures further amplify the computational requirements. The memory demands also increase due to the larger datasets produced at higher resolutions. Although computationally demanding, future studies could build on this framework by using multiple climate models and scenarios to provide a more comprehensive and reliable assessment of future fire danger conditions in India's forest ecosystems.

Other than climate variables, socio-economic and anthropogenic factors also play a significant role in fire risk. Integrating variables like population density, land use patterns, and industrial or agricultural proximity into fire risk assessments would provide a more nuanced assessment of fire ignition and spread dynamics. Incorporating these socio-economic drivers, especially in regions with high human activity adjacent to forested areas, would improve the specificity and accuracy of fire risk models. Similarly, the structural diversity of India's forests—ranging from dense tropical to sparse deciduous ecosystems—calls for species-specific assessments. By including more detailed vegetation data, future studies could tailor fire risk assessments to the unique characteristics and vulnerabilities of different forest types.

In addition to future projections of fire weather by end-century, accurate short-term forecasting is also necessary for effective fire management. Integrating real-time weather forecasts with the FDRS framework could enable a more dynamic system. This approach would support proactive firefighting efforts, better allocation of resources, and timely

warnings for vulnerable areas. Climate extremes, including extended droughts or intense heatwaves, are becoming more frequent and affect fire risks. These events, which deviate from typical fire weather indices focused on averages, require further study. Fire weather forecasting would require integrating such extremes into models. Additionally, exploring feedback loops between climate extremes and forest fires—such as the impact of increased carbon emissions from fires on atmospheric warming—would provide insights into the potential for fire-climate feedback mechanisms that could intensify future fire regimes.

A holistic approach to fire management will require integrating these research findings into operational policy-making frameworks. Including the inferences from this thesis in policy formation could guide the design of adaptive interventions in fire management. Moreover, long-term planning based on scenario-based projections of fire hazard. Engaging local communities and stakeholders to develop fire management frameworks, which blend traditional knowledge with advanced scientific insights, could enhance resilience across forested landscapes.

References

- Abatzoglou, J. T., & Williams, A. P. (2016). Impact of anthropogenic climate change on wildfire across western US forests. *Proceedings of the National Academy of Sciences of the United States of America*, 113(42), 11770–11775.
<https://doi.org/10.1073/PNAS.1607171113>
- Abatzoglou, J. T., Williams, A. P., & Barbero, R. (2019). Global emergence of anthropogenic climate change in fire weather indices. *Geophysical Research Letters*, 46(1), 326–336.
- Abedi, M., Zaki, E., Erfanzadeh, R., & Naqinezhad, A. (2018). Germination patterns of the scrublands in response to smoke: The role of functional groups and the effect of smoke treatment method. *South African Journal of Botany*, 115.
<https://doi.org/10.1016/j.sajb.2017.03.010>
- Abram, N. J., Henley, B. J., Environment, A. S. G.-... E. &, & undefined 2021. (n.d.). Connections of climate change and variability to large and extreme forest fires in southeast Australia. *Nature.Com*. <https://www.nature.com/articles/s43247-020-00065-8>
- Ahmad, F., & Goparaju, L. (2018). Climate change and its impact on Forest Fire in the state of Himachal Pradesh and Uttarakhand states of India: Remote Sensing and GIS Analysis. *Contemporary Trends in Geoscience*, 7(2).
<https://doi.org/10.2478/ctg-2018-0016>
- Amiro, B. D., Logan, K. A., Wotton, B. M., Flannigan, M. D., Todd, J. B., Stocks, B. J., & Martell, D. L. (2004). Fire weather index system components for large fires in the Canadian boreal forest. *International Journal of Wildland Fire*, 13(4), 391–400.
- Andraju, P., Kanth, A. L., Kumari, K. V., & Rao, S. V. B. (2019). Performance Optimization of Operational WRF Model Configured for Indian Monsoon Region. *Earth Systems and Environment*, 3(2). <https://doi.org/10.1007/s41748-019-00092-2>
- Arnell, N. W., Freeman, A., & Gazzard, R. (2021). The effect of climate change on indicators of fire danger in the UK. *Environmental Research Letters*, 16(4), 44027.
- Ashrit, R., Rani, S. I., Kumar, S., Karunasagar, S., Arulalan, T., Francis, T., Routray, A., Laskar, S. I., Mahmood, S., Jerney, P., Maycock, A., Renshaw, R., George, J. P.,

- & Rajagopal, E. N. (2020). IMDAA Regional Reanalysis: Performance Evaluation During Indian Summer Monsoon Season. *Journal of Geophysical Research: Atmospheres*, 125(2). <https://doi.org/10.1029/2019JD030973>
- Attada, R., Kumar, P., & Dasari, H. P. (2018). Assessment of Land Surface Models in a High-Resolution Atmospheric Model during Indian Summer Monsoon. *Pure and Applied Geophysics*, 175(10). <https://doi.org/10.1007/s00024-018-1868-z>
- Augustin, F., Girardin, M. P., Terrier, A., Grondin, P., Lambert, M. C., Leduc, A., & Bergeron, Y. (2022). Projected changes in fire activity and severity feedback in the spruce–feather moss forest of western Quebec, Canada. *Trees, Forests and People*, 8(10022), 9.
- Badarinath, K. V. S., Kharol, S. K., & Chand, T. K. (2007). Use of satellite data to study the impact of forest fires over the northeast region of India. *IEEE Geoscience and Remote Sensing Letters*, 4(3), 485–489.
- Bar, S., Acharya, P., Parida, B. R., Sannigrahi, S., Maiti, A., Barik, G., & Kumar, N. (2024). Investigation of fire regime dynamics and modeling of burn area over India for the twenty-first century. *Environmental Science and Pollution Research*, 31(41). <https://doi.org/10.1007/s11356-024-32922-w>
- Barbero, R., Abatzoglou, J. T., Larkin, N. K., Kolden, C. A., & Stocks, B. (2015). Climate change presents increased potential for very large fires in the contiguous United States. *International Journal of Wildland Fire*, 24(7), 892–899.
- Barik, A., Sahoo, S. K., Kumari, S., & Roy, S. B. (2021). 10 km gridded hydrometeorological dataset developed by dynamical downscaling of the bias-corrected CMIP5 CESM RCP8.5 projections over India for current (2006-2015) and future (2091-2100) periods using WRF. In *World Data Center for Climate (WDCC) at DKRZ*. https://doi.org/https://doi.org/10.26050/WDCC/WRF10km_wbc_C5_forc_oIndia
- Bedia, J., Golding, N., Casanueva, A., Iturbide, M., Buontempo, C., & Gutiérrez, J. M. (2018). Seasonal predictions of Fire Weather Index: Paving the way for their operational applicability in Mediterranean Europe. *Climate Services*, 9. <https://doi.org/10.1016/j.cliser.2017.04.001>

- Bedia, J., Herrera, S., Gutiérrez, J. M., Benali, A., Brands, S., Mota, B., & Moreno, J. M. (2015). Global patterns in the sensitivity of burned area to fire-weather: Implications for climate change. *Agricultural and Forest Meteorology*, 214–215.
<https://doi.org/10.1016/j.agrformet.2015.09.002>
- Berrisford, P., Dee, D., Fielding, K., Fuentes, M., Kallberg, P., Kobayashi, S., & Uppala, S. (2011). The ERA-Interim Archive - Version 2.0. In *ERA report series*.
- Bruyère, C. L., Done, J. M., Holland, G. J., & Fredrick, S. (2014). Bias corrections of global models for regional climate simulations of high-impact weather. *Climate Dynamics*, 43(7–8). <https://doi.org/10.1007/s00382-013-2011-6>
- Canadell, J. G., Meyer, C. P., Cook, G. D., ... A. D.-N., & undefined 2021. (n.d.). Multi-decadal increase of forest burned area in Australia is linked to climate change. *Nature.Com*. <https://www.nature.com/articles/s41467-021-27225-4>
- Carbutt, C., & Kirkman, K. (2022). Ecological Grassland Restoration—A South African Perspective. In *Land* (Vol. 11, Issue 4). <https://doi.org/10.3390/land11040575>
- Carvalho, A., Flannigan, M. D., Logan, K., Miranda, A. I., & Borrego, C. (2008). Fire activity in Portugal and its relationship to weather and the Canadian Fire Weather Index System. *International Journal of Wildland Fire*, 17(3).
<https://doi.org/10.1071/WF07014>
- Castro, C. L., Pielke, R. A., & Leoncini, G. (2005). Dynamical downscaling: Assessment of value retained and added using the Regional Atmospheric Modeling System (RAMS). *Journal of Geophysical Research D: Atmospheres*, 110(5).
<https://doi.org/10.1029/2004JD004721>
- Challinor, A. J., Ewert, F., Arnold, S., Simelton, E., & Fraser, E. (2009). Crops and climate change: Progress, trends, and challenges in simulating impacts and informing adaptation. *Journal of Experimental Botany*, 60(10).
<https://doi.org/10.1093/jxb/erp062>
- Chaturvedi, R. K., Joshi, J., Jayaraman, M., Bala, G., & Ravindranath, N. H. (2012). Multi-model climate change projections for India under representative concentration pathways. *Current Science*, 791–802.
- Choudhury, D., Nath, D., & Chen, W. (2024). Asian summer monsoon responses under RCP4.5 and RCP8.5 scenarios in CESM large ensemble simulations.

- Environmental Research Communications*, 6(7), 071004.
<https://doi.org/10.1088/2515-7620/ad5b3b>
- Cochran, W. G. (1952). The χ^2 Test of Goodness of Fit. *The Annals of Mathematical Statistics*, 23(3), 315–345. <http://www.jstor.org/stable/2236678>
- Countryman, C. M. (1972). The fire environment. In *Forestry handbook*. Pacific Southwest Forest and Range Experiment Station.
- Cruz, M. G., Sullivan, A. L., Gould, J. S., Sims, N. C., Bannister, A. J., Hollis, J. J., & Hurley, R. J. (2012). Anatomy of a catastrophic wildfire: the Black Saturday Kilmore East fire in Victoria, Australia. *Forest Ecology and Management*, 284, 269–285.
- Damage due to Forest Fire*. (2023).
- de Groot, W. J., Goldammer, J. G., Keenan, T., Brady, M. A., Lynham, T. J., & Justice, C. O. (n.d.). ... & O'Loughlin, K. (2006). Developing a global early warning system for wildland fire. *Forest Ecology and Management*, 234, 1.
- De Jong, M. C., Wooster, M. J., Kitchen, K., Manley, C., Gazzard, R., & McCall, F. F. (2016). Calibration and evaluation of the Canadian Forest Fire Weather Index (FWI) System for improved wildland fire danger rating in the United Kingdom. *Natural Hazards and Earth System Sciences*, 16(5). <https://doi.org/10.5194/nhess-16-1217-2016>
- DeMaris, A. (1995). A Tutorial in Logistic Regression. *Journal of Marriage and the Family*, 57(4). <https://doi.org/10.2307/353415>
- Dhar, T., Bhatta, B., & Aravindan, S. (2023). Forest fire occurrence, distribution and risk mapping using geoinformation technology: A case study in the sub-tropical forest of the Meghalaya, India. *Remote Sensing Applications: Society and Environment*, 29. <https://doi.org/10.1016/j.rsase.2022.100883>
- Dimitrakopoulos, A. P., Bemmerzouk, A. M., & Mitsopoulos, I. D. (2011). Evaluation of the Canadian fire weather index system in an eastern Mediterranean environment. *Meteorological Applications*, 18(1), 83–93.
- Dimitrakopoulos, A. P., & Papaioannou, K. K. (2001). Flammability assessment of Mediterranean forest fuels. *Fire Technology*, 37(2), 143–152.

- Dowdy, A. J., Mills, G. A., Finkele, K., & Groot, W. De. (2009). *Australian fire weather as represented by the McArthur forest fire danger index and the Canadian forest fire weather index (p. 91)*. Centre for Australian Weather and Climate Research.
- Dudhia, J. (1989). Numerical study of convection observed during the Winter Monsoon Experiment using a mesoscale two-dimensional model. *Journal of the Atmospheric Sciences*, 46(20). [https://doi.org/10.1175/1520-0469\(1989\)046<3077:NSOCOD>2.0.CO;2](https://doi.org/10.1175/1520-0469(1989)046<3077:NSOCOD>2.0.CO;2)
- E. Lopez Gunn Caretta M.A., A. M. M. A. R. A. B. A. G. Y. H. T. K. L. J. L., & and S. Supratid R. Morgan, S. M. (2016). *Water. In: Climate Change 2022: Impacts, Adaptation and Vulnerability. Contribution of Working Group II to the Sixth Assessment Report of the Intergovernmental Panel on Climate Change* (Vol. 15, Issue 2, pp. 1–23).
- Edwards, P. N. (2000). Chapter 2 A brief history of atmospheric general circulation modeling. In *International Geophysics* (Vol. 70, Issue C). [https://doi.org/10.1016/S0074-6142\(00\)80050-9](https://doi.org/10.1016/S0074-6142(00)80050-9)
- Epanechnikov, V. (1969). Nonparametric estimation of a multidimensional probability density. *Teoriya Veroyatnostei i Ee Primeneniya*, 14(1), 156–161.
- et al. Skamarock WC. (2008). A description of the advanced research WRF version 3, NCAR Tech. Note, NCAR/TN-468+STR. *Natl. Cent. for Atmos. Res. Boulder, Colorado, June*.
- Fanin, T., Biogeosciences, G. R. V. D. W.-, & undefined 2017. (n.d.). Precipitation–fire linkages in Indonesia (1997–2015). *Bg.Copernicus.Org*. <https://bg.copernicus.org/articles/14/3995/2017/>
- Fathima Nuzla Ismail, Brendon J. Woodford, Sherlock A. Licorish, & Aubrey D. Miller. (2024). An assessment of existing wildfire danger indices in comparison to one-class machine learning models. *Natural Hazards*.
- Field, R. D. (2020). Evaluation of Global Fire Weather Database reanalysis and short-term forecast products. *Natural Hazards and Earth System Sciences*, 20(4), 1123–1147.

- Flannigan, M. D., Amiro, B. D., Logan, K. A., Stocks, B. J., & Wotton, B. M. (2006a). Forest fires and climate change in the 21st century. *Mitigation and Adaptation Strategies for Global Change*, 11(4), 847–859.
- Flannigan, M. D., Amiro, B. D., Logan, K. A., Stocks, B. J., & Wotton, B. M. (2006b). Forest fires and climate change in the 21st century. *Mitigation and Adaptation Strategies for Global Change*, 11(4), 847–859.
- Flannigan, M. D., Logan, K. A., Amiro, B. D., Skinner, W. R., & Stocks, B. J. (2005). Future area burned in Canada. *Climatic Change*, 72(1), 1–16.
- Flannigan, M. D., Stocks, B. J., & Wotton, B. M. (2000). Climate change and forest fires. *Science of the Total Environment*, 262(3), 221–229.
- Flato, G., Marotzke, J., Abiodun, B., Braconnot, P., Chou, S. C., Collins, W., Cox, P., Driouech, F., Emori, S., Eyring, V., Forest, C., Gleckler, P., Guilyardi, E., Jakob, C., Kattsov, V., Reason, C., & Rummukainen, M. (2013). IPCC 2013 AR5 - Chapter 9: Evaluation of Climate Models. *Climate Change 2013: The Physical Science Basis. Contribution of Working Group I to the Fifth Assessment Report of the Intergovernmental Panel on Climate Change*.
- Fulé, P. Z., Garkoti, S. C., & Semwal, R. L. (2021). Frequent burning in chir pine forests, Uttarakhand, India. *Fire Ecology*, 17(1), 1–11.
- Giglio, L., Descloitres, J., Justice, C. O., & Kaufman, Y. J. (2003). An enhanced contextual fire detection algorithm for MODIS. *Remote Sensing of Environment*, 87(2–3), 273–282.
- Gincheva, A., Pausas, J. G., Torres-Vázquez, M. Á., Bedia, J., Vicente-Serrano, S. M., Abatzoglou, J. T., Sánchez-Espigares, J. A., Chuvieco, E., Jerez, S., Provenzale, A., Trigo, R. M., & Turco, M. (2024). The Interannual Variability of Global Burned Area Is Mostly Explained by Climatic Drivers. *Earth's Future*, 12(7).
<https://doi.org/10.1029/2023EF004334>
- Gonzalez, P., Neilson, R. P., Lenihan, J. M., & Drapek, R. J. (2010). Global patterns in the vulnerability of ecosystems to vegetation shifts due to climate change. *Global Ecology and Biogeography*, 19(6), 755–768.

- Groot, W. J. D., Field, R. D., Brady, M. A., Roswintarti, O., & Mohamad, M. (2007). Development of the Indonesian and Malaysian fire danger rating systems. *Mitigation and Adaptation Strategies for Global Change*, 12(1), 165–180.
- Gunwani, P., & Mohan, M. (2017). Sensitivity of WRF model estimates to various PBL parameterizations in different climatic zones over India. *Atmospheric Research*, 194. <https://doi.org/10.1016/j.atmosres.2017.04.026>
- Gunwani, P., Sati, A. P., Mohan, M., & Gupta, M. (2021). Assessment of physical parameterization schemes in WRF over national capital region of India. *Meteorology and Atmospheric Physics*, 133(2). <https://doi.org/10.1007/s00703-020-00757-y>
- Halofsky, J. E., Peterson, D. L., & Harvey, B. J. (2020). Changing wildfire, changing forests: the effects of climate change on fire regimes and vegetation in the Pacific Northwest, USA. *Fire Ecology*, 16(1), 1–26.
- Heinimann, A., Mertz, O., Froking, S., Christensen, A. E., Hurni, K., Sedano, F., Chini, L. P., Sahajpal, R., Hansen, M., & Hurtt, G. (2017). A global view of shifting cultivation: Recent, current, and future extent. *PLoS ONE*, 12(9). <https://doi.org/10.1371/journal.pone.0184479>
- Herawati, H., & Santoso, H. (2011). Tropical forest susceptibility to and risk of fire under changing climate: A review of fire nature, policy and institutions in Indonesia. *Forest Policy and Economics*, 13(4), 227–233.
- Hong, S. Y., Noh, Y., & Dudhia, J. (2006). A new vertical diffusion package with an explicit treatment of entrainment processes. *Monthly Weather Review*, 134(9). <https://doi.org/10.1175/MWR3199.1>
- Hurrell, J. W., Holland, M. M., Gent, P. R., Ghan, S., Kay, J. E., Kushner, P. J., Lamarque, J. F., Large, W. G., Lawrence, D., Lindsay, K., Lipscomb, W. H., Long, M. C., Mahowald, N., Marsh, D. R., Neale, R. B., Rasch, P., Vavrus, S., Vertenstein, M., Bader, D., ... Marshall, S. (2013). The community earth system model: A framework for collaborative research. *Bulletin of the American Meteorological Society*, 94(9). <https://doi.org/10.1175/BAMS-D-12-00121.1>

- Hutto, R. L., Keane, R. E., Sherriff, R. L., Rota, C. T., Eby, L. A., & Saab, V. A. (2016). Toward a more ecologically informed view of severe forest fires. *Ecosphere*, 7(2). <https://doi.org/10.1002/ecs2.1255>
- India State Forest Report 2021*. (2022).
- Jain, M., Saxena, P., Sharma, S., & Sonwani, S. (2021). Investigation of Forest Fire Activity Changes Over the Central India Domain Using Satellite Observations During 2001–2020. *GeoHealth*, 5(12). <https://doi.org/10.1029/2021GH000528>
- Janjic, Z. (2002). Nonsingular Implementation of the Mellor-Yamada Level 2.5 Scheme in the NCEP Meso model. *NCEP Office Note*, 437.
- Janjić, Z. I. (2000). Comments on “Development and Evaluation of a Convection Scheme for Use in Climate Models.” *Journal of the Atmospheric Sciences*, 57(21). [https://doi.org/10.1175/1520-0469\(2000\)057<3686:codaeo>2.0.co;2](https://doi.org/10.1175/1520-0469(2000)057<3686:codaeo>2.0.co;2)
- John R Porter. (2022). *Food Systems. In Our Warming Planet: Climate Change Impacts and Adaptation Food Systems. In Our Warming Planet: Climate Change Impacts and Adaptation (pp. 254-275)(pp. 254-275)*.
- Jones, M. W., Abatzoglou, J. T., Veraverbeke, S., Andela, N., Lasslop, G., Forkel, M., Smith, A. J. P., Burton, C., Betts, R. A., van der Werf, G. R., Sitch, S., Canadell, J. G., Santín, C., Kolden, C., Doerr, S. H., & Quéré, C. Le. (2022). Global and Regional Trends and Drivers of Fire Under Climate Change. In *Reviews of Geophysics* (Vol. 60, Issue 3). <https://doi.org/10.1029/2020RG000726>
- Kain, J. S., & Kain, J. (2004). The Kain - Fritsch convective parameterization: An update. *Journal of Applied Meteorology*, 43(1). [https://doi.org/10.1175/1520-0450\(2004\)043<0170:TKCPAU>2.0.CO;2](https://doi.org/10.1175/1520-0450(2004)043<0170:TKCPAU>2.0.CO;2)
- Kale, M. P., Ramachandran, R. M., Pardeshi, S. N., Chavan, M., Joshi, P. K., Pai, D. S., Bhavani, P., Ashok, K., & Roy, P. S. (2017). Are Climate Extremities Changing Forest Fire Regimes in India? An Analysis Using MODIS Fire Locations During 2003–2013 and Gridded Climate Data of India Meteorological Department. *Proceedings of the National Academy of Sciences India Section A - Physical Sciences*, 87(4). <https://doi.org/10.1007/s40010-017-0452-8>

- Kalogiannidis, S., Chatzitheodoridis, F., Kalfas, D., Patitsa, C., & Papagrorgiou, A. (2023). Socio-Psychological, Economic and Environmental Effects of Forest Fires. *Fire*, 6(7). <https://doi.org/10.3390/fire6070280>
- Karali, A., Hatzaki, M., Giannakopoulos, C., Roussos, A., Xanthopoulos, G., & Tenentes, V. (2014). Sensitivity and evaluation of current fire risk and future projections due to climate change: the case study of Greece. *Natural Hazards and Earth System Sciences*, 14(1), 143–153.
- Kidson, J. W., & Thompson, C. S. (1998). A comparison of statistical and model-based downscaling techniques for estimating local climate variations. *Journal of Climate*, 11(4). [https://doi.org/10.1175/1520-0442\(1998\)011<0735:ACOSAM>2.0.CO;2](https://doi.org/10.1175/1520-0442(1998)011<0735:ACOSAM>2.0.CO;2)
- Kirchmeier-Young, M. C., Gillett, N. P., Zwiers, F. W., Cannon, A. J., & Anslow, F. S. (2019). Attribution of the Influence of Human-Induced Climate Change on an Extreme Fire Season. *Earth's Future*, 7(1), 2–10.
- Kodandapani, N., Cochrane, M. A., & Sukumar, R. (2004). Conservation threat of increasing fire frequencies in the Western Ghats, India. *Conservation Biology*, 18(6). <https://doi.org/10.1111/j.1523-1739.2004.00433.x>
- Krikken, F., Lehner, F., Haustein, K., Drobyshev, I., & Oldenborgh, G. J. Van. (n.d.). *Attribution of the role of climate change in the forest fires in Sweden 2018*. <https://doi.org/10.5194/nhess-2019-206>
- Krishnan, R., Sanjay, J., Gnanaseelan, C., Mujumdar, M., Kulkarni, A., & Chakraborty, S. (2020). Assessment of climate change over the Indian region: A report of the ministry of earth sciences (MOES), government of India. In *Assessment of Climate Change over the Indian Region: A Report of the Ministry of Earth Sciences (MoES), Government of India*. <https://doi.org/10.1007/978-981-15-4327-2>
- Li, D., Feng, J., Xu, Z., Yin, B., Shi, H., & Qi, J. (2019). Statistical bias correction for simulated wind speeds over CORDEX-East Asia. *Earth and Space Science*, 6(2), 200–211.
- Littell, J. S., Peterson, D. L., Riley, K. L., Liu, Y., & Luce, C. H. (2016). A review of the relationships between drought and forest fire in the United States. *Global Change Biology*, 22(7), 2353–2369. <https://doi.org/10.1111/GCB.13275>

- Liu, Y., Goodrick, S. L., & Stanturf, J. A. (2013). Future US wildfire potential trends projected using a dynamically downscaled climate change scenario. *Forest Ecology and Management*, 294, 120–135.
- Liu, Y., Stanturf, J., & Goodrick, S. (2010). Trends in global wildfire potential in a changing climate. *Forest Ecology and Management*, 259(4), 685–697.
- Mahto, S. S., & Mishra, V. (2019). Does ERA-5 Outperform Other Reanalysis Products for Hydrologic Applications in India? *Journal of Geophysical Research: Atmospheres*, 124(16). <https://doi.org/10.1029/2019JD031155>
- Martonne, E. De. (1923). *Aridité et indices d'aridité* (pp. 1935–1938).
- Matt Jolly, W., Freeborn, P. H., Page, W. G., & Butler, B. W. (2019). Severe fire danger index: A forecastable metric to inform firefighter and community wildfire risk management. *Fire*, 2(3). <https://doi.org/10.3390/fire2030047>
- McHugh, M. L. (2013). The chi-square test of independence. *Biochemia Medica*, 23(2), 143–149.
- Mishra, V., Bhatia, U., & Tiwari, A. D. (2020). Bias-corrected climate projections for South Asia from Coupled Model Intercomparison Project-6. *Scientific Data*, 7(1). <https://doi.org/10.1038/s41597-020-00681-1>
- Mlawer, E. J., Taubman, S. J., Brown, P. D., Iacono, M. J., & Clough, S. A. (1997). Radiative transfer for inhomogeneous atmospheres: RRTM, a validated correlated-k model for the longwave. *Journal of Geophysical Research Atmospheres*, 102(14). <https://doi.org/10.1029/97jd00237>
- Mohanty, A., & Mithal, V. (2022). Managing Forest Fires in a Changing Climate. *Council on Energy, Environment and Water: New Delhi, India*. <https://www.ceew.in/sites/default/files/ceew-research-on-states-prone-to-forest-wildfires-india-and-mitigation-methods.pdf>
- Monaghan, A. J., Steinhoff, D. F., Bruyere, C. L., & Yates, D. (2014). NCAR CESM global bias-corrected CMIP5 output to support WRF/MPAS research. In *Research Data Archive at the National Center for Atmospheric Research, Computational and Information Systems Laboratory, Boulder, Colorado* (Vol. 25, Issue 03).

- Moritz, M. A., Parisien, M.-A., Batllori, E., Krawchuk, M. A., Dorn, J. Van, Ganz, D. J., & Hayhoe, K. (2012). Climate change and disruptions to global fire activity. *Ecosphere*, 3(6), art49. <https://doi.org/10.1890/ES11-00345.1>
- Murthy, K. K., Sinha, S. K., Kaul, R., & Vaidyanathan, S. (2019). A fine-scale state-space model to understand drivers of forest fires in the Himalayan foothills. *Forest Ecology and Management*, 432. <https://doi.org/10.1016/j.foreco.2018.10.009>
- Navarro-Racines, C., Tarapues, J., Thornton, P., Jarvis, A., & Ramirez-Villegas, J. (2020). High-resolution and bias-corrected CMIP5 projections for climate change impact assessments. *Scientific Data*, 7(1). <https://doi.org/10.1038/s41597-019-0343-8>
- Naveh, Z. (1994). *The Role of Fire and Its Management in the Conservation of Mediterranean Ecosystems and Landscapes*. https://doi.org/10.1007/978-1-4613-8395-6_9
- Nielsen, F. (2016). *Hierarchical Clustering* (pp. 195–211). https://doi.org/10.1007/978-3-319-21903-5_8
- Niu, G. Y., Yang, Z. L., Mitchell, K. E., Chen, F., Ek, M. B., Barlage, M., Kumar, A., Manning, K., Niyogi, D., Rosero, E., Tewari, M., & Xia, Y. (2011). The community Noah land surface model with multiparameterization options (Noah-MP): 1. Model description and evaluation with local-scale measurements. *Journal of Geophysical Research Atmospheres*, 116(12). <https://doi.org/10.1029/2010JD015139>
- Patil, N. S., & Laddimath, R. S. (2021). Regional assessment of impacts of climate change: A statistical downscaling approach. In *Springer Climate*. https://doi.org/10.1007/978-3-030-67865-4_2
- Patil, R., & Kumar, P. P. (2016). WRF model sensitivity for simulating intense western disturbances over North West India. *Modeling Earth Systems and Environment*, 2(2). <https://doi.org/10.1007/s40808-016-0137-3>
- Paulson, C. A. (1970). The Mathematical Representation of Wind Speed and Temperature Profiles in the Unstable Atmospheric Surface Layer. *Journal of Applied Meteorology*, 9(6). [https://doi.org/10.1175/1520-0450\(1970\)009<0857:tmrows>2.0.co;2](https://doi.org/10.1175/1520-0450(1970)009<0857:tmrows>2.0.co;2)

- Pausas, J. G., & Keeley, J. E. (2019). Wildfires as an ecosystem service. *Frontiers in Ecology and the Environment*, 17(5). <https://doi.org/10.1002/fee.2044>
- Pechony, O., & Shindell, D. T. (2010). Driving forces of global wildfires over the past millennium and the forthcoming century. *Proceedings of the National Academy of Sciences*, 107(45), 19167–19170.
- Peel, M. C., Finlayson, B. L., & McMahon, T. A. (2007). Updated world map of the Köppen-Geiger climate classification. *Hydrology and Earth System Sciences*, 11(5), 1633–1644.
- Piñol, J., Terradas, J., & Lloret, F. (1998). Climate warming, wildfire hazard, and wildfire occurrence in coastal eastern Spain. *Climatic Change*, 38(3). <https://doi.org/10.1023/A:1005316632105>
- Prathipati, V. K., Viswanadhapalli, Y., Chennu, V. N., & Dasari, H. P. (2021). Study of Active and Break Spell Phenomena of Indian Summer Monsoon Using WRF Downscaled Data. *Pure and Applied Geophysics*. <https://doi.org/10.1007/s00024-021-02837-5>
- Qian, J. H., Seth, A., & Zebiak, S. (2003). Reinitialized versus continuous simulations for regional climate downscaling. *Monthly Weather Review*, 131(11). [https://doi.org/10.1175/1520-0493\(2003\)131<2857:RVCSFR>2.0.CO;2](https://doi.org/10.1175/1520-0493(2003)131<2857:RVCSFR>2.0.CO;2)
- Quilcaille, Y., Batibeniz, F., Ribeiro, A. F. S., Padrón, R. S., & Seneviratne, S. I. (2023). Fire weather index data under historical and shared socioeconomic pathway projections in the 6th phase of the Coupled Model Intercomparison Project from 1850 to 2100. *Earth Syst. Sci. Data*, 000583391(15).
- Rai, D., & Pattnaik, S. (2019). Evaluation of WRF planetary boundary layer parameterization schemes for simulation of monsoon depressions over India. *Meteorology and Atmospheric Physics*, 131(5). <https://doi.org/10.1007/s00703-019-0656-3>
- Rajeevan, M., Kesarkar, A., Thampi, S. B., Rao, T. N., Radhakrishna, B., & Rajasekhar, M. (2010). Sensitivity of WRF cloud microphysics to simulations of a severe thunderstorm event over Southeast India. *Annales Geophysicae*, 28(2). <https://doi.org/10.5194/angeo-28-603-2010>

- Randall, R. A. W. D. A. (2007). Climate Models and Their Evaluation. In *Evaluation* (Vol. 323).
- Ratnam, J. V, Behera, S. K., Krishnan, R., Doi, T., & Ratna, S. B. (2017). Sensitivity of Indian summer monsoon simulation to physical parameterization schemes in the WRF model. *Climate Research*, 74(1). <https://doi.org/10.3354/cr01484>
- Ravindranath, N. H., Joshi, N. V, Sukumar, R., & Saxena, A. (2006). Impact of climate change on forests in India. In *Current Science* (Vol. 90, Issue 3). <https://doi.org/10.1007/s41775-024-00229-9>
- Reddy, B. R., Srinivas, C. V, Shekhar, S. S. R., Baskaran, R., & Venkatraman, B. (2020). Impact of land surface physics in WRF on the simulation of sea breeze circulation over southeast coast of India. *Meteorology and Atmospheric Physics*, 132(6). <https://doi.org/10.1007/s00703-020-00726-5>
- Renard, Q., Plissier, R., Ramesh, B. R., & Kodandapani, N. (2012). Environmental susceptibility model for predicting forest fire occurrence in the Western Ghats of India. *International Journal of Wildland Fire*, 21(4). <https://doi.org/10.1071/WF10109>
- Roy, P. S., Behera, M. D., Murthy, M. S. R., Roy, A., Singh, S., & Kushwaha, S. P. S. (2015). ... & Ramachandran, R. M. *New Vegetation Type Map of India Prepared Using Satellite Remote Sensing: Comparison with Global Vegetation Maps and Utilities*, 39, 142–159.
- Samiuddin, M., & El-Sayyad, G. M. (1990). On nonparametric kernel density estimates. *Biometrika*, 77(4), 865–874.
- Santoso, M. A., Christensen, E. G., Yang, J., & Rein, G. (2019). Review of the transition from smouldering to flaming combustion in wildfires. *Frontiers in Mechanical Engineering*, 5, 49.
- Schaefer, J. T. (1990). The Critical Success Index as an Indicator of Warning Skill. *Weather and Forecasting*, 5(4). [https://doi.org/10.1175/1520-0434\(1990\)005<0570:tcsiaa>2.0.co;2](https://doi.org/10.1175/1520-0434(1990)005<0570:tcsiaa>2.0.co;2)
- Scheiter, S., Higgins, S. I., Beringer, J., & Hutley, L. B. (2015). Climate change and long-term fire management impacts on Australian savannas. *New Phytologist*, 205(3), 1211–1226.

- Scheper, A. C., Verweij, P. A., & van Kuijk, M. (2021). Post-fire forest restoration in the humid tropics: A synthesis of available strategies and knowledge gaps for effective restoration. *Science of the Total Environment*, 771. <https://doi.org/10.1016/j.scitotenv.2020.144647>
- Scholze, M., Knorr, W., Arnell, N. W., & Prentice, I. C. (2006). A climate-change risk analysis for world ecosystems. *Proceedings of the National Academy of Sciences of the United States of America*, 103(35). <https://doi.org/10.1073/pnas.0601816103>
- Schroeder, M. J., & Buck, C. C. (1970). *Fire weather: a guide for application of meteorological information to forest fire control operations* (No. 360). US Department of Agriculture.
- Schwalm, C. R., Glendon, S., & Duffy, P. B. (2020). RCP8.5 tracks cumulative CO₂ emissions. *Proceedings of the National Academy of Sciences of the United States of America*, 117(33). <https://doi.org/10.1073/PNAS.2007117117>
- Seneviratne, S. I., Zhang, X., Adnan, M., Badi, W., Dereczynski, C., Luca, A. Di, Ghosh, S., Iskandar, I., Kossin, J., Lewis, S., Otto, F., Pinto, I., Satoh, M., Vicente-Serrano, S. M., Wehner, M., & Zhou, B. (2021). Weather and Climate Extreme Events in a Changing Climate. In *Climate Change 2021 – The Physical Science Basis* (pp. 1513–1766). Cambridge University Press. <https://doi.org/10.1017/9781009157896.013>
- Shah, S. U., Yebra, M., Van Dijk, A. I. J. M., & Cary, G. J. (2022). A New Fire Danger Index Developed by Random Forest Analysis of Remote Sensing Derived Fire Sizes. *Fire*, 5(5). <https://doi.org/10.3390/fire5050152>
- Sharma, U. (2020). Effect of forest fire on nitrogen mineralization in different land uses under Chir Pine (*Pinus roxburghii*) forest in North Western Himalayas. *Journal of Pharmacognosy and Phytochemistry*, 9(6), 1233–1236.
- Singh, R. D., Gumber, S., Tewari, P., & Singh, S. P. (2016). Nature of forest fires in Uttarakhand: Frequency, size and seasonal patterns in relation to pre-monsoonal environment. *Current Science*, 111(2). <https://doi.org/10.18520/cs/v111/i2/398-403>
- Singh, S., & Suresh Babu, K. V. (2021). *Forest Fire Susceptibility Mapping for Uttarakhand State by Using Geospatial Techniques*. https://doi.org/10.1007/978-3-030-76116-5_11

- Singh, T., Saha, U., Prasad, V. S., & Gupta, M. Das. (2021). Assessment of newly-developed high resolution reanalyses (IMDAA, NGFS and ERA5) against rainfall observations for Indian region. *Atmospheric Research*, 259. <https://doi.org/10.1016/j.atmosres.2021.105679>
- Srinivas, C. V, Hariprasad, D., Rao, D. V. B., Anjaneyulu, Y., Baskaran, R., & Venkatraman, B. (2013). Simulation of the Indian summer monsoon regional climate using advanced research WRF model. *International Journal of Climatology*, 33(5). <https://doi.org/10.1002/joc.3505>
- Srivastava, P., & Garg, A. (2013). Forest fires in India: Regional and temporal analyses. *Journal of Tropical Forest Science*, 228–239.
- Stocks, B. J., Lawson, B. D., Alexander, M. E., Wagner, C. V, McAlpine, R. S., Lynham, T. J., & Dube, D. E. (1989). The Canadian forest fire danger rating system: an overview. *The Forestry Chronicle*, 65(6), 450–457.
- Sun, Q., Miao, C., Hanel, M., Borthwick, A. G. L., Duan, Q., Ji, D., & Li, H. (2019). Global heat stress on health, wildfires, and agricultural crops under different levels of climate warming. *Environment International*, 128. <https://doi.org/10.1016/j.envint.2019.04.025>
- Thomas, T. M., Bala, G., & Vemavarapu, S. V. (2023). How do the characteristics of monsoon low pressure systems over India change under a warming climate? A modeling study using the NCAR CESM. *Climate Dynamics*, 61(11–12). <https://doi.org/10.1007/s00382-023-06837-0>
- Thompson, G., Field, P. R., Rasmussen, R. M., & Hall, W. D. (2008). Explicit forecasts of winter precipitation using an improved bulk microphysics scheme. Part II: Implementation of a new snow parameterization. *Monthly Weather Review*, 136(12). <https://doi.org/10.1175/2008MWR2387.1>
- Tian, L., Jin, J., Wu, P., yue Niu, G., & Zhao, C. (2020). High-resolution simulations of mean and extreme precipitation with WRF for the soil-erosive Loess Plateau. *Climate Dynamics*, 54(7–8). <https://doi.org/10.1007/s00382-020-05178-6>
- Tian, X., McRae, D. J., Jin, J., Shu, L., Zhao, F., & Wang, M. (2011). Wildfires and the Canadian Forest Fire Weather Index system for the Daxing'anling region of China. *International Journal of Wildland Fire*, 20(8), 963–973.

- Trzaska, S., & Schnarr, E. (2014). A Review of Downscaling Methods for Climate Change Projections. African and Latin American Resilience to Climate Change (ARCC). *United States Agency for International Development by Tetra Tech ARD*, September, 1–42.
http://www.ciesin.org/documents/Downscaling_CLEARED_000.pdf
- Turco, M., Abatzoglou, J. T., Herrera, S., Zhuang, Y., Jerez, S., Lucas, D. D., AghaKouchak, A., & Cvijanovic, I. (2023). Anthropogenic climate change impacts exacerbate summer forest fires in California. *Proceedings of the National Academy of Sciences of the United States of America*, 120(25).
<https://doi.org/10.1073/pnas.2213815120>
- Turco, M., Rosa-Cánovas, J. J., Bedia, J., Jerez, S., Montávez, J. P., Llasat, M. C., & Provenzale, A. (2018). Exacerbated fires in Mediterranean Europe due to anthropogenic warming projected with non-stationary climate-fire models. *Nature Communications*, 9(1). <https://doi.org/10.1038/s41467-018-06358-z>
- Tyukavina, A., Potapov, P., Hansen, M. C., Pickens, A. H., Stehman, S. V., Turubanova, S., Parker, D., Zalles, V., Lima, A., Kommareddy, I., Song, X. P., Wang, L., & Harris, N. (2022). Global Trends of Forest Loss Due to Fire From 2001 to 2019. *Frontiers in Remote Sensing*, 3. <https://doi.org/10.3389/frsen.2022.825190>
- Ullah, S., You, Q., Sachindra, D. A., Nowosad, M., Ullah, W., Bhatti, A. S., Jin, Z., & Ali, A. (2022). Spatiotemporal changes in global aridity in terms of multiple aridity indices: An assessment based on the CRU data. *Atmospheric Research*, 268. <https://doi.org/10.1016/j.atmosres.2021.105998>
- Upton, G. J. (1992). Fisher's exact test. *Journal of the Royal Statistical Society: Series A (Statistics in Society)*, 155(3), 395–402.
- Vadrevu, K. P., Giglio, L., & Justice, C. (2013). Satellite based analysis of fire–carbon monoxide relationships from forest and agricultural residue burning (2003–2011). *Atmospheric Environment*, 64, 179–191.
- Vadrevu, K. P., Lasko, K., Giglio, L., Schroeder, W., Biswas, S., & Justice, C. (2019). Trends in vegetation fires in south and southeast Asian countries. *Scientific Reports*, 9(1), 1–13.

- van Vuuren, D. P., Edmonds, J., Kainuma, M., Riahi, K., Thomson, A., Hibbard, K., Hurtt, G. C., Kram, T., Krey, V., Lamarque, J. F., Masui, T., Meinshausen, M., Nakicenovic, N., Smith, S. J., & Rose, S. K. (2011). The representative concentration pathways: An overview. *Climatic Change*, 109(1).
<https://doi.org/10.1007/s10584-011-0148-z>
- van Wees, D., van Der Werf, R., G., Randerson, J. T., Andela, N., Chen, Y., & Morton, D. C. (2021). The role of fire in global forest loss dynamics. *Global Change Biology*, 27(11), 2377.
- Vancutsem, C., Achard, F., Pekel, J. F., Vieilledent, G., Carboni, S., Simonetti, D., Gallego, J., Aragão, L. E. O. C., & Nasi, R. (2021). Long-term (1990–2019) monitoring of forest cover changes in the humid tropics. *Science Advances*, 7(10).
<https://doi.org/10.1126/sciadv.abe1603>
- Vasilakos, C., Kalabokidis, K., Hatzopoulos, J., Kallos, G., & Matsinos, Y. (2007). Integrating new methods and tools in fire danger rating. *International Journal of Wildland Fire*, 16(3). <https://doi.org/10.1071/WF05091>
- Verma, S., Singh, D., Mani, S., & Jayakumar, S. (2017). Effect of forest fire on tree diversity and regeneration potential in a tropical dry deciduous forest of Mudumalai Tiger Reserve, Western Ghats, India. *Ecological Processes*, 6(1), 1–8.
- Wagner, C. E. Van. (1987). Development and structure of the Canadian forest fire weather index system. In *Forestry*. In Can. For. Serv.
<http://scholar.google.com/scholar?hl=en&btnG=Search&q=intitle:Development+and+Structure+of+the+Canadian+Forest+Fire+Weather+Index+System#0>
- Wang, X., Parisien, M. A., Taylor, S. W., Candau, J. N., Stralberg, D., Marshall, G. A., Little, J. M., & Flannigan, M. D. (2017). Projected changes in daily fire spread across Canada over the next century. *Environmental Research Letters*, 12(2).
<https://doi.org/10.1088/1748-9326/aa5835>
- Wang, X., Tolsdorf, V., Otto, M., & Scherer, D. (2021). WRF-based dynamical downscaling of ERA5 reanalysis data for High Mountain Asia: Towards a new version of the High Asia Refined analysis. *International Journal of Climatology*, 41(1). <https://doi.org/10.1002/joc.6686>

- Wood, A. W., Leung, L. R., Sridhar, V., & Lettenmaier, D. P. (2004). Hydrologic implications of dynamical and statistical approaches to downscaling climate model outputs. *Climatic Change*, 62(1–3).
<https://doi.org/10.1023/B:CLIM.0000013685.99609.9e>
- Wotton, B. M. (2009). Interpreting and using outputs from the Canadian Forest Fire Danger Rating System in research applications. *Environmental and Ecological Statistics*, 16(2), 107–131.
- Wotton, B. M., & Flannigan, M. D. (1993). Length of the fire season in a changing climate. *The Forestry Chronicle*, 69(2), 187–192.
- Wotton, B. M., of ..., C. A. N.-I. J., & undefined 2010. (2010). Forest fire occurrence and climate change in Canada. *CSIRO Publishing*, 19, 253–271.
<https://doi.org/10.1071/WF09002>
- Xia, G., Cervarich, M. C., Roy, S. B., Zhou, L., Minder, J. R., Jimenez, P. A., & Freedman, J. M. (2017). Simulating impacts of real-world wind farms on land surface temperature using the WRF model: Validation with observations. *Monthly Weather Review*, 145(12). <https://doi.org/10.1175/MWR-D-16-0401.1>
- Xu, Z., & Yang, Z. L. (2012). An improved dynamical downscaling method with GCM bias corrections and its validation with 30 years of climate simulations. *Journal of Climate*, 25(18). <https://doi.org/10.1175/JCLI-D-12-00005.1>
- Yule, G. U. (1897). On the theory of correlation. *Journal of the Royal Statistical Society*, 60(4), 812–854.
- Zackrisson, O., Nilsson, M.-C., & Wardle, D. A. (1996). Key Ecological Function of Charcoal from Wildfire in the Boreal Forest. *Oikos*, 77(1).
<https://doi.org/10.2307/3545580>